UNIVERSITEIT VAN PRETORIA
UNIVERSITY OF PRETORIA
YUNIBESITHI YA PRETORIA

Dried Xanthan Gum/Nanocellulose for Thermoplastic Starch Reinforcement

Zian Hoek

UNIVERSITEIT VAN PRETORIA
UNIVERSITY OF PRETORIA
YUNIBESITHI YA PRETORIA

Dried Xanthan Gum/Nanocellulose for Thermoplastic Starch Reinforcement

Zian Hoek
18076272

Dissertation for the partial fulfilment of the requirements of the degree

Master of Engineering (Chemical Engineering)

Supervisor

Focke, Walter Wilhelm

Co-supervisor

Mrs. E. du Toit

Department of Chemical Engineering
University of Pretoria
South Africa

CVD 800

2024-02-05

Dried Xanthan Gum/Nanocellulose for Thermoplastic Starch Reinforcement

Abstract

The world is facing a plastic crisis. Biodegradable plastics are not yet suitable to solve the problem. Two issues are cost and strength. Thermoplastic starch, or TPS, is a biodegradable polymer produced by gelatinising starch granules in the presence of a plasticiser, such as glycerol. It is biodegradable, low-cost, and renewable, but its tensile properties, retrogradation, and permeability leave much to be desired.

Nanocellulose fibres (CNFs) are a way to remediate this problem by reinforcing the polymer matrix. Nanocellulose is a perfect reinforcing material for green polymers, as it has appreciable mechanical properties, high surface area, and is biodegradable. There is an issue though; nanocellulose can not be dried. This is due to a process called hornification; the irreversible agglomeration of cellulose upon drying. Nanocellulose fibres, when sold, contain at least 75% water. This adds a lot to the shipping cost and makes it less cost-competitive. Non-polar polymers are also incompatible with water. Therefore, producing redispersible dried nanocellulose is a major concern.

The addition of other biopolymers, called capping agents, prior to drying is one way to prevent hornification. Biopolymers, such as lignin, gelatin, and carboxy methyl cellulose, have been tested. Xanthan gum, a hydrocolloid, is one biopolymer that has not received much attention as a potential capping agent. Xanthan gum is a suitable additive due to its unique properties such as shear thinning behaviour, anionic charge, extreme thickening ability, and stability over a large temperature and pH range.

The starch investigated is derived from amura (*Tacca involucrata*)— a tuber grown in Nigeria. Amura grows naturally in Nigeria and would not intrude on the native ecology. It is rarely used as a food source, as it has a bitter taste and needs refinement to make it edible. Amura can thus contribute to the economy of a developing nation without impacting food security.

The aim of the study was threefold: establish the suitability of amura as a source for TPS, characterise the redispersibility of dried CNFs when dried with xanthan gum, and investigate the interaction of xanthan gum and CNFs on the tensile properties of TPS.

There is a paucity of research on amura starch as a source for TPS; thus the native starch and the TPS film were briefly characterised. The native starch's amylose content, crystallinity,

and gelatinisation temperature were determined and indicated it is an A-type starch— similar to yellow amura described in the literature. The TPS was produced using film casting with glycerol as a plasticiser, assessed at three different concentrations, and conditioned at three different humidities. The TPS retrogradation, water vapour permeability, and tensile properties were investigated, showing similar behaviour as TPS from the literature. The TPS showed a maximum tensile strength at 35% glycerol and 53% RH, which where central values. This result is unexpected, but not unheard of in literature.

Various ratios of nanocellulose/xanthan were high-shear mixed, oven-dried, and redispersed to a 0.03 wt% concentration. The dried redispersed samples were compared to dispersions of non-dried samples of similar concentrations. The dried CNFs were redispersed using different mixing intensities and methods, such as high-shear mixing from 4000 rpm – 8000 rpm and ultrasonication. The fibre diameters were estimated using turbidimetry, which showed dried redispersed CNFs had diameters of 149.0 nm and 147.4 nm when shear mixed and ultrasonicated, respectively. CNFs with 25 wt% xanthan added had diameters of 147.0 nm for both shear mixing and ultrasonication. Scanning electron microscopy (SEM), done on freeze dried samples, confirmed this observation. Pure, dried CNFs that were redispersed only with shear mixing showed large agglomerates. No agglomerates were observed with CNFs that had 25 wt% xanthan added prior to drying, even when redispersed only using shear mixed. Solutions made from dried, pure CNFs showed a marked difference in rheological behaviour compared to non-dried CNF solutions. In contrast, the shear-thinning slopes of dried-then-redispersed and non-dried CNF solutions with 15 wt% xanthan added were identical, showing that xanthan addition could conserve the rheological properties.

The impact of CNF and xanthan on the tensile properties of TPS was assessed using a central composite design, which revealed a positive interaction term. It was theorised that this was due to the CNF and xanthan forming an interlaced web throughout the TPS matrix. Dried or non-dried CNF/xanthan mixtures were dispersed in TPS matrices and tensile testing revealed no conclusive difference between TPS with dried CNFs or with non-dried CNFs, regardless of xanthan gum addition. TPS with 5% pure, non-dried CNFs had a tensile strength of 14.3±2.9 MPa, compared to 15.3±1.0 MPa for TPS with dried CNFs. The strongest and stiffest sample was the TPS with dried CNF/xanthan (25% xanthan content), with a CNF-to-starch addition of 5 wt%. This sample had a tensile strength of 23.0 MPa and a modulus of 1.476 GPa. Compared to pure TPS, with a tensile strength of 5.4 MPa and a modulus of 0.307 GPa, the improvement is significant.

Amura starch was shown to be suitable for producing TPS films. This work proved that xanthan is an effective capping agent for CNFs, allowing for full redispersion after drying. Furthermore, combining CNFs and xanthan showed synergism when used to reinforce TPS. Previously dried CNF/xanthan could successfully be used to reinforce amura TPS films. The work has applica-

tions in the production of redispersible dried CNFs that are effective at producing biopolymers with appreciable tensile properties. It is recommended that research extends to lower levels of xanthan gum addition as well as to other biodegradable polymers besides TPS.

keywords: Xanthan gum, thermoplastic starch, cellulose nanofibrils, dispersion, hornification

Acknowledgements

I first want to say thank you to my parents, for their years of support and giving me the freedom to become who I am. Thank you to my significant other, Fransu, for celebrating the highs and nurturing the lows. I would like to say thank you to my supervisor, Prof. W. Focke, for asking the right questions, giving the best answers, and for all the rooibos tea at Artisans. I am grateful for my co-supervisor, Mrs E du Toit, for she was able to give the clearest of answers to the vaguest of questions, and was always delightful and pleasant. Thank you Anya and Daniele, my two trusty undergraduates, whom without the research would not have progressed as swiftly as it has. Thank you Roger and Joy, my two fellow postgraduates, who provided a much needed break from the lab from time to time. Thank you Dr James Wesley-Smith, for providing the most magnificent microscopy images I have ever laid eyes on. Thank you Dr Maria Atanasova for the XRD analyses. I would like to acknowledge Dr Deon Brink for his assistance with the adsorption analysis. I would like to say thanks to PAMSA and Sappi for the financial and research support, and especially to Sanet Minnaar and Ismael Amer for their support in technical analyses.

"And always, he fought the temptation to choose a clear, safe course, warning 'That path leads ever down into stagnation.'"

— Princess Irulan quoting Paul Atreides
Dune

Contents

List of Figures

List of Tables

Nomenclature

Constants

π	Circumference of a circle divide by its diameter	–
N_A	Avogadro's number 6.02×10^{23}	mol^{-1}

Greek

2θ	Diffraction angle	$^\circ$
α	Intercept change from dried to non-dried	–
β	Slope change from dried to non-dried	–
$\dot{\gamma}$	Shear rate	s^{-1}
η	Dynamic viscosity	mPa s
λ	Wavelength of light	cm
μ	Mass-length ratio	Da/cm
ϕ_f	Volume fraction of fibre	–
ϕ_m	Volume fraction of matrix	–
σ	Tensile strength	MPa
τ	Turbidity	cm^{-1}

Roman

Δm	Mass change of sample	g
ΔP	Water vapour pressure difference across sample	kPa
Δt	Change in time	d
Δt	Time interval	d
$\frac{dn}{dc}$	Specific refractive index increment	mL g^{-1}
ND	Categorical variable indicating non-dried state	–
A	Area of sample	m^2
c	Concentration of polymer solution	g mL^{-1}

C_e	Equilibrium concentration of adsorbate	$\mathrm{g\,L^{-1}}$
d	Diameter of polymer molecule	m
E	Young's modulus	GPa
E_c	Composite Young's modulus	GPa
E_f	Fibre Young's modulus	GPa
E_m	Matrix Young's modulus	GPa
$F_{\max}$	Maximum force between two spheres	N
K	Consistency index of fluid	$\mathrm{Pa\,s^n}$
K_f	Freundlich constant	$\mathrm{g\,g^{-1}}$
K_L	Langmuir constant	$\mathrm{g^{-1}}$
M_w	Molecular weight of adsorbate	$\mathrm{g\,mol^{-1}}$
MM	Molar mass	$\mathrm{g\,mol^{-1}}$
n	Flow behaviour index of fluid	–
n'	Refractive index of polymer solution	–
n_f	Freundlich exponent	–
q_e	Equilibrium adsorption capacity	$\mathrm{g\,g^{-1}}$
q_H	Hydrophobic surface adsorption capacity	$\mathrm{g\,g^{-1}}$
$q_{\max}$	Maximum adsorption capacity	$\mathrm{g\,g^{-1}}$
r	Radius	cm
RH	Relative humidity	%
S_a	Cross-sectional area of adsorbate molecule	$\mathrm{m^2}$
SSA	Specific surface area of adsorbent	$\mathrm{m^2\,g^{-1}}$
t	Thickness of sample	m
T_c	Closing temperature of gelatinisation	°C
T_g	Glass transition temperature	°C

T_o	Onset temperature of gelatinisation	°C
T_p	Peak temperature of gelatinisation	°C
WVP	Water vapour permeability	$\mathrm{g\,m^{-1}\,d^{-1}\,kPa^{-1}}$
$WVTR$	Water vapour transmission rate	$\mathrm{g\,m^{-2}\,d^{-1}}$

1 Introduction

Synthetic polymers, or more colloquially, plastics, are one of the most impactful advancements in materials science. The discovery of celluloid in 1869 and bakelite in 1907 paved the way for a large field of study known today as polymer science (American Chemical Society, 2023). Plastics are incredible materials with low cost, low density, and a wide range of mechanical properties — ranging from ductile to rigid. Plastic's largest advantage compared to other materials is the ease of conversion into the final product (Bisinella *et al.* 2018; Mackenzie, 2022). The low melting point and shear thinning behaviour allow for fast production processes, such as injection moulding and film blowing (Osswald, 2017: 174–179).

However, synthetic plastics have drawbacks, with plastic pollution being a pressing environmental concern. The matter is of such importance that it was explicitly stated in 2 of the 17 sustainable development goals (12 and 14) set by the UN in 2015, and has relevance to 4 others (United Nations, 2015). Some of these polymers, especially PVC and its additives, like phthalates, have had detrimental health effects on society (Swan & Colino, 2021).

The demand that caused 460 Mt of plastic to be produced in 2019 is not dwindling soon; in actuality, it is set to triple by 2060 (OECD, 2022). Finding greener alternatives is a crucial step towards meeting the sustainable development goals. Biodegradable polymers offer a viable solution, with polylactic acid (PLA) and polybutylene adipate terephthalate (PBAT) leading the market (European Bioplastics, 2022).

Among the various biopolymers, thermoplastic starch (TPS) stands out for its low cost, compatibility with modern production methods, and negligible environmental impact (Mordor Intelligence, 2023; Wiedmann & Strobel, 1991). TPS is a biodegradable polymer produced by gelatinising starch with a plasticiser, such as glycerol. TPS is not perfect though, and has several drawbacks, such as poor mechanical properties, sensitivity to moisture, and retrogradation (Van Soest *et al.* 1996c; Van Soest & Vliegenthart, 1997).

Numerous strategies have been explored to remediate these disadvantages, including, but not limited to, chemical modification, novel plasticisers, cross-linking, and reinforcing fillers (Felipe Bergel *et al.* 2020; Ma & Yu, 2004; Jiugao, Ning & Xiaofei, 2005; Ghanbari *et al.* 2018). A promising filler for TPS is nanocellulose fibre (CNF). CNFs are nanoscale cellulose fibres produced via mechanical refinement of cellulose pulp (Huang, Dufresne & Lin, 2019: 54). Once at the nanoscale, the fibres showcase remarkable mechanical strength and stiffness, a high aspect ratio, and biodegradability (Kafy *et al.* 2017; Iwamoto *et al.* 2009; Xu *et al.* 2013).

However, CNFs are sold as an aqueous solution or paste with > 75 % water (Foster *et al.* 2018). This limits the application of CNFs in some polymers and increases the shipping cost.

The water can not be removed due to hornification; the irreversible agglomeration of CNFs due the formation of hydrogen bonds and lactone bridges upon drying (Fernandes Diniz, Gil & Castro, 2004). Producing redispersible, dried CNFs that remain functional in biodegradable polymers, such as TPS, is essential for progressing the biopolymer field.

Various strategies had been developed to produce redispersible dried CNFs. Examples are different drying methods, ionic additives, surface modification, and adding other polymers (capping agents) (Xu *et al.* 2022). Natural capping agents that showed good success are carboxy methyl cellulose (CMC), lignin, and gelatin (Lowys, Desbrières & Rinaudo, 2001; Liu, 2018; Kwak *et al.* 2019). Xanthan gum is a natural hydrocolloid that has unique rheological, thickening, and stabilizing properties. Beaumont *et al.* (2017) briefly explored xanthan gum as a capping agent for TENCEL® gel, a nanospherical gel derived from cellulose. The work showed promise and supports the exploration of xanthan gum as capping agent for CNFs.

The aim of the study is to produce redispersible dried CNFs that can still effectively reinforce TPS by using xanthan gum as a capping agent. The TPS was produced from a novel starch called amura (*Tacca involucrata*)— a tuber crop grown in Nigeria— which had little to no research reporting on its use for TPS production (Omojola, 2013; Zaku *et al.* 2009). There were thus three objectives. First, briefly characterise native amura starch and investigate its suitability as a source for TPS. Next, quantitatively evaluate xanthan gum's efficacy as a capping agent to produce redispersible dried CNFs. And finally, investigate how xanthan affects the ability of CNFs to strengthen TPS, both when the CNF/xanthan is non-dried, and when it is dried and redispersed.

For this purpose, the amylose content, gelatinisation temperature, and crystalline structure of the native starch were determined to establish the baseline characteristics of the starch using iodine indication, DSC, and XRD, respectively. TPS was produced via film casting. Glycerol was added as the plasticiser at 3 different concentrations. The TPS was stored under 3 different humidities. This allowed for the investigation of the retrogradation behaviour, vapour permeability, and tensile properties of the TPS.

Four levels of xanthan gum addition, relative to the CNFs, were investigated. Mixtures were high-shear mixed and oven-dried. Five mixing intensities were investigated for subsequent redispersion of dried material. The dispersibility of the dried CNFs was characterised using turbidimetry, SEM/TEM, and rheometry. The zeta potential and colloidal stability were also investigated.

A central composite face-centred design (CCF) was developed to investigate the effect of CNFs and xanthan gum on the tensile properties of amura TPS. The CCF allowed for the accurate estimation of the effects of xanthan and CNF on the TPS. This includes quadratic and interaction effects. Dried and non-dried CNF/xanthan mixtures were added to TPS at both 2.5 wt% and

5 wt% CNF loadings relative to the mass starch allowing for comparison between non-dried and dried-then-redispersed CNF/xanthan as reinforcing fillers.

2 Literature

2.1 Thermoplastic starch

Starch is an organic polymer that consists of glucose monomers. There are 2 types of starch polymers, amylose and amylopectin. Amylose is a linear chain of glucose monomers, more specifically called (1→4)-linked α-D-glucopyronosal units. Amylopectin is a branched chain polymer, with the main chain consisting of (1→4)-linked α-D-glucopyronosal units, with branches of (1→6)-linked α-D-glucopyronosal units (BeMiller, 2019: 163–164). The structures of amylose and amylopectin are shown in Figure 1.

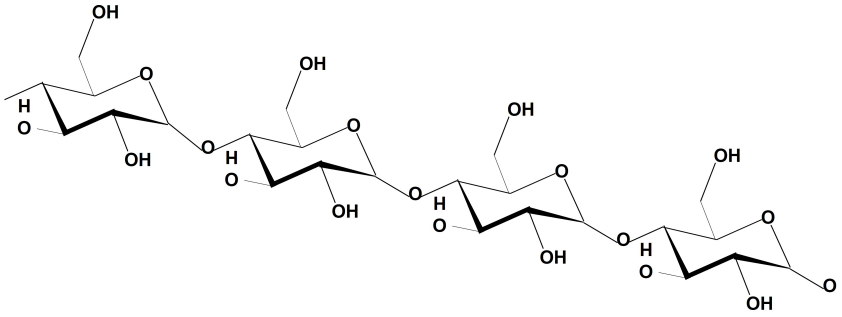

(a) Amylose.

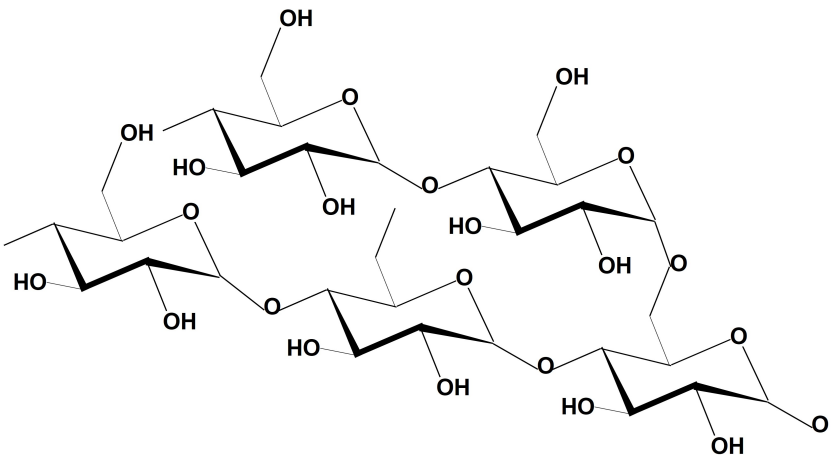

(b) Amylopectin.

Figure 1: Structures of amylose and amylopectin. Adapted from BeMiller & Whistler (2009: 151).

Starch can be obtained from many sources such as grains, seeds, tubers, and legumes. The amount of amylopectin and amylose differs substantially between sources, with starches containing almost no amylose, called waxy starches, to high amylose starches (BeMiller, 2019:

169). Amylopectin chains are considerably larger than amylose chains due to its branching, with a molar mass (MM) of 50–500 Mg/mol (BeMiller & Whistler, 2009: 152). In comparison, amylose has a MM of 0.136–3.5 Mg/mol (Sjöö & Nilsson, 2018: 5) and a DP of up to 600 glucose units (BeMiller & Whistler, 2009: 152). Amylopectin is shorter, with the longest chains being only 60 glucose units on average (BeMiller & Whistler, 2009: 152).

Amylopectin forms a double-helix structure that creates the crystalline part of the starch (BeMiller, 2019: 167). The degree of crystallinity for starches had been shown to range from 27 % for maize to 35 % for tapioca (Singh *et al.* 2007). The crystallinity was shown to decrease if the starch is mechanically refined, with a mere 45 s of refinement (≈6 W·h) halving maize's crystallinity (Dome *et al.* 2020).

There are 3 types of starch crystals, A, B and C. A is common in cereals, B in high amylose maize and potatoes, and C in legumes and certain tubers such as sweet potato and yams (Hizukuri, Kaneko & Takeda, 1983; Cai *et al.* 2014; Guo *et al.* 2020). A-type starch is a tightly packed coordination of double helices. B is very similar in structure but one of the helices is replaced by a column of water (BeMiller, 2019: 167-168). C is a combination of the 2 (Guo *et al.* 2020). There are V-type crystals that are formed by amylose post-gelatinisation (Janssen & Moscicki, 2010: 79). After gelatinisation/plasticisation, the starch is completely amorphous. The amylose recrystallises rapidly upon cooling. The reformed crystals are deemed V_h, V_e, and E_h. The E_h crystals are not stable and will eventually revert to V_h. The subscript h stands for hydrated and a means anhydrous (Janssen & Moscicki, 2010: 79). It was shown there is a correlation between the length of amylopectin chains and the starch crystal type, with long chains being type A, short ones type B, and intermediate chains type C (Hizukuri *et al.* 1983). The amount of amylose also correlated, with low amylose starches being type A, high amylose type B, and intermediate levels type C (Cheetham & Tao, 1998).

Starch polymer chains agglomerate into semi-crystalline granules (Ebnesajjad, 2013: 130). These are held together by hydrogen bonds. If one can disrupt these bonds, one can produce thermoplastic starch (TPS) (Baillie, 2004: 133). TPS is a biodegradable plastic that has been, and still is, extensively studied, as shown in Figure 2. To disrupt the hydrogen bonds one requires a plasticiser, as well as applied thermal and/or shear stress (Ebnesajjad, 2013: 133). How plasticisers work is explained by 3 theories. The lubrication theory postulates that plasticisers act as lubricants, allowing polymer chains to glide more easily past each other. The gel theory explains that polymer chains are loosely connected and that plasticisers can disturb these bonds and thus increase the motion of polymer chains. The free volume theory states that the plasticiser increases the free volume, which is the volume available to molecular motion, which explains the lowering in glass transition temperature (T_g) with increasing plasticiser content (Daniels, 2009).

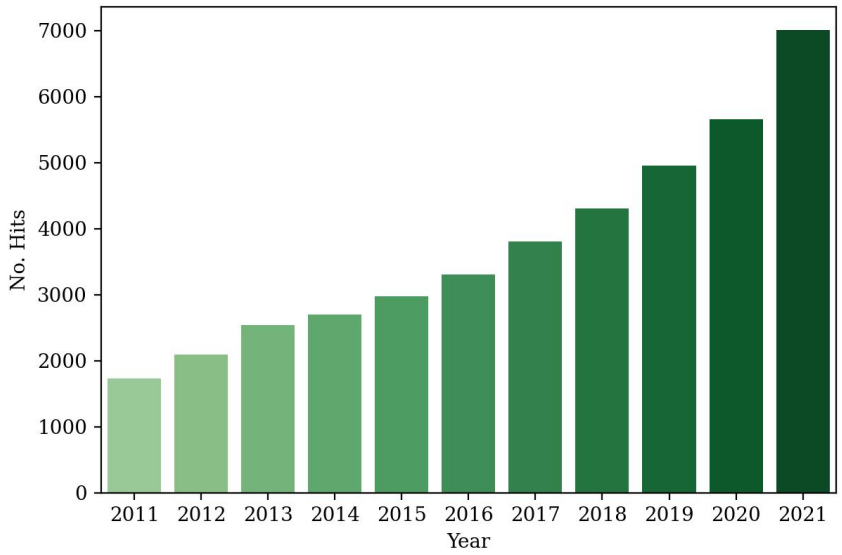

Figure 2: Hits in each year for the search term "thermoplastic starch" on Google Scholar.

A good plasticiser must be compatible with the polymer, have a lower T_g, and shouldn't leach out of the polymer. This last point makes water an unsuitable plasticiser for starch on its own, as it easily evaporates or absorbs based on the relative humidity (RH) of the air (Leroy *et al.* 2022). This causes the mechanical properties to pendulum between brittle and elastic, all depending on the RH (Chocyk *et al.* 2015; Leroy *et al.* 2022). It is for that reason that less volatile plasticisers are added to thermoplastic starch. The T_g is the temperature at which a polymer goes from being rubbery and elastic to glassy and stiff (Young & Lovell, 2011: 385). The T_g tends to decrease linearly with the addition of plasticisers such as water and glycerol (de Graaf, Karman & Janssen, 2003; Van Soest & Vliegenthart, 1997).

In order to effectively plasticise starch, one needs to take the starch above its gelatinisation temperature (Ebnesajjad, 2013: 133). There is an onset temperature, T_o, a peak temperature, T_p, and a closing temperature, T_c. The values had been reported to range between 53 °C–74 °C and 63 °C–86 °C for T_o and T_p respectively (Ubwa *et al.* 2012). The amount of amylose was shown to have an impact on the T_o and T_p, although there is some confusion. Varavinit *et al.* (2003) studied rice starch and found that the gelatinisation temperatures increased with higher amylose content. Sasaki, Yasui & Matsuki (2000) on the other hand studied wheat starch and found that higher amylose starches had lower gelatinisation temperatures. Regarding the impact of plasticisers, water decreased the T_o, but glycerol had been found to increase the T_o.

There had been a lot of debate about why glycerol increased the T_o. One theory was that glycerol competed for water and, being more hygroscopic than starch, withheld water from plasticising the starch (Nashed, Rutgers & Sopade, 2003). Tan *et al.* (2004) showed that the T_o had a large dependency on the concentration of glycerol relative to total plasticiser, rather than the amount of glycerol itself and that higher concentrations of glycerol lead to a higher

T_o. The theory is that glycerol, being a more viscous and larger molecule than water, requires more thermal energy to diffuse into the starch granule. Van Soest *et al.* (1996a) showed at low water concentrations glycerol lowered the T_p, with T_o remaining somewhat constant, but at high water concentrations both T_o and T_p will increase due to the addition of glycerol.

The influence of glycerol is somewhat complex. At low concentrations of water and glycerol, glycerol can have an anti-plasticising effect, where the stiffness of the TPS increases with increasing glycerol content. This reaches a maximum where the stiffness once more decreases, and glycerol acts as a plasticiser (Chang, Abd Karim & Seow, 2006; Zhang & Han, 2010; Mikus *et al.* 2014). For glycerol, this maximum occurs at a concentration in the range of 10 %wt–15 %wt (Chang *et al.* 2006; Zhang & Han, 2010; Mikus *et al.* 2014). Other plasticisers show the same effect. Sorbitol shows anti-plasticisation from 21–27 %wt, much higher than glycerol's (Mikus *et al.* 2014; Gaudin *et al.* 1999; Gaudin *et al.* 2000). A theory for why this may be is that sorbitol can make more hydrogen bonds with starch, which can possibly cross-link the starch, making sorbitol not act as a plasticiser (Özeren *et al.* 2020).

A good plasticiser should not form a lot of hydrogen bonds with the starch, otherwise, physical cross-linking will occur. This is why Özeren *et al.* (2020) found glycerol to be the best plasticiser out of the ones tested, with sorbitol and glucose being the worst. The number of plasticisers tested was only six and this is not a complete overview of all plasticisers for starch. Glycerol had been shown to phase separate at high concentrations, causing the mechanical properties of the TPS to be jeopardised (Mikus *et al.* 2014). The amount at which this occurred was at a 70:30 ratio of starch:glycerol. Some tested plasticisers are shown in Table 1.

Choline chloride is an example of a deep eutectic solvent (DES) and imidazolium chloride is an ionic liquid, both of which showed better performance as plasticiser compared to glycerol (Zdanowicz & Spychaj, 2011). Monosaccharides had been analysed for use as plasticisers, where fructose proved to impart a higher tensile strength, higher elongation at break, and lower water vapour permeability (WVP) than glycerol (Zhang & Han, 2006). It was reported that amides are stronger plasticisers than polyols. It was also discovered that the higher the molar mass of the plasticiser the weaker its plasticisation effect (Zuo *et al.* 2015). Isosorbide was shown to be an interesting plasticiser. It is a crystalline powder, whereas glycerol is a liquid. TPS containing isosorbide showed no retrogradation over a 9 month period. Isosorbide plasticised starch also showed better mechanical properties and lower permeability than glycerol plasticised starch (Battegazzore *et al.* 2015).

Retrogradation is the process of recrystallisation of TPS. Post plasticisation, the amylose within starch quickly recrystallises to V_h, V_a, and E_h crystals, depending on the conditions (Van Soest & Knooren, 1997; Van Soest *et al.* 1996d). It was shown that under high water content, no V_h and E_h will form (Van Soest & Knooren, 1997). V_a only forms at very low moisture levels

Table 1: Various plasticisers used for starch.

Group	Plasticiser	Reference
Polyols	Glycerol	Van Der Burgt, Van Der Woude & Janssen (1996)
	Ethylene glycol	Da Róz *et al.* (2006)
	Sorbitol	Esmaeili, Pircheraghi & Bagheri (2017)
	Isosorbide	Battegazzore *et al.* (2015)
Amides	Formamide	Zuo *et al.* (2015)
	Acetamide	Ma & Yu (2004)
	Ethylenebisformamide	Yang, Yu & Ma (2006)
	Urea	Ma & Yu (2004)
Saccharides	Fructose Mannose Glucose	Zhang & Han (2006)
Other	Water	Ebnesajjad (2013: 133)
	Ethanolamine	Huang, Yu & Ma (2005)
	Choline chloride	Zdanowicz & Spychaj (2011)
	Imidazolium chloride	Zdanowicz & Spychaj (2011)

(Van Soest & Vliegenthart, 1997). Some of the amylose might even form double helices to form B-type crystals (Van Soest & Essers, 1997). Amylose recrystallises rapidly due to its high mobility and length (Van Soest & Essers, 1997).

Amylopectin on the other hand is large and bulky, with the chains having very little mobility (Yu & Christie, 2005). The amylopectin takes a longer time to recrystallise into B-type crystals (Yu & Christie, 2005; Van Soest, de Wit & Vliegenthart, 1996b; Van Soest & Knooren, 1997; Van Soest *et al.* 1996c). Due to the large size of amylopectin, it does not retrograde if it is below its T_g, as the molecular motion is hindered, preventing the chains from coiling (Van Soest *et al.* 1996b). It has been shown that recrystallisation is favourable for mechanical properties up to a point (Van Soest *et al.* 1996c; Van Soest *et al.* 1996b). Amylopectin recrystallises both intermolecularly and intramolecularly, with intermolecular recrystallisation strengthening the matrix. Intramolecular recrystallisation on the other hand causes shrinkage and internal stress that eventually causes cracks on the polymer surface (Van Soest *et al.* 1996c; Van Soest *et al.* 1996b). Due to amylopectin recrystallising only above its T_g, one can create completely amorphous TPS by plasticising waxy starch and cooling it to below the T_g. The T_g is dependent on the plasticiser and RH. One can also make highly amorphous TPS by adding high amounts of water to the TPS pre-extrusion, as that will cause no V_h or E_h crystals to form from amylose (Van Soest & Knooren, 1997).

Humidity and plasticiser play a critical role in the T_g and the recrystallisation behaviour of the starch (Van Soest & Knooren, 1997). Some plasticisers can deter retrogradation. Ma &

Yu (2004) showed that the use of amides lessens retrogradation in comparison to polyols. Ethanolamine, isosorbide and fructose all showed similar improvements (Huang, Yu & Ma, 2005; Battegazzore *et al.* 2015; Zhang & Han, 2006). It had been found that at low RH, meaning 50 %, amylopectin will not recrystallise, which is thought to be due to the increase in T_g (Van Soest *et al.* 1996b). At very high RH, such as 90 %, one gets rapid recrystallisation (Van Soest *et al.* 1996b). Glycerol, if the water content is kept constant, will actually lower crystallinity, but due to its hygroscopic behaviour, it will invariably increase the moisture content and so increase the crystallinity (Van Soest & Knooren, 1997). The higher the moisture content of the TPS the more it recrystallises. Higher moisture content is caused by higher RH and higher plasticiser content (Da Róz *et al.* 2006). It should well be noted that plasticisers that are worse plasticisers than glycerol absorb less moisture (Da Róz *et al.* 2006).

It had also been shown that amylopectin and amylose can co-crystallise (Rindlav-Westling, Stading & Gatenholm, 2002; Lian *et al.* 2018). A critical concentration of amylose, $\approx$ 25%, was shown to be the point where the crystallinity of the amylopectin will increase (Rindlav-Westling *et al.* 2002). A theory of why this was observed is that the amylose and amylopectin form co-crystals, which then act as a nucleation agent for amylopectin to crystallise further (Rindlav-Westling *et al.* 2002). It was also shown that below this critical amylose content phase separation occurred between the 2 starches (Rindlav-Westling *et al.* 2002; Leloup, Colonna & Buleon, 1991). This was especially prevalent with native starch as it was very difficult to homogenise the amylose and amylopectin (Rindlav-Westling *et al.* 2002). It was postulated that if the amylose content is high enough, a continuous network of amylose forms throughout the matrix, allowing higher crystallinity and better mechanical properties (Rindlav-Westling *et al.* 2002).

The structural differences between amylopectin and amylose play a large part in the mechanical properties of TPS. It is hypothesised that the main reason glycerol requires more energy to plasticise starch than water is due to the enthalpy of unwinding the amylopectin coils. This is due to the glycerol being larger and heavier; thus more energy is required to move them with the amylopectin chains (Tan *et al.* 2004). This unwinding is shown in Figure 3. It was found that amylose allows for stronger and stiffer films (Yu & Christie, 2005; Van Soest & Vliegenthart, 1997; Van Soest & Essers, 1997; Myllärinen *et al.* 2002). This is due to the long chains of amylose entangling more easily (Yu & Christie, 2005). Amylopectin makes very ductile films due to the fact that amylose can not make a lot of hydrogen bonds, allowing for easy slippage between the molecules (Yu & Christie, 2005; Van Soest & Vliegenthart, 1997). This was seen with amylopectin having a lower viscosity (Yu & Christie, 2005). One study claimed that amylopectin makes stronger films (Altayan, Darouich & Karabet, 2021), but most papers suggest amylose is the best for tensile strength.

There are various ways of producing TPS. An easy way to do it is to use film casting, where

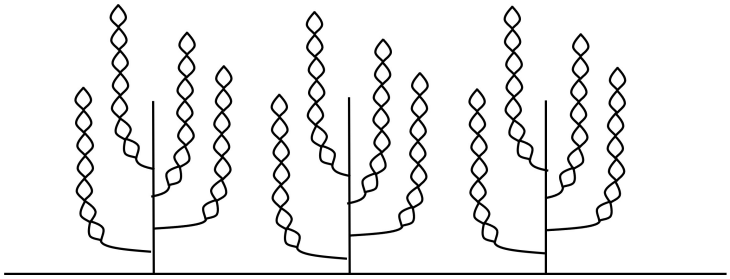

(a) Twisted form of amylopectin.

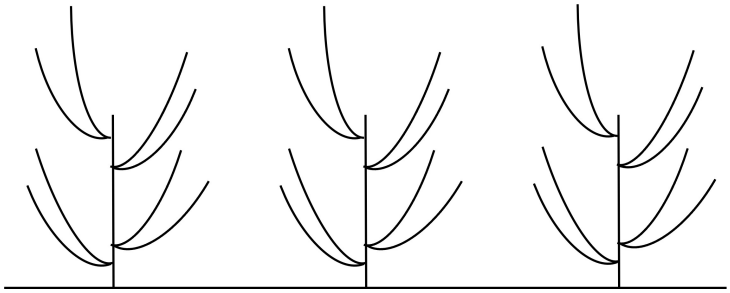

(b) Unfurled form of amylopectin.

Figure 3: Effect of plasticisation on amylopectin. Based on Bertoft (2013), Yu & Christie (2005), and BeMiller (2019: 166).

starch is heated with excess water and another plasticiser to above its T_p. The solution is then cast in a holder, such as a petri dish, where it is then left to dry, either via air or oven (Leloup *et al.* 1991; Zhang & Han, 2006). This method is time-consuming and, if one decides to use an oven, requires a lot of energy to evaporate all the water. Therefore more mechanical methods, such as melt blending and extrusion compounding, are much more economical. It had also been found that extrusion compounding creates co-continuous networks between amylose and amylopectin, which was not observed with film casting (Van Soest & Essers, 1997; Leloup *et al.* 1991).

The major advantage TPS has over other polymers is that it is completely biodegradable and comes from a highly renewable resource (Dogossy & Czigany, 2011; Nevoralová *et al.* 2019). Despite the pros, it has many drawbacks. It does not have appreciable stiffness or tensile strength (de Graaf *et al.* 2003; Mali *et al.* 2006). Literature values for the tensile strength and modulus of TPS made from various starches and with various glycerol contents, in parts per hundred starch (phs), are shown in Table 2. High-density polyethylene, for reference, has a modulus of 0.5 GPa – 1.1 GPa. TPS could weaken and crack with time due to retrogradation (de Graaf *et al.* 2003). It is highly permeable to water and oxygen (Mali *et al.* 2006; Arvanitoyannis & Biliaderis, 1999). Higher RH was shown to negatively influence the mechanical properties (Van Soest *et al.* 1996c).

TPS has been shown to absorb considerable amounts of water from the environment as it ages if the RH is high (Huang *et al.* 2005; Schmitt *et al.* 2015). To combat this, many researchers have tried methods such as modifying the starch, adding fillers, or cross-linking, in an attempt

Table 2: Tensile properties, σ and E, of TPS made from various starches with different glycerol levels and storage humidities.

Starch type	RH (%)	Glycerol (phs)	σ (MPa)	E (MPa)	Reference
Rice	62	33.3	2.1	–	Laohakunjit & Noomhorm (2004)
		42.8	1.8	–	
		53.9	1.0	–	
Corn	75	42.8	6	270	Esmaeili, Pircheraghi & Bagheri (2017)
		56.2	1.5	20	
Pea	50	40	5.8	97.5	Zhang & Han (2006)
		60	5.8	82.6	
		80	2.2	22.8	
		100	1.4	7.8	
Potato	54	25.0	25.5	890	Talja *et al.* (2007)
		42.8	9.0	350	
		66.7	2.5	40	
Wheat	NA	17.6	42	–	de Graaf, Karman & Janssen (2003)
		25.0	27	–	
		33.3	8	–	

to improve upon the physical characteristics. Some of the methods are shown in Table 3.

Table 3: Various methods of improving thermoplastic starch.

Modification	Influence	Reference
	Surface modification	
Acetylation	Used acetic anhydride. Very effective at hydrophobising starch foams and decreasing water adsorption. Produced stronger starch films.	(Felipe Bergel *et al.* 2018; Nevoralová *et al.* 2019)
Esterification	Done with maleic anhydride or propionic acid. Effective at decreasing the water adsorption, but not as effective as acetylation. Also produces much weaker TPS.	(Felipe Bergel *et al.* 2018; Nevoralová *et al.* 2019)
Carbamation	Various isocyanates, such as phenyl isocyanate, was shown to be effective at decreasing the polarity of the TPS surface and thus making it more hydrophobic.	(Carvalho, Curvelo & Gandini, 2005)

Modification	Influence	Reference
Silylation	Was done with 3-chloropropyl trimethoxysilane and methyltrimethoxysilane. Foams made containing this starch were considerably more hydrophobic.	(Felipe Bergel *et al.* 2020)
Hydroxy propylation + Oxidation	Was shown to allow film blowing of TPS, whereas native TPS was insufficient.	(Thunwall *et al.* 2008)
	Crosslinking	
Citric acid	Could reduce retrogradation. Lowered viscosity and weakened tensile properties. Also lowered water absorption. Citrate ions from choline citrate could improve the tensile properties.	(Jiugao *et al.* 2005; Zdanowicz, Jędrzejewski & Pilawka, 2019)
Malic acid	Was able to reduce retrogradation. Made very ductile samples	(Niazi, Zijlstra & Broekhuis, 2015)
Boric acid	Crosslinked via UV irradiation. Considerable improvement in tensile strength. Did increase the moisture uptake. Showed reduction in retrogradation.	(Khan *et al.* 2019)
	Reinforcement	
Nanoclays	Mostly montmorillonite composites. Showed to improve both WVP and tensile strength.	(Müller, Laurindo & Yamashita, 2012; Zhang *et al.* 2013)
Metal oxides	Example is zinc oxide. Improved mechanical properties, decreased WVP, and was able to absorb UV rays.	(Ma *et al.* 2009)
Cellulose	Both raw fibre and nanofibres had been studied. Both show increases in tensile strength, stiffness, and WVP. Decreases transmittance of films.	(Savadekar & Mhaske, 2012; Karimi *et al.* 2014; Wang *et al.* 2017; Babaee *et al.* 2015)
Chitosan	Increased mechanical properties and decreased WVP. Also delayed the mould onset.	(Balla *et al.* 2021)

2.2 Amura

Amura (*Tacca involucrata*) is a tuber crop native to Nigeria (Zaku *et al.* 2009). It is part of the family *Dioscoracea*, with the yam being the most well-known member (The Editors

of Encyclopaedia, 2008). It is estimated that, in Nigeria alone, 20 Mt of *Tacca* tubers are estimated to grow annually and go virtually unused (Omojola, 2013). It is a low protein, low lipid starch (Zaku *et al.* 2009). These can be favourable attributes, as it has been shown that the addition of lipids and protein negatively impacts TPS (Diyana *et al.* 2021; Corradini *et al.* 2007).

There were two types of amura starch found, yellow starch and white starch. White had a bit larger granule with a larger size distribution. Yellow showed A-type starch crystals, whereas white showed C-type starch crystals. Gelatinisation for yellow amura had an onset at 74.1 °C and a peak at 76.2 °C, whereas white amura had onset and peak gelatinisation temperatures of 77.3 °C and 80.1 °C respectively (Nwokocha, Senan & Williams, 2011). The amylose content was reported to be 28.07 ± 0.04 % (Zaku *et al.* 2009). It was reported that white amura is had a C-type crystal structure, and yellow amura had an A-type crystal structure.

Amura starch was found to have a high bulk density, 0.81 ± 0.03 g/cm^3, which was higher than what was found for other starches such as maize (Zaku *et al.* 2009). Amura needs prior preparations to make it edible as it contains toxins. It is therefore not commonly consumed and regarded as a famine food (Janick & Freedman, 2022).

A close relative of amura is *Tacca leontopetaloides*, commonly known as Polynesian arrowroot. There are studies where *Tacca leontopetaloides* was used for making biopolymers. Amin *et al.* (2017) showed how glycerol concentrations impacted the tensile strength and water adsorption of the *Tacca* films. It was found that lower glycerol levels lead to lower water content and higher tensile strength. Makhtar *et al.* (2013) and Makhtar *et al.* (2014) made polymer composites using *T. leontopetaloides*.

The amylose content of amura is near the suspected minimum critical point for achieving a continuous amylose matrix. The low lipid and protein content is favourable as well. It occurs naturally in Nigeria; thus, starch production can support a developing economy. The fact that it is not often eaten means it won't detract from the food supply if used for TPS production. All these points support the idea that amura is a worthwhile starch to investigate.

2.3 Nanocellulose

Cellulose consists of (1→4)-linked β-D-glucopyronosal units (BeMiller, 2019: 224). The only difference between cellulose and starch is that cellulose has β–linkages, meaning the glycosidic bond is above the ring, and starch has α–linkages. It is the most abundant natural polymer in the world (Huang *et al.* 2019: 1). Cellulose is found in the cell membranes of plants (BeMiller, 2019: 224). It is due to the abundance of cellulose that research efforts into nanocellulose (NC)

have grown exponentially, as shown in Figure 4. There are five types of nanocellulose: cellulose nanocrystals (CNC), cellulose nanofibrils (CNF), bacterial nanocellulose (BNC), algal nanocellulose, and tunicate nanocellulose (Foster *et al.* 2018). Tunicates are, as of writing, the sole source of animal-derived nanocellulose (Seddiqi *et al.* 2021; Trache *et al.* 2017). BNC is a unique version of cellulose since it has no impurities, unlike plant-based cellulose that contains some residual lignin and hemicellulose (Huang *et al.* 2019: 95). Most nanocellulose is produced from plant-based stock. Sources range from hardwood and softwood pulp (Fall, Burman & Wågberg, 2014), pineapple leaves (Mahardika *et al.* 2018), cassava (Teixeira *et al.* 2009), and sugar beet (Hietala, Sain & Oksman, 2017).

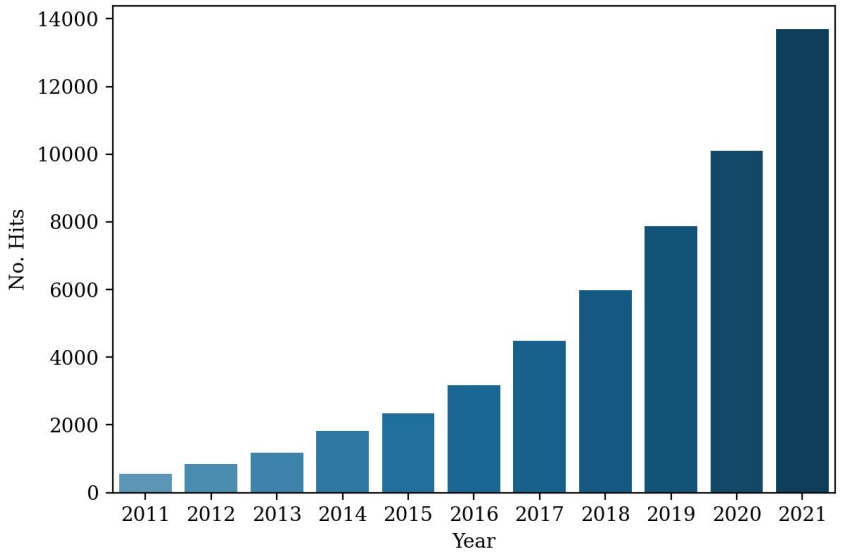

Figure 4: Hits in each year for the search term "nanocellulose" on Google Scholar from 2011–2021.

The difference between CNCs and CNFs is size and geometry. CNC typically has a length <300 nm and a diameter <70 nm (Huang *et al.* 2019; Nechyporchuk, Belgacem & Bras, 2016: 33-35). CNFs have a diameter ranging from 5 nm–50 nm, depending on whether the fibres are bundled or not, and the length reaches a few μm's (Huang *et al.* 2019; Nechyporchuk *et al.* 2016: 78). CNFs have a much higher aspect ratio than CNCs, which is due to the much larger ratio between length and diameter. This is favourable when it comes to polymer reinforcement, as the interfacial area between the NC and the polymer matrix is higher (Xu *et al.* 2013; Kamboj *et al.* 2022).

NC is produced either via chemical and/or mechanical methods. CNCs are usually made via acid hydrolysis with H_2SO_4 or HCl (Trache *et al.* 2017). Organic acids, such as citric acid, had also been used with success (Zhou *et al.* 2019). The acid hydrolysis attacks the amorphous region of the cellulose. The crystals, being more resilient, remain after the hydrolysis (Huang *et al.* 2019: 21). CNFs are usually made via mechanical methods such as high shear blenders, homogenisation, and ultrasonication (Uetani & Yano, 2011; Pääkkö *et al.* 2007; Mahardika *et al.* 2018). The addition of chemical pretreatment can greatly reduce the energy required

to produce CNFs. Pretreatments include oxidation, enzymatic hydrolysis, and alkaline/acid hydrolysis (Michelin *et al.* 2020; Malucelli *et al.* 2019; Soares Faria *et al.* 2020). For further information on the production of NC, please refer to the excellent reviews of Trache *et al.* (2017), Khalil *et al.* (2014), and Nechyporchuk *et al.* (2016). A breakdown of the CNF production process is shown in Figure 5.

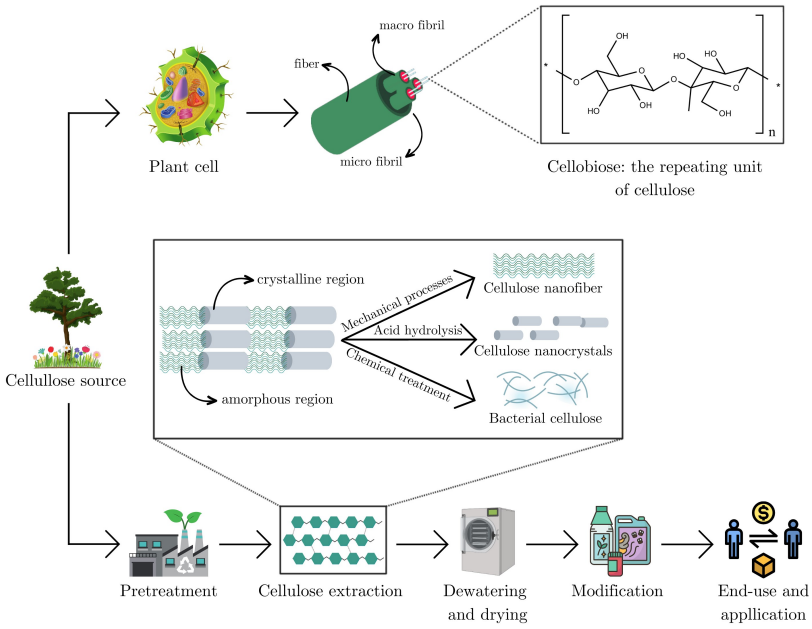

Figure 5: Production of CNF from raw material to consumer product. Used with permission from Niemand (2023).

Nanocellulose has numerous incredible physical properties and with applications in a variety of fields. It has three main physical properties that make it of high value: high strength and stiffness, a reactive surface area, and it is renewable as well as biodegradable. The mechanical properties vary based on measurement technique and source. Information on the modulus of nanocellulose is shown in Table 4. The table shows that the modulus is influenced by source, measuring method, and size. As one can see with the flax fibres, smaller diameter fibres had a higher modulus (Lamy & Baley, 2000). The aspect ratio, the ratio between surface area and volume, increases for a cylinder when the diameter decreases. This means that there is more interfacial area between the fibre and the polymer, allowing for greater interaction.

Information on the tensile strength of CNFs, as of writing, is scarce. There is information on the tensile strength of CNC. The theoretical maximum of a cellulose crystal is reported as 7.5 GPa–7.7 GPa (Mark, 1967). Saito *et al.* (2012) used a model that relied on the length and width of a fibril. They estimated the tensile strength of tunicate and wood-based CNFs that were TEMPO-oxidized. Tunicate CNF had a tensile range of 1.5 GPa–6.4 GPa, depending on the method used for determining both the mean and the width. Wood-based CNF had a

Table 4: Modulus and tensile strength of NC from various sources and measurement methods.

Type	Modulus (GPa)	Method	Source	Reference
CNF (TEMPO)[1]	145.2	AFM	Tunicate	(Iwamoto *et al.* 2009)
CNF (acid)[2]	150.4	AFM	Tunicate	
BNC	78	AFM	Bacteria	(Guhados, Wan & Hutter, 2005)
BNC	79–88	Raman	Bacteria	(Tanpichai *et al.* 2012)
CNF	29–36	Raman	Wood	
Fibre (34.5 μm)	39.03	-	Flax	(Lamy & Baley, 2000)
Fibre (6.8 μm)	78.68	-	Flax	
Long Fibre CNF	23.9	-	-	(Kafy *et al.* 2017)
Glass fibre	76–81	-	-	(Wypych, 2021: 299)
Aramid fibre	20–21	-	-	(Wypych, 2021: 279)

[1] TEMPO = (2,2,6,6-tetramethylpiperidinyl-1-oxyl) oxidation
[2] acid = acid hydrolysis

tensile range of 0.8 GPa–3.5 GPa. The tunicate CNFs were a little bit wider and much longer than the wood-based CNFs. Long fibres spun from NC were found to have a tensile strength of 383.3 MPa (Kafy *et al.* 2017). Glass fibres have a tensile strength of 3.1 GPa–3.8 GPa (Wypych, 2021: 299). Aramid fibres' tensile strength ranges from 2.5 GPa–3.2 GPa. As one can see, CNFs are competitive with the most common commercial fibres.

The glucose monomer of nanocellulose has three hydroxyl groups that are available for reaction. These hydroxyl groups are located on C6, C3 and C2. The reactivity order is C6>C3>C2 (Huang *et al.* 2019: 7). This allows for surface modification of the cellulose (Huang *et al.* 2019: 4). Various modifications impart different properties to CNFs and CNCs. Some of the most common modifications are shown in Figure 6. The reactions are explained in Table 5. The main use of surface modification is to improve the compatibility of NC with non-polar polymers. NC is hydrophilic; thus it aggregates very easily in hydrophobic polymers due to phase incompatibility.

There are more surface modifications, such as the grafting of polymers onto the cellulose backbone, ring-opening polymerisation, and living radical polymerisation (Huang *et al.* 2019: 126-136). For a more in-depth discussion on surface modification, there are great reviews done by Rol *et al.* (2019) and Ghasemlou *et al.* (2021).

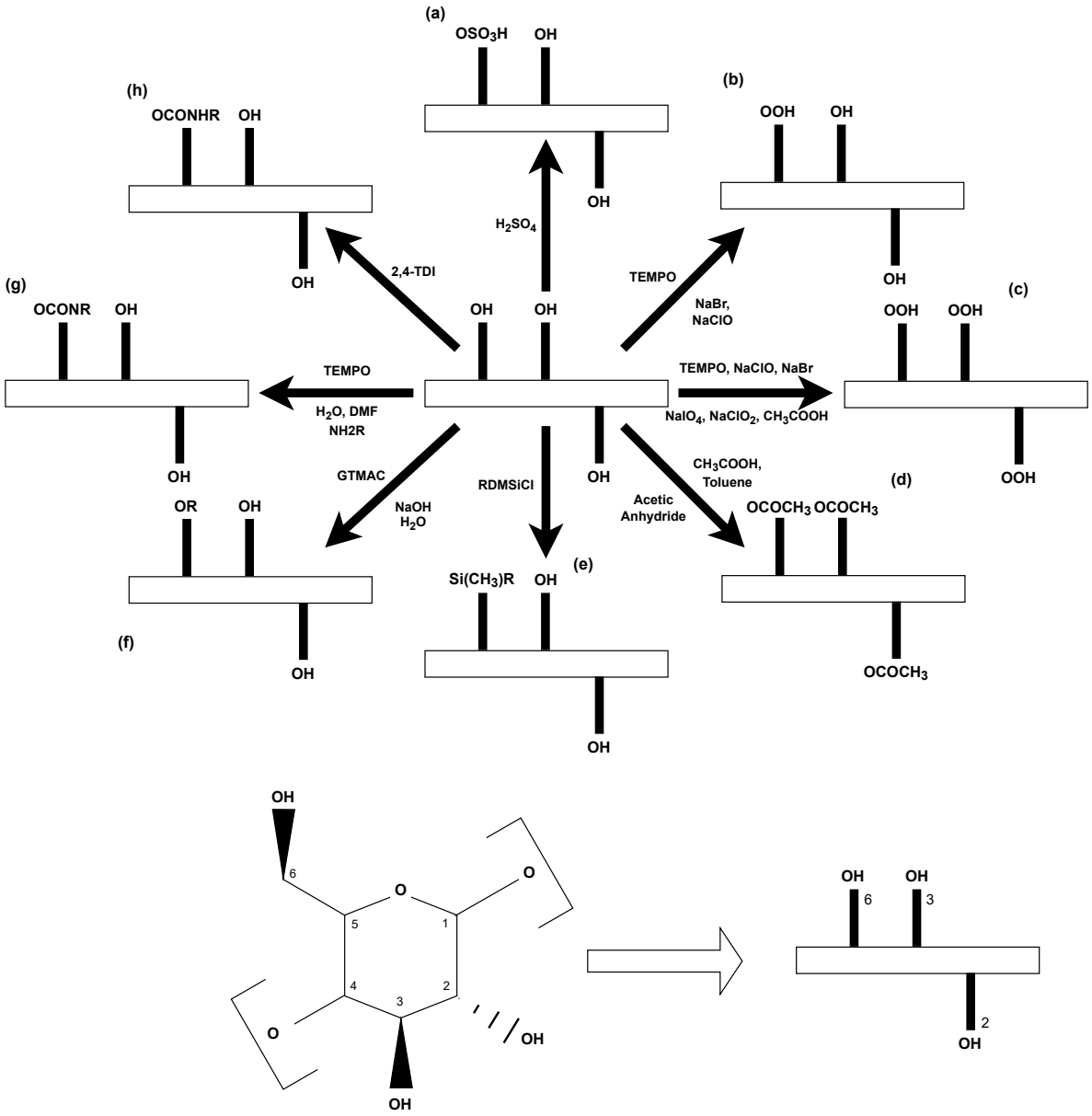

TEMPO = 2,2,6,6-Tetramethylpiperidinyloxy, DMF = Dimethyl formamide, GTMAC = Glycidyltrimethylammonium chloride, DMSiCl = Dimethylsilyl chloride, TDI = Toluene diisocyanate, R = Carbon chain

Figure 6: Various methods of surface functionalisation of nanocellulose, inspired by (Huang, Dufresne & Lin, 2019: 6).

Table 5: Reactions shown in Figure 6.

No.	Reaction	Description	Reference
a	Sulfonation	Happens to CNC's produced via H_2SO_4 hydrolysis. Degree of substitution is dependent on concentration and temperature of hydrolysis.	(Peng *et al.* 2019)
b	Oxidation	TEMPO oxidation only affects C6. Easy way of creating a carboxyl group, which tends to be easier to react with.	(Abou-Zeid *et al.* 2018)
c	Oxidation	Periodate oxidation attacks the C2 and C3 carbons, and cleaves their bonds, breaking the glucose ring. Allows for maximum degree of substitution.	(Abou-Zeid *et al.* 2018)
d	Acetylation	Acetyl group being bounded to the chain. Method is also applicable to other esterification reactions.	(Kim, Nishiyama & Kuga, 2002)
e	Silynation	Makes the cellulose more hydrophobic. The R refers to any length of carbon side chain. Dimethylsilyl chloride compounds are commonly used.	(Goussé *et al.* 2002)
f	Etherification	Done by opening an epoxy functional group and binding the open carbon to the OH of the glucose monomer. Many types of epoxies can be reacted this way.	(Zaman *et al.* 2012)
g	Amidation	Attachment of an amide group. Is applicable to many amides.	(Johnson, Zink-Sharp & Glasser, 2011)
h	Carbamation	Also known as urethanisation; attachment of a carbamide/urethane group on the main chain. Commonly done with isocyanates. Very similar to the amidation reaction.	(Abushammala, 2019)

There is a wide array of potential applications for nanocellulose due to its favourable mechanical and chemical properties. The ability of nanocellulose to alter the rheology of mixtures makes it a good food additive for things such as mayonnaise (Heggset *et al.* 2020). It is also

used for food packaging due to the favourable barrier properties, the reinforcement it gives, and the ability to carry anti-microbial additives (Hubbe *et al.* 2017; Saxena *et al.* 2010). The fields in which NC is applicable are shown in Table 6.

Table 6: Fields and uses of NC.

Field	Use	Reference
Food	Due to its ability to modify the rheology of suspensions, NC is used as a stabiliser. It is also added as a non-caloric filler.	(Perumal *et al.* 2022)
Packaging	There is a lot of interest in its use for food packaging. It lowers oxygen permeability while reinforcing the material. With some modifications, it can become a barrier to water and oils.	(Hubbe *et al.* 2017; Ahankari *et al.* 2021)
Paper	Used both for paper reinforcement as well as a coating.	(Li *et al.* 2021)
Oil	Used to modify the rheology and stabilise the oil to prevent phase separation.	(Combariza, Martínez-Ramírez & Blanco-Tirado, 2021)
Construction	Capable of reinforcing cement and improving the internal bonding strength, modulus of rupture, and modulus of elasticity. Also alters the rheology.	(Balea *et al.* 2019)
Electronics	Can be used in conjunction with metal particles and conductive polymers to create conductive inks. Also used with printed electronics.	(Dias *et al.* 2020; Hoeng, Denneulin & Bras, 2016)
Medicine	Used in drug delivery systems thanks to its small size. Its reinforcing abilities, permeability, and hydrophilicity make it ideal for wound dressing. It is also usable in tissue engineering.	(Nicu, Ciolacu & Ciolacu, 2021)
Cosmetics	Used for emulsion stabilisation as well as a carrier for active ingredients. Can replace some microplastics.	(Almeida *et al.* 2021)
Wood adhesive	Reinforces wood panels. Also modifies the rheology of adhesives.	(Vineeth, Gadhave & Gadekar, 2019)

Field	Use	Reference
Water treatment	Can be used as an absorbent of pollutants such as heavy metals, oils and dyes. Membrane filter composites can be made with NC.	(Mautner, 2020; Mahfoudhi & Boufi, 2017)
Polymers	Reinforces polymer matrix, imparting higher stiffness and tensile strength. Also aids in barrier properties. Very useful to strengthen biodegradable polymers such as poly(lactic acid) (PLA). It needs compatibilisation with hydrophobic polymers.	(Kargarzadeh *et al.* 2018; Dufresne, 2017; Dufresne, 2018)

2.4 Nanocellulose for polymer reinforcement

The very high stiffness of CNFs makes it an attractive polymer reinforcer. Together with its low density, renewable source, and biodegradability, nanocellulose is a viable alternative to other polymer fibre additives. It can be applied to rubbers, thermosets, and thermoplastics (Kargarzadeh *et al.* 2018; Dufresne, 2017). Fibres reinforce polymers by taking more of the stress or strain being applied on the matrix. When the stress applied is in the longitudinal direction of the fibres, assuming perfect alignment (anisotropy), there is uniform strain. This is because both the fibres and the matrix elongate equally. When the stress is applied perpendicular to the fibres, there is uniform stress, as the matrix and fibres elongate separately, but under the same load. These are the two extreme scenarios. Equation 1 and 2 show the formulas for tensile modulus under uniform strain and uniform stress, respectively (Young & Lovell, 2011: 604–606). E is the modulus, ϕ, is the volume fraction, and subscript c, m, and f stands for composite, matrix, and filler, respectively. In real life, one would expect the modulus to range between these 2 extremes, assuming no slippage occurs between the fibres and polymer matrix.

$$E_c = \phi_m E_m + \phi_f E_f \tag{1}$$

$$\frac{1}{E_c} = \frac{\phi_m}{E_m} + \frac{\phi_f}{E_f} \tag{2}$$

In the case of a polymer being hydrophobic, surface modification or the use of a surfactant is necessary to ensure proper transfer of mechanical stress. Too much of a polarity difference between the NC and the polymer might have a negative impact on the composite.

Some of the most common thermoplastics in use are hydrophobic. This includes polyolefins such as polyethylene (PE) and polypropylene (PP), as well as biodegradable polymers such as poly(lactic acid) (PLA). To improve dispersion within these polymers, three methods are applied: coupling agents/surfactants, surface functionalisation, and grafting. There are three coupling agents commonly used: maleated PP/PE (Li *et al.* 2014; Suzuki *et al.* 2014; Iwamoto *et al.* 2014), poly(ethylene oxide) (PEO) (Pereda, Kissi & Dufresne, 2014; Zhang *et al.* 2017; Li *et al.* 2014), also known as poly(ethylene glycol) (PEG), and poly(vinyl alcohol) (PVA) (Kiziltas *et al.* 2016; Haque *et al.* 2017). Each of these compatibilisers is amphiphilic and can thus bind to both the CNFs and polymer matrix.

The most common surface functionalisation methods were silanisation (Qian *et al.* 2018), esterification/acetylation (Jonoobi *et al.* 2012), and carbamation (Espino-Pérez *et al.* 2013). Surface functionalisation was used a lot with PLA composites (Dufresne, 2018; Kargarzadeh *et al.* 2018). It is effective because it increases the hydrophobicity of the NC surface. One can graft polymers onto the NC chain to impart the properties of the grafted polymer on the NC. PLA could be grafted onto NC using ring-opening polymerisation, and PEG could be grafted using a carboxylation-amidation reaction (Lizundia *et al.* 2016; Lin & Dufresne, 2013). Both improved the hydrophobic character of the NC.

TPS is hydrophilic, just as NC (Huang *et al.* 2019: 182). Therefore, the interfacial adhesion between the polymer matrix and the fibres tends to be appreciable. There was, however, still be a noticeable degree of agglomeration of the fibres observed (Teixeira *et al.* 2009). Csiszár, Kun & Fekete (2021) showed that the glycerol amount influences the reinforcing abilities of CNCs. If the glycerol content was too high (40%), it disrupted the interaction between the NC and the TPS.

Figure 7 shows various experiments where TPS was reinforced with CNFs with the mechanical properties reported. As one can see, there is considerable variation. All, except two papers, used film casting. Teixeira *et al.* (2009) used melt blending and Hietala, Mathew & Oksman (2013) used extrusion. Savadekar & Mhaske (2012) achieved some spectacular results, reporting a very high tensile strength with very low loadings. The peak loading was also achieved very early. What made this paper unique is the addition of acetic acid with glycerol and the large diameter of the CNFs, which was 424 ± 158 nm. This might explain why the strength of the composite suddenly dropped at 1 % loading.

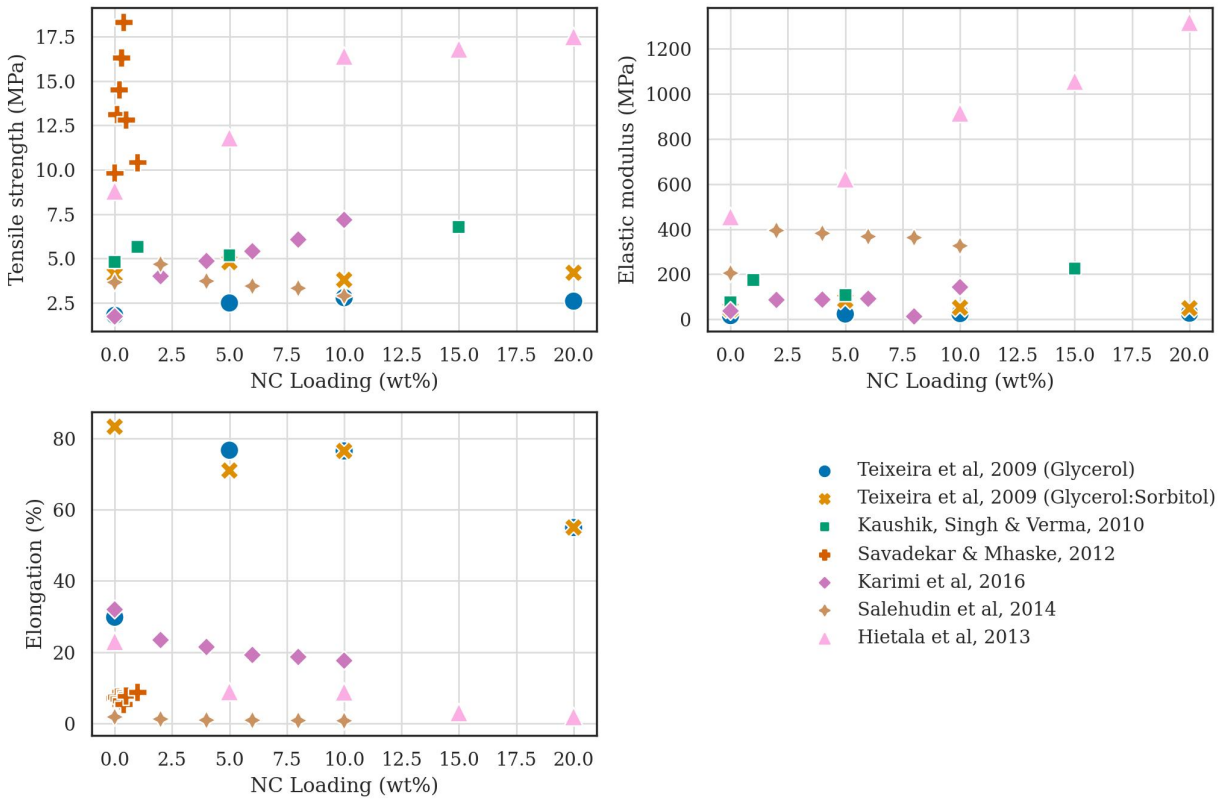

Figure 7: Effect of CNF on the mechanical properties of TPS at various loadings.

It is surprising to see that the extruded sample did extremely well in comparison to the rest. The modulus of the extruded samples is comparable to some commonly used polymers such as LDPE (130 MPa–348 MPa), HDPE (500 MPa–1100 MPa) and polypropylene (1700 MPa) (Wypych, 2016: 172, 194, 532). One could expect the extruder to damage the fibres due to the shear stress applied and elevated temperatures. The temperatures used in extrusion tend to run higher than with film casting (Pushpadass *et al.* 2009; Kaushik, Singh & Verma, 2010). Higher temperatures risk degrading the polymers. The extruder paper is the only paper that showed a continuous increase in tensile strength. This might be due to the extrusion being able to more effectively disperse the fibres. The effect of plasticisers is also visible in Figure 7. The glycerol:sorbitol samples had higher tensile strength than the pure glycerol sample. One can also note that the optimal CNF loading is lower for the glycerol:sorbitol samples than the glycerol sample. One can also see in this paper that the addition of sorbitol had a larger influence on the mechanical properties than adding CNFs (Teixeira *et al.* 2009).

The majority of research papers covering the reinforcement of TPS with CNFs rather use solution casting or melt blending. The high amounts of water in NC are problematic with extrusion,

as the high temperatures used can cause the water to boil (Meng *et al.* 2019). This was observed in preliminary experiments done in our labs. NC is usually supplied in a water-filled form with the NC no higher than 25 wt% (Foster *et al.* 2018). The high amounts of water will lower the initial amylose recrystallisation, which is not favourable, and will limit the shear the extruder can apply, which might lead to lower mixing of the NC. To overcome the boiling problem, Hietala *et al.* (2013) increased the screw speed to 200 rpm. This caused a vacuum that helped in evaporating the water before the polymer went through the die. Despite this, water still remained in the polymer and the polymer had to be dried post-extrusion. The very high screw speed is also undesirable.

When NC is dried, it undergoes a process called hornification. Hornification is the irreversible bonding of cellulose fibres where both hydrogen bonds and lactone bridges form (Fernandes Diniz *et al.* 2004). This causes the loss of the unique properties of NC, as it can not be fully redispersed after drying without considerable effort.

Ultrasonication is a method that allows for near-full redispersion of dried NC. Ultrasonication works by causing cavitation, which is the formation, growth, and implosion of microscopic bubbles within a liquid medium (Nowak, 2010: ix). The energy released by the bubbles imploding is immense, with values as high as 5000 K and 1800 atm reported (Nowak, 2010: 2). These implosions created liquid jet streams that can effectively break agglomerates and redisperse them (Mattox, 2010: 498).

It had been shown that, with enough specific energy (J/g) applied through ultrasonication, one could almost completely redisperse even air-dried NC (Beck, Bouchard & Berry, 2012). The amount needed though was quite immense, totaling 1900 J/g. Ultrasonication is not a solution though. Currently, it has a high energy cost due to low efficiency and loss of energy to heat dissipation (Li *et al.* 2013; Hoo *et al.* 2022). It was also shown to become less energy efficient at larger production scales (Li *et al.* 2017; Hoo *et al.* 2022). It is thus of utmost importance that, whatever drying method is developed, it works via mechanical mixing alone.

2.5 Drying of nanocellulose

A way to get around the water issue is to dry the NC while minimising agglomeration. There are 4 methods assessed in the literature: oven/air drying (OD/AD), spray drying (SD), freeze-drying (FD), and supercritical drying (SCD) (Xu *et al.* 2022). Oven drying and air drying are the most economical ways of drying and most suggested for the characteristics of NC but come with the problem that agglomeration is rampant (Peng, Gardner & Han, 2012a; Žepič *et al.* 2014; Van't Land, 2011: 23). During AD and OD, there are 3 drying stages. During the first stage, free water is dried at a constant rate and shrinkage is observed due to capillary

forces. A decrease in drying rate is then observed and shrinkage is halted. The diffusion of water to the surface is fast enough to keep up with the drying rate. A second decrease in drying rate occurs where the drying rate becomes limited by the diffusion of the bound water (Ben Abdelouahab *et al.* 2021; Peng *et al.* 2012a). It is postulated that the last step is where most of the agglomeration occurs due to the very strong capillary forces and lack of water allowing the CNFs to make contact (Peng *et al.* 2012a). An illustration of how drying leads to hornification is shown in Figure 8

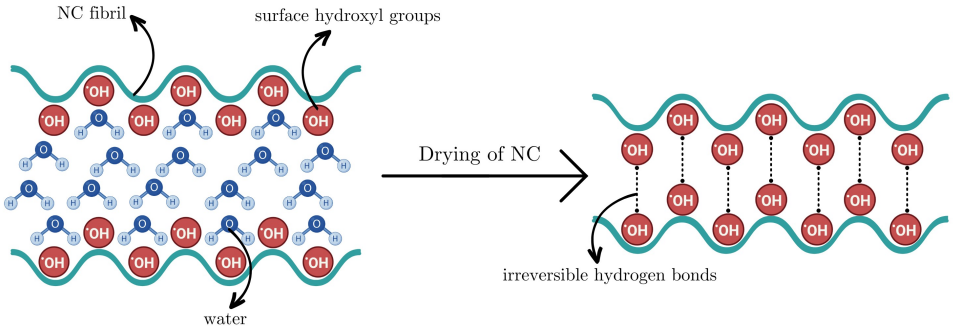

Figure 8: Drying mechanism of CNFs that leads to hornification. Used with permission from Niemand (2023).

Spray drying works by spraying a heated liquid through a nozzle called an atomiser into a stream of hot air. The drying works on a similar principle as oven drying. The only additional steps are the atomisation prior to drying and the air cleaning post-drying (Van't Land, 2011: 133). The droplets are dried at a rapid pace. Spray drying usually requires a large liquid-to-solids ratio, meaning that high amounts of energy are required for vaporisation for every kg product dried. This makes SD less economical than OD (Van't Land, 2011: 133). Nonetheless, it is useful if the end product is better than the OD product, and still allows for high production rates (Van't Land, 2011: 134).

Spray drying has the advantage that it makes a very fine powder, but these powders tend to be spherical agglomerates of NC ranging from 2 µm–7 µm (Peng *et al.* 2012a; Peng, Han & Gardner, 2012b; Khoshkava & Kamal, 2014; Beck *et al.* 2012). The powders tend to have high crystallinity and higher thermal stability, which made it suggested as the best drying method for polymer reinforcement purposes (Peng *et al.* 2013). Spray-dried powders made two types of agglomerates, depending on whether there were CNFs outside of the droplet or not (Peng *et al.* 2012a). Droplets with fibres sticking out did not make spherical agglomerates, but rather ones that look like a bundle of fibres. If all fibres were within the droplet during drying, the agglomerate is very spherical (Peng *et al.* 2012a). SD nanocellulose tended to be irreversibly agglomerated (Beck *et al.* 2012; Meneguin *et al.* 2020; Khoshkava & Kamal, 2014; Žepič *et al.* 2014).

Freeze drying, also known as lyophilisation, is a method that takes water to a temperature

and pressure where it can sublimate instead of boil (Van't Land, 2011: 235). It has a few disadvantages to other drying methods, such as being time-consuming (Van't Land, 2011: 236). It is also considerably more expensive than SD and OD due to the high energy consumption (Hui, 2008: 217). FD produces laterally agglomerated fibres (Peng *et al.* 2012a; Žepič *et al.* 2014). At high concentrations, 0.5%–1.0%, there are lamellar structures that form (Han *et al.* 2013). It is postulated that during the initial freezing phase, the ice crystals push the fibres into close proximity to one another, allowing for agglomeration (Beck *et al.* 2012; Khoshkava & Kamal, 2014; Han *et al.* 2013). At low concentrations, 0.5 %, the FD CNF's are ultrafine fibres. The agglomerates tend to be smaller than those with SD (Peng *et al.* 2012a; Žepič *et al.* 2014). The FD samples still tended to not be well suited for redispersion, though were better than SD (Khoshkava & Kamal, 2014; Beck *et al.* 2012).

SCD replaces the water with liquid CO_2, which is then taken to its supercritical point where liquid and gas become indistinguishable. SCD overall produces the best powders but comes with the highest economical cost (Peng *et al.* 2012a).

A major factor that determines whether CNFs will agglomerate or not is the surface charge of the fibres (Fall *et al.* 2011; Beck *et al.* 2012). If it is high enough, the electrostatic repulsion will repel the fibres from each other, limiting the hornification of the fibres. If the charge is too low, the fibres start to aggregate (Beck *et al.* 2012). The surface charge can be lowered by lowering the pH or adding salts to increase the ionic charge of the liquid (Beck *et al.* 2012). Fall *et al.* (2011) developed a model for CNF aggregation using the DLVO (Derjaguin, Landau, Verwey, and Overbeek) theory.

The theory postulates that the van der Waals forces and electrostatic forces are independent of each other and can be linearly added to determine the total force of 2 particles on each other (Birdie, 2010: 143-145). The attractive forces are larger than the repulsive forces at large distances or small distances. This causes a secondary and a primary minimum. At intermediate distances the repulsion is larger than the attraction, causing an energy maximum. Higher concentrations and larger valencies of salts lower this maximum. Due to thermal energy causing Brownian motion, the particles might overcome this energy maximum and go into the primary minimum. This is aggregation. The higher the maximum the more stable the suspension and the less likely aggregation becomes (Tardos, 2015: 97-99).

Fall *et al.* (2011) showed that fibres with larger surface charges can resist aggregation at a lower pH and higher salt concentrations. A pH below 3 and a sodium concentration larger than 100 mM tends to cause aggregation of the fibres. Hamid *et al.* (2016) reported that a zeta potential, negative or positive, with an absolute value above 30 mV, can resist agglomeration. The acid/protonated form of NC has shown to form agglomerates that can not be dispersed again (Beck *et al.* 2012). When 94 % of the protons on the OH groups were substituted with

Na^+, full redispersion is possible, no matter the drying method, as long as sufficient sonication energy was applied (Beck *et al.* 2012). Based on this DLVO theory, a few methods have been developed to overcome the irreversible aggregation of fibres, with some shown in Figure 9.

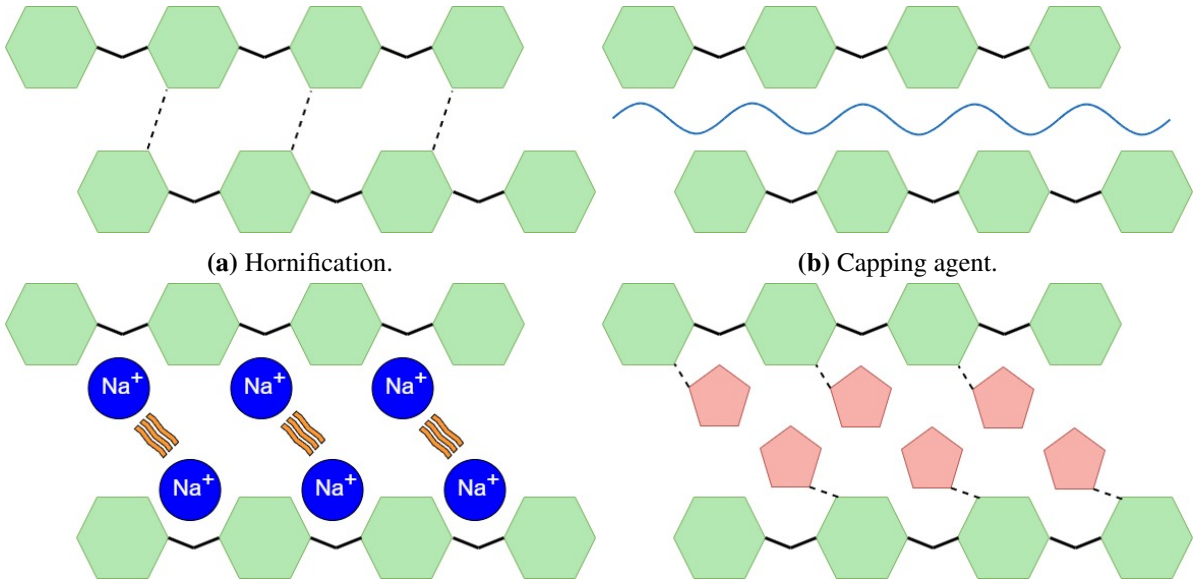

(a) Hornification. **(b)** Capping agent. **(c)** Ions. **(d)** Surfactants.

Figure 9: Three methods of preventing NC agglomeration using additives.

Surface charge modification is thus an obvious method for preventing agglomeration. It works by adding charged functional groups onto the CNF surface. Sulfonation, which occurs during H_2SO_4 hydrolysis, adds sulfate half-ester groups that give zeta-potential values as low as -43.8 mV (Niu *et al.* 2017). H_3PO_4 hydrolysed NC has phosphate groups on them, which also adds surface charge (Kokol *et al.* 2015). Carboxymethylation is another surface modification method to increase surface charge (Eyholzer *et al.* 2010; Beaumont *et al.* 2016).

TEMPO oxidation adds more carboxyl groups, which are easily deprotonated. Most CNFs are in and of themselves not void of carboxyl groups. There tends to be some residual hemicellulose left on the CNF surface, which has carboxyl groups on it (Morán *et al.* 2008; Missoum, Bras & Belgacem, 2012). The pectin within some sources of NC can also be purposefully preserved to ensure there are carboxyl groups present (Hietala *et al.* 2017).

The carboxylate groups allow for easier ion addition, where the carboxylate groups bind to a metal ion, which prevents H-bonds from forming instead (Fukuzumi *et al.* 2014; Missoum *et al.* 2012). It has been shown that larger counter ions are better at preventing aggregation. Potassium was shown to be better at preventing aggregation than sodium (Yang *et al.* 2021). Benítez & Walther (2017) tested 3 ions: Li^+, Na^+, Cs^+, and found that the larger the counter ion, the better the redispersion of the dried NC. This also held up for alkyl ammonium ions, where longer alkyl chains showed better redispersion (Benítez & Walther, 2017). The valency of the ions is also important. Monovalent ions have been shown to cause weak aggregation

that can be separated with mechanical energy, whereas divalent and trivalent ions, such as Fe^{+2}, can increase the degree of aggregation (Zhu *et al.* 2021). Fairman (2014) showed that cetyltrimethylammonium bromide (CTAB), a cationic ion, was effective at limiting, although not completely stopping, fibre aggregation. An interesting result was that air drying was better than drying at 120 °F. The proposed reason for this is that the mobility of the CTAB ions is higher at elevated temperatures, and thus attachment to the CNF was less likely. It was also shown that CTAB is only effective at low concentrations and at high concentrations the CTAB aids aggregation (Shang *et al.* 2019).

Solvent exchange is another viable method for preventing aggregation. This has been done with various alcohols, with *tert*-butanol showing promising results (Hanif *et al.* 2018; Jiang & Hsieh, 2014; Zhou *et al.* 2019). One advantage of *tert*-butanol is that oven drying is much faster, in comparison to water, and thus requires less energy (Hanif *et al.* 2018). In addition to that, the presence of *tert*-butanol on its own prevents agglomeration to a large extent (Hanif *et al.* 2018). It was found that non-polar solvents, such as toluene, are much better at preventing aggregation than polar ones (Araki & Arita, 2017). Zhu *et al.* (2021) tested water, ethanol and *tert*-butanol. They found that alcohols do well in preventing aggregation, with *tert*-butanol doing better than ethanol. They postulated 3 reasons for alcohols being more effective: H-bonding, surface tension, and steric hindrance. Alcohols can make three H-bonds, whereas water can make four. Water's high surface tension means that during drying the fibres will be pulled together more via mechanical forces. It was also shown that the solvents with low polarity produced more redispersible NC.

The last main method is steric hindrance, which works with the addition of large additives, commonly called capping agents. If the fibrils are limited in their motion and proximity to each other, the maximum energy barrier can not be breached easily. Carboxymethyl cellulose (CMC) is commonly added to microcrystalline cellulose (MCC), both of which are common food additives, to prevent aggregation of the MCC (BeMiller, 2019: 228). This has been tested with NC as well, with good success. Polymers added to aid in steric hindrance are called capping agents. Sometimes the addition of smaller molecules, such as glycerol or glucose, can hinder the formation of hydrogen bonds by making hydrogen bonds themselves with the CNFs. These act as surfactants. Many substances have been tested and some are listed in Table 7.

There are a few notable observations from Table 7. Some of the capping agents/surfactants are easily removed, usually just by washing with water. These are lignin, fish gelatin, and maltodextrin (Liu, 2018; Kwak *et al.* 2019; Asquez-Cock *et al.* 2017). This is advantageous if one wants to use pure nanocellulose. There is also considerable variation with certain capping agents and their efficacy, especially CMC. One reason is the method of preparation. The adsorption of CMC and PEG gave the best results out of the papers cited. The adsorption is done by stirring the CNF and CMC/PEG together at elevated temperatures (Butchosa & Zhou, 2014;

Table 7: Summary of capping agents and surfactants for preventing aggregation of CNFs.

Additive	Method	wt%	Efficacy	Reference
Lignin	FD, VD	5–50	+++	(Nordenström *et al.* 2021)
	OD	10–50	++	(Kim *et al.* 2022)
	AD	1.6–25	++	(Liu, 2018)
CMC	OD	5–43	++	(Lowys, Desbrières & Rinaudo, 2001)
	FD	5–50	+	(Nordenström *et al.* 2021)
	SD	30	+++	(Nardi, Silveira & Siqueira, 2020)
	OD	5–40	+++	(Butchosa & Zhou, 2014)
	OD	25	++	(Beaumont *et al.* 2017)
PVA	OD	150–250	+	(Velásquez-Cock *et al.* 2018)
Maltodextrin	OD	100-250	+	(Asquez-Cock *et al.* 2017)
	SD	100	+	(Meneguin *et al.* 2020)
Glycerol	OD	12.5–50	++	(Moser, Henriksson & Lindström, 2018)
Mannitol	SD	100	++	(Meneguin *et al.* 2020)
Glucose	OD	20	++	(Zhang *et al.* 2021)
PEG	FD	0.1–8	+++	(Cheng *et al.* 2015)
	PD	50–400	++	(Santmarti, Tammelin & Lee, 2020)
	FD	5–50	++	(Nordenström *et al.* 2021)
Fish gelatin	OD	5–25	++	(Kwak *et al.* 2019)
Mixed glucan	VD	11–35	++	(Zha *et al.* 2023)
Xanthan gum	OD	25	++	(Beaumont *et al.* 2017)

+: High amounts of capping agent were needed; aggregation was largely present.
++: Moderate amounts of capping agent were needed; aggregation was moderately prevented.
+++: Low amounts of capping agent were needed; aggregation was completely prevented.
VD: Vacuum dried OD: Oven dried AD: Air dried
PD: Pressure dried SD: Spray dried FD: Freeze dried

Cheng *et al.* 2015). Butchosa & Zhou (2014) tested preparing CMC/CNF mixtures with and without heating during mixing, and the preheated sample outperformed the unheated sample. More ionic CMC was shown to be better at preventing agglomeration (Lowys *et al.* 2001).

2.6 Xanthan gum

Xanthan gum is a complex carbohydrate produced during fermentation by the bacteria *Xanthomonas campestris* (BeMiller, 2019: 261). It consists of a cellulose backbone, where every 2nd glucopyranosal monomer has a trisaccharide chain bonded on C_2 via a glycosidic bond. The trisaccharide chains consist of a mannose monomer with an acetyl group on C_6, a glucose monomer with a carboxyl group on C6, and another mannose monomer, which about 50% of the time has a pyruvic acid, bonded as a cyclic acetyl, connected to C_4 and C_6 (BeMiller, 2019: 262). The chemical structure is illustrated in Figure 10. The trisaccharide chains lay on the main backbone, protecting the main chain from chemical attacks and giving it incredible stiffness (BeMiller, 2019: 262–264). The protection allows xanthan gum to be usable in any temperature of liquid water and shows no change in properties between a pH of 6–9 and little change over 1–11. The addition of 0.1% NaCl removes all rheological dependence on pH (BeMiller, 2019; Butler, 2016: 263).

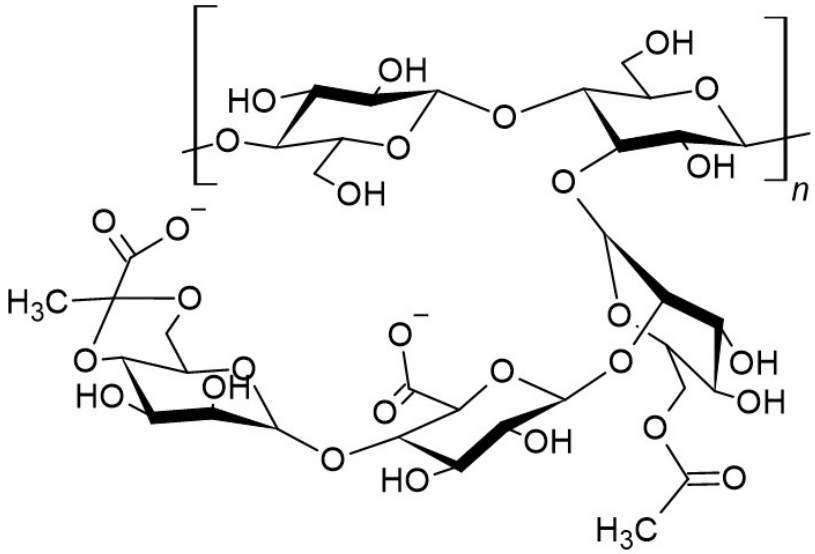

Figure 10: Chemical structure of xanthan gum with pyruvate cyclic group.

Xanthan gum is used as a rheology modifier, especially in the food industry, as it has a very favourable Newtonian plateau, is extremely shear thinning, and can, even at low concentrations, increase viscosity drastically (BeMiller, 2019; Butler, 2016: 266–267). Xanthan gum was shown to have a viscosity of ≈ 900 mPa s at a concentration of 0.2 %, a shear rate of 0.4 s^{-1}, in a 0.1 w% NaCl solution, and at 25 °C (García-Ochoa *et al.* 2000). Xanthan gum shows synergism

with various other hydrocolloids, such as κ-carrageenan and locust bean gum (BeMiller, 2019: 264–265).

The work by Beaumont *et al.* (2017), as shown in the last row of Table 7, studied the effect of numerous additives, including xanthan, on producing redispersible cellulose. The work focused mainly on TENCEL® gel, a nanostructured gel consisting of spherical cellulose particles. Various additives were analysed, with xanthan gum and CMC singled out as being very promising. Methods used to test the degree of agglomeration were particle size distribution, viscosity, colloidal stability, and water retention. Both oven drying and freeze drying were assessed. The additives were tested at a single concentration.

The particle size distribution of the oven-dried xanthan-cellulose samples was shown to be lower than the pure, never-dried NC sample. The impact of xanthan on the particle size distribution was not discussed. The xanthan could not have caused the cellulose particles to become smaller, but most likely had a smaller particle size and thus made the distribution seem smaller. The effect of drying on the viscosity was compared to the xanthan-cellulose sample before drying. Xanthan is a very strong thickening agent, thus it will increase the viscosity a lot (Wyatt & Liberatore, 2009). The comparison of the mixture prior to and after drying shows a slight decrease in viscosity post-drying. The one concern is that the xanthan addition makes the viscosity appear to be very close, as the xanthan caused a three-fold increase in viscosity of the cellulose dispersion (Beaumont *et al.* 2017). There is a chance that the difference seen is due to pure cellulose aggregation, and the xanthan just makes the relative difference look small. It is thus not so simple to conclude that the small decrease in viscosity confirms a small degree of aggregation.

Nonetheless, the results of Beaumont *et al.* (2017) supports the further exploration of xanthan gum as a capping agent for CNFs. Xanthan is an anionic polymer, due to having multiple carboxylate groups on the side chains (Wu & McClements, 2015; Wyatt & Liberatore, 2009; BeMiller, 2019: 262). The zeta potential had been shown to be -61.8 mV (Chun, Kim & Lee, 2009). This implies that it could be a good capping agent, even better than CMC. The results by Beaumont *et al.* (2017) are thus very promising and xanthan should be a very good capping agent. Further investigation is required though, especially of the effect of different xanthan gum concentrations.

Xanthan had been used in conjunction with NC in previous studies. One showed that a film made from NC and xanthan was strongest with a 60:40 NC to xanthan ratio, showing that xanthan had a contribution to make to the NC (Langari *et al.* 2019). The Young's modulus was very low though, having a maximum of 14.67 MPa. CNCs have been used with xanthan to produce bio-inks (Baniasadi *et al.* 2022). The bio-inks are developed specifically for tissue engineering purposes.

Xanthan had been used with thermoplastic starch as well. Melo *et al.* (2011) made TPS films via casting and extrusion while adding 2 %–10 % xanthan. Xanthan addition could moderately improve the mechanical properties as long as the storage humidity was not too high. One thing to take note of in this paper is the minimal glycerol use at 20 wt%. Da Matta *et al.* (2011) tested xanthan on pea starch and found that it made almost no contribution to the mechanical properties of TPS except for making it slightly stiffer. This is surprising as the opposite was found with xanthan added to NC. Starch gels had a decrease in elasticity with the addition of xanthan gum (Mandala, Palogou & Kostaropoulos, 2002). The increase in stiffness and decrease in elongation might be due to the high persistence length of xanthan, which is defined by Zhang *et al.* (2019) as, "... the distance over which the orientation of the bonds persists." In other words, it is the longest length where there is no bending of the polymer chain. Xanthan's persistence length was shown to range between 100 nm–120 nm, whereas polystyrene, in a good solvent, showed a persistence length of 0.8 nm (Sato, Norisuye & Fujita, 1984; Chun *et al.* 2009; Ahlawat, Deopa & Patil, 2022).

Xanthan gum had been shown to interact with the amylose in the starch, wrapping around it and decreasing its swelling power (Nawab *et al.* 2016). The retrogradation of the amylose was also hindered by the xanthan gum, as it prevented amylose-amylose bonds from forming after gelatinisation (Nawab *et al.* 2016; Lutfi *et al.* 2017).

Xanthan gum solutions show shear thinning behaviour (BeMiller, 2019: 263–265). For extrusion and injection moulding, this can be favourable behaviour. Xanthan could thus be an effective capping agent that will allow for CNFs to be dried and incorporated into starch. The removal of the xanthan might not be necessary due to its favourable interaction with starch and NC. Its ability to add stiffness is favourable for the production of TPS.

The work by Beaumont *et al.* (2017) was a large inspiration for the current study. There is a paucity of research on the effect of xanthan gum on CNF, especially as a capping agent. There is also nearly no information on the effect of capping agents on the NC and the polymer matrix the NC is added to. Peng *et al.* (2018) looked at the addition of lignin/NC to polypropylene, but besides this work, very little has been explored.

3 Experimental

3.1 Materials

Valida S191C 8% Batch SB-20-0126-01 was used as the source of CNF and was supplied by Sappi. The consistency was 8.2%. The xanthan gum used was Ingredion Ticaxan xantham gum 80 mesh supplied by IMCD. Amura starch was supplied by the National Root Crops Research Institute (NRCRI), Umudike in collaboration with the Raw Materials Research and Development Council (RMRDC), Abuja, Nigeria. All other chemicals used were supplied by Acechem.

3.2 Methods

3.2.1 Dried CNF capping and redispersion

Dried CNF dispersion preparation

The nanocellulose was diluted to a 1 % concentration by adding deionised water. The required xanthan gum was added before mixing. Note that the xanthan portion added is relative to the dry mass CNF. Mixing was done using a Silverson L4RT high shear mixer at 8000 rpm for 3 min. Half of the sample was separated to keep as the non-dried sample, and the other half was put in a plastic petri dish to dry at 50 °C in an oven for 24 h. Table 8 shows the sample nomenclature used throughout the paper.

Table 8: Nomenclature used for the various samples throughout the report.

Xanthan (%)	State	Group	Individual
0	Wet Dried	X0	W1 D1
15	Wet Dried	X15	W2 D2
25	Wet Dried	X25	W3 D3
50	Wet Dried	X50	W4 D4

Mixing intensity sample preparation

Dried CNF/Xanthan was diluted with deionised water to a concentration of 0.03 wt%. The mixing samples were prepared according to Table 9. Note that the mixing was done cumulatively. For instance, sample L was made by mixing at 4000 rpm for 1 min. A portion of this sample was removed and named sample L. Sample M was then prepared by mixing the remaining solution at 5500 rpm for 30 sec. A portion of the sample is separated as sample M. The process is continued till sample U, which is the final remaining portion that is ultrasonicated. Ultrasonication was done using a Jeken PS-10A ultrasonic cleaner with a frequency of 40 kHz and 70 W power. It was used for all ultrasonicated samples.

Table 9: Mixing intensities for various samples.

Sample	Name	rpm	Time
L	Low	4000	1 min
M	Medium	5500	30 sec
H	High	7000	30 sec
B	Blitz	8000	30 sec
U	Ultrasonic	NA	5 min

The reason for analysing this is due to Equation 3,

$$F_{\max} = 3\pi\eta\dot{\gamma}r_1 r_2 \tag{3}$$

where $F_{\max}$ is the maximum force one can apply on the particles, μ is the viscosity, $\dot{\eta}$ is the shear rate, and r_1 and r_2 is the radius of the particles. The formula was derived by Tadmor (1976). As one can note, the smaller the particles, the less force one can apply to them. This means that as agglomerates get broken into smaller and smaller particles, the smaller the force is applied to them. Eventually, the force will be too small to overcome the inter-particle bonds keeping the agglomerates together. It is thus expected to see a decrease in agglomerate size as one increases the mechanical energy supplied.

3.2.2 TPS sample preparation

Pure TPS samples

The TPS films were made using a film casting method. For the pure TPS samples, meaning no xanthan and CNF, the method was as follows. Starch, 12 g, was weighed in a glass beaker. The respective amount of glycerol was quickly added to prevent too much moisture absorption

from the glycerol. Water, 600 mL, was added and the mixture was stirred. The samples were heated to 85 °C for a duration of 30 min with constant magnetic stirring. Once fully gelatinised, the samples were cast into round silicon moulds and dried overnight in a convection oven set at 50 °C. Silicon moulds made the removal of films convenient by minimising risk of sample damage. The samples were put into their respective humidity chambers once dried. The storage temperature ranged between 22 °C – 24 °C.

Pure TPS samples were prepared, stored, and named according to Table 10a. The humidities of the saturated salt solutions are shown in Table 10b. Glycerol content added is expressed in parts per hundred starch (phs).

Table 10: Sample nomenclature for neat TPS to analyse the effect of glycerol and humidity, using saturated salt solutions (Greenspan, 1977), on amura TPS.

(a) Sample nomenclature.

Salt	Glycerol (phs)		
	30	35	40
K_2CO_3	K30	K35	K40
$Mg(NO_3)_2$	Mg30	Mg35	Mg40
NaCl	Na30	Na35	Na40

(b) Saturated salt humidities (20 °C–25 °C).

Salt	%RH (20 °C)	%RH (25 °C)
K_2CO_3	43.16	43.16
$Mg(NO_3)_2$	54.38	52.89
NaCl	75.47	75.29

TPS with non-dried CNF/xanthan

The TPS samples containing the CNF and xanthan were prepared slightly differently. Xanthan is very good at capturing and holding air bubbles. The samples prepared in a similar fashion as the neat TPS were therefore littered with them after drying. This is shown in Figure 11. This phenomenon could be alleviated by double-casting the films, which consisted of redissolving and degassing the TPS film and casting it again. All reinforced samples had 30 phs glycerol, relative to the mass starch. The first cast had one additional step to the neat TPS method; the CNF and xanthan, in non-diluted form, were added directly to the starch before the water. Glycerol was also added at this step. Once water was added, the slurry was high shear mixed at 8000 rpm for 1 min before heating.

After drying, the first casts were blitzed into powder using a spice grinder. The samples were redissolved into 300 mL of deionised water and brought to 85 °C under constant stirring. The redissolved samples were high shear mixed once more for 1 min at 8000 rpm using a Silverson L4RT. A volume of 100 mL of deionised water was added to cool the sample. Degassing was done using a vacuum chamber. The vacuum chamber pressure was changed step-wise from 50 kPa to 40 kPa to 30 kPa. The pressure was changed once bubble formation on the surface stalled. The surface bubbles were scraped off before changing the pressure. The samples were recast and dried again at 50 °C.

(a) Single-cast. **(b)** Double-cast.

Figure 11: Bubble formation in films that were cast once vs cast twice.

CNF/xanthan gum's impact on TPS reinforcement.

A face-centred central composite design (CCF) was used to analyse the effect of nanocellulose and xanthan gum on the mechanical properties of TPS. The design allows for both interaction effects and quadratic terms to be analysed with enough degrees of freedom (Verseput, 2000). Two centre points were included. Note that the CNF and xanthan content is expressed in parts per hundred starch (phs), not the mass of the polymer. The design is shown in Table 11.

Table 11: Full CCF design with 2 centre points at 2 levels for CNF and xanthan.

(a) CCF design layout for CNF and xanthan.

Design No.	CNF	Xan
1	-1	-1
2	-1	+1
3	+1	-1
4	+1	+1
5	0	0
6	-1	0
7	+1	0
8	0	-1
9	0	+1
10	0	0

(b) Values for CNF and xanthan levels of the CCF design.

Level	CNF (phs)	Xan (phs)
-1	2.5	1.25
0	3.75	1.875
+1	5	2.5

TPS with dried CNF/xanthan

The dried CNF with/without xanthan gum were prepared similarly to the non-dried samples. The only difference is how the CNF/xanthan was included. The dried CNF/xanthan was added to the water and then sheared at 8000 rpm for 2 min. The water was then added to the starch and glycerol, and shear mixed for 30 s at 8000 rpm.

Table 12b shows the experimental design for the dried CNF/xanthan reinforced TPS. This is to allow for the comparison of dried CNF and non-dried CNF, with or without xanthan, for the reinforcement of TPS. Some of the TPS samples with dried CNF do not have an adequate counterpart in the CCF design. The compliments are showcased in Table 12a. Table 12a also has the designs for the neat TPS that was double-cast, as well as TPS samples with only xanthan gum. The xanthan values are the %wt in reference to the mass CNF, except with samples 3 and 4 in Table 12a. These two are the pure xanthan samples with no CNF added and the wt% then refers to the starch.

Table 12: Experimental design for other non-dried samples and dried CNF/xanthan reinforced samples.

(a) Non-dried

Sample	CNF	Xan wt%
1	-1	0
2	+1	0
3	NA	1.25
4	NA	2.5
5	NA	0
6	-1	15
7	+1	15
8	-1	25

(b) Dried

Sample	CNF	Xan wt%
9	-1	0
10	+1	0
11	-1	15
12	+1	15
13	-1	25
14	+1	25
15	-1	50
16	+1	50

3.3 Analytical techniques

3.3.1 Amylose content

Amylose plays a large role in the tensile and crystalline properties of starch. Thus it is important to know the starch's amylose content. The method was adapted from Ambouroue Avaro *et al.* (2011). The starch was dried at 135 °C for 1 hr. An iodine solution, containing 20 g/L KI and 2 g/L I_2, was prepared in deionised water. A total of 100 ± 0.01 mg of dried starch, weighed immediately after being removed from the oven, was added to a conical flask. A volume of 1 mL 95% ethanol and 9 mL 1 M NaOH was added to the starch. The slurry was put in a boiling water bath for 10 min. After removal, it was allowed to cool at room temperature for 10 min. A 100 mL of deionised water was added to the starch. In a 100 mL volumetric flask

5 mL of the starch solution, 1 mL of 1 N acetic acid, and 2 mL of iodine solution were added. The volumetric flask was then filled with distilled water till 100 mL was reached. The solution was allowed to incubate for 30 min. UV-Vis absorbance analysis was done at 620 nm on a Cary 60 UV-Vis. Equation 4 was used to estimate the amylose content as a percentage.

$$\text{Amylose\%} = (5.83539 + 1.47157 \times \ln(\text{Abs620}))^2 \tag{4}$$

3.3.2 DSC

Differential scanning calorimetry was done on the pure starch samples to determine the T_o, T_p and T_c. It was done using a Mettler Toledo HP DSC 827e. Starch was diluted in deionised water at a ratio of 3:1 water to starch and 9 mg of slurry was used. The pressure was set at 40 bar. The temperature was changed from 30 °C–100 °C with a heating rate of 10 °C/min.

3.3.3 XRD

X-ray diffraction (XRD) analysis was done on both the pure starch and TPS samples. X-ray diffractograms were recorded on a Bruker D2 PHASER XRD Instrument with Cu-Kα radiation (λ=1.54060). The system was equipped with a LYNXEYE detector with a 4.99° PSD opening. Samples were scanned from 5°–45° 2θ at a rate of 0.02°/s. The generator settings were 30 kV and 10 mA. XRD samples were analysed using the `cryst` package in R (Valenzuela & Rodriguez-Llamazares, 2016). The function used was the `crystMW` function, that implements the Brückner method (Brückner, 2000). The function parameters used for starch was `N=10, iter=50`, for fresh TPS `N=15, iter = 50`, and for retrograded TPS `N=20, iter = 50`.

3.3.4 DMA

Dynamic mechanical analysis (DMA) was used to determine the T_g of the neat TPS samples. A Perkin Elmer DMA 8000 was used. Samples were placed in Perkin-Elmer RoHS compliant, 304 annealed stainless steel pockets. The temperature range varied based on the glycerol content and storage humidity of the samples. The K30 and Mg30 samples (Section 3.2.2) were analysed from room temperature to 70 °C. All other samples were done from −40 °C – 60 °C. The heating rate was 2 °C/min, and the frequency was varied between 1 Hz and 10 Hz.

3.3.5 WVP

Water vapour permeability (WVP) was done on the pure TPS films do determine the effect of both humidity and glycerol content on the barrier properties of the TPS. The method was adapted from Mali *et al.* (2006). The desiccators were conditioned for 1 day with a saturated salt solution in each desiccator. The cells were filled with ≈5 g anhydrous $CaCl_2$. A round TPS film was cut from each sample and secured on each cell. The cells were weighed each day until the mass change started to plateau. The WVP was then calculated using Equation 5–7 (Cazón *et al.* 2022).

$$WVTR = \frac{\Delta m}{A\Delta t} \tag{5}$$

$$\text{Permeance} = \frac{WVTR}{\Delta P} \tag{6}$$

$$WVP = \text{Permeance} \cdot \text{thickness} \tag{7}$$

3.3.6 FTIR

Fourier transform infrared spectroscopy (FTIR) was done on the pure starch, neat TPS samples, the dried CNF/xanthan, and the pure xanthan gum powder. FTIR analysis was done using a Bruker Alpha FTIR. The scan resolution was 4 cm^{-1} and 32 scans were taken. The scan range was 7000 cm^{-1} – 500 cm^{-1}. The scans were baseline corrected, smoothed, and then rescaled so that each has the same max peak height.

3.3.7 Zeta potential measurement

Zeta potential was measured using a Malvern Zetasizer Nano S. Both non-dried CNF/xanthan and dried CNF/xanthan were redispersed to a concentration of 0.03 wt% in a 10 mM KNO_3 deionised water solution. The samples were redispersed via high shear mixing at 8000 rpm for 3 min using the Silverson. Samples were ultrasonicated for 10 min to degas and further disperse the fibres. The samples were injected into DTS1070 cuvettes. Equilibration time and temperature were 3 min and 25 °C, respectively. A total of twelve scans, done in triplicate, were taken on each sample. Three samples of each mixture were tested.

3.3.8 TEM

The non-dried CNF/xanthan solutions from the zeta potential measurements were used. A drop of each sample (≈5 μL) was placed on one side of a Formvar-coated TEM grid. Within 15 s,

the grid was brought into contact with an equal volume of 1% aqueous phosphotungstic acid (PTA). The grid was immediately brought into side-on contact with a wedge of filter paper to remove the excess. The grid was air-dried with mild agitation. A JEOL 1010 TEM, at 100 kV, was used to image the grids. A pixel ruler, taken from RapidTables, was used to estimate the fibre diameters.

3.3.9 Viscosity measurement

The sample preparation was as follows. The non-dried CNF/xanthan samples, as mentioned in Section 3.2.1, were diluted by adding equal mass water to the non-dried sample portion. This gives a solution of ≈0.5 wt% CNF. The dried CNF/xanthan samples were redispersed in deionised water to a similar concentration and mixed for 3 min at 8000 rpm. The viscosity was recorded on an Anton Paar MCR 92 rheometer in a CC 27 cup. Each sample was allowed to equilibrate to 25 °C for 10 min. Pre-shear mixing was done at a shear rate of 50 s^{-1} for 3 sec. The sample was then left for a further 3 min before measurement started. The sample was analysed at a shear rate of 0.01 s^{-1}–100 s^{-1}. The samples showed shear thinning behaviour, so the viscosity could be related to the shear rate using a power law model shown in Equation 8

$$\eta = K\dot{\gamma}^{n-1} \tag{8}$$

with η being the viscosity, $\dot{\gamma}$ the shear rate, and K the flow consistency index (Osswald, 2017: 63). One can linearise the Equation by applying a logarithmic transformation, shown in Equation 9

$$\ln \eta = \ln K + (n-1) \ln \dot{\gamma} \tag{9}$$

The aim of the viscosity test is to prove that xanthan gum allows for more of the rheology to be conserved when the CNF is dried and redispersed. This was assessed by fitting a linear line

$$\ln \eta = \ln K + (n-1) \ln \dot{\gamma} + \alpha \mathrm{ND} + \beta \ln \dot{\gamma} \mathrm{ND} \tag{10}$$

ND is a categorical variable that is 1 when the sample was non-dried and 0 if the sample was previously dried; α and β thus correct for the intercept and slope difference between previously dried and non-dried samples. The methodology of representing Equation 10 is in accordance with the methodology commonly used in statistics and data science when doing linear regression with a categorical variable (James *et al.* 2021: 83).

3.3.10 SEM

The dilute B–samples from Section 3.2.1, the U–CNF sample, the non-dried samples from the zeta-potential test, and a pure xanthan sample, ultrasonicated, were used for the SEM imaging. The samples were first freeze-dried. This allowed for the structure of the native suspension to be maintained. A 1 mL aliquot of each sample was placed upon a 2×2 cm square of aluminium foil and immersed in liquid N_2. Once frozen, each foil containing the samples was transferred straight to the pre-cooled stage of a freeze dryer set at -40 °C. The freeze dryer used was a Virtis SP Scientific Advantage Pro. Samples were dried under vacuum (1.33–0.40 kPa) by slow and stepwise warming from -40 °C to room temperature over a period of two days. The dried samples were mounted on double-sided carbon adhesive dots on SEM stubs, coated with 7 nm of sputtered chromium. A Zeiss Supra55 SEM at 3 kV was used for imaging. Images were taken from multiple points to capture the full representation of each sample. A pixel ruler, taken from RapidTables, was used to estimate the fibre diameters.

3.3.11 Turbidity

The samples used were the mixed intensity samples as described in Section 3.2.1. Five scans of each sample were taken, as there was considerable variance in certain samples. A total of three replicates were done. The λ ranged from 320 nm–860 nm with a step size of 60 nm. Scan time was 2 s. A Cary 60 UV-Vis spectrophotometer was used to measure the absorbance. The effect of xanthan was taken into account by assuming the absorbance is additive. Xanthan gum samples, prepared to each concentration as they would be in the CNF/xanthan samples, were scanned at each wavelength. The absorbance values for the CNF/xanthan samples were then corrected.

Carr & Hermans (1978) derived an equation that allowed them to estimate the diameter of fibrin fibres in suspension by using turbidity measurements. Turbidity here does not refer to the NTU type but to the formula, $\tau = \ln(10)A/t$, with τ being the turbidity, A the absorbance, and t the sample thickness in cm. The theory assumes that the fibrin is a thin, long rod in suspension. The scattering caused by the particles can be estimated using this assumption. The scattering is related to the turbidity. The derived formula proposed by Carr & Hermans (1978) is shown in Equation 11

$$\tau = \left(\frac{88\pi^3 n' c}{15\lambda^3 N}\right)\left(\frac{\mathrm{d}n}{\mathrm{d}c}\right)^2 \mu \tag{11}$$

where λ is the wavelength, n' is the refractive index, dn/dc is the specific refractive index increment, c is the concentration, and μ is the mass-length ratio. Equation 11 assumes that

$\tau \propto \lambda^{-3}$. According to Carr & Hermans (1978), this does not hold once the mass-length ratio, μ, becomes very large. In this case, if one assumes the rods to be cylindrical, one can apply a series expansion and obtain Equation 12

$$\frac{c}{\tau\lambda^3} = \frac{N_A}{\left(\frac{88}{15}\right)\pi^3 n \left(\frac{dn}{dc}\right)^2 \mu}\left[1 + \frac{23}{77}\pi^2 n'^2 d^2 \frac{1}{\lambda^2}\right] \tag{12}$$

where d is the diameter. With Equation 12 one can determine two sizing parameters, μ and d. One can do this by using $\frac{c}{\tau\lambda^3}$ as the y and $1/\lambda^2$ as the x. A linear line can then be fit, and using the slope and intercept the d and μ can be determined, respectively. Carr & Hermans (1978) made the assumption that $d << \lambda$. If one does not make that assumption, one gets the equation proposed by Yeromonahos, Polack & Caton (2010), shown in Equation 13

$$\tau\lambda^5 = \frac{1}{N_A} 2\pi^3 c n' \mu \left(\frac{dn}{dc}\right)^2 \left(\frac{44}{15}\right)\left[\lambda^2 - \frac{184}{154}\pi^2 n'^2 r^2\right] \tag{13}$$

where one can use linear fit of $\tau\lambda^5$ and λ^2 to determine r and μ, with r being the fibre radius.

Equation 11 was used with some success on CNF by Shimizu *et al.* (2016), where the μ values were determined and then related to the diameter of the fibres. In this study, the 3 various methods are all analysed for their applicability. Even if the estimated parameters do not reflect the true values, it may give insight into differences between samples. The value for $\frac{dn}{dc}$ used was 0.16 mL g^{-1}, taken from Shimizu *et al.* (2016), and the n' was 1.33.

3.3.12 Specific surface area determination

The specific surface area (SSA) was determined using a Congo red adsorption test as described in Ougiya *et al.* (1998), Kwak *et al.* (2019), and Velásquez-Cock *et al.* (2018). The test is done to quantify the change in surface area when the CNFs agglomerate upon drying. CNF/xanthan solutions, both dried-then-redispersed and non-dried, were prepared similarly to the zeta potential samples but without KNO_3. A phosphate buffer was prepared with the help of the calculator from AAT Bioquest, Inc. (2023). For a 2 L batch, 1600 mL of deionised water was added to a glass jar. To make a 0.1 M phosphate solution, 9.80 g of $Na_2HPO_4 \cdot 12\,H_2O$ and 20.70 g of NaH_2PO_4 were added to the solution. The pH was adjusted to 6 by either adding 1 M HCl or 1 M NaOH solution. More deionised water was added to fill the volume to 2 L.

The solutions were dialysed in the phosphate buffer over three days, with the phosphate buffer being replaced daily. After dialysis, NaCl was added to the CNF/Xanthan solution to a concentration of 0.004 wt%. Each sample was divided into five. Each sample received a different

amount of Congo red, varying from 5%–30% relative to the mass of CNF and xanthan in solution. The samples were left overnight in a water bath at 60 °C. The samples were centrifuged at 10000 rpm for 7 min. Duplicates of each sample were analysed in a Hitachi U-3900 UV-Vis spectrophotometer at a wavelength of 492 nm.

The absorbance was used to determine the concentration of Congo red in the supernatant, C_e. This information could be used to determine the mass Congo red adsorbed onto the fibres, q_e. This could be used to fit a Langmuir isotherm model, shown in Equation 14 (Langmuir, 1918). Other models were assessed as well. A common adsorption isotherm is the one derived by Freundlich (1909), which is shown in Equation 15

$$q_e = q_{max}\frac{K_L C_e}{1 + K_L C_e} \tag{14}$$

$$q_e = K_f C_e^{1/n} \tag{15}$$

Cellulose is mostly hydrophilic but does possess a hydrophobic triclinic surface on its crystal lattice (Mazeau & Wyszomirski, 2012). This means there is a possibility of hydrophobic bonding having an influence on dye adsorption. Mazeau & Wyszomirski (2012) showed that a significant portion of Congo red dye adsorbed onto the hydrophobic surfaces of cellulose. A modified Langmuir, taken from VanDer Kamp *et al.* (2005), was used to take the hydrophobic surface adsorption into account. VanDer Kamp *et al.* (2005) studied the importance of the hydrophobic surfaces of activated carbon on the adsorption of large dye molecules. The modified Langmuir is shown in Equation 16

$$q_e = q_{max}\frac{K_L C_e}{1 + K_L C_e} + q_H \tag{16}$$

where the variable q_H is the hydrophobic adsorption capacity. This hydrophobic surface is assumed to have irreversible adsorption and thus $K_H C_e >> 1$. This model is referred to as Langmuir2.

The specific surface area can be calculated from the q_{max} using Equation 17,

$$SSA = \frac{q_{\max} \cdot Na \cdot Sa}{M_w \times 10^{21}} \tag{17}$$

with M_w being the molar mass of Congo Red (696.7 g/mol) and Sa the surface area of the cellulose covered by the Congo red (1.73 nm^2) (Kwak *et al.* 2019; Ougiya *et al.* 1998).

The curve-fitting was done using Scipy's `curve_fit` and `least_squares` functions (Virtanen *et al.* 2020). The loss function was `linear` and the `trf` regression method was used.

To determine the standard error of the regression coefficients, bootstrapping was used. Bootstrapping is a sampling method that allows for an accurate estimation of the mean and standard deviation of samples (Davison & Hinkley, 1997). In the case of regression, it works as follows. Generate the bootstrap data set by choosing data points from the original data set at random. This is done with replacement, meaning the same point can be chosen multiple times. Fit the curve to the bootstrapped dataset. Store the coefficients. Repeat this process; the mean and standard deviation of all the coefficients generated are the main coefficients and their standard error, respectively. This allows for more accurate determination of coefficients and their certain standard error when doing non-linear regression (Davison & Hinkley, 1997). A thousand bootstrapped samples were generated and fitted, with the bootstrap sample size being equal to the size of the dataset.

In order to ensure that the addition of the q_H term in Equation 16 does not cause over-fitting, k-fold cross validation, with k=10, was used (James *et al.* 2021: 203). The process works where the data is split into k equally sized parts, or folds. The data is trained on k-1 of the folds and then tested on the remaining fold. The process is repeated so that every fold is used once as the testing fold. The root mean squared error is then calculated and compared between the equations. This allowed one to see whether the q_H causes over-fitting. The k-folds were generated using the `KFold` function from scikit-learn (Pedregosa *et al.* 2011).

3.3.13 Sedimentation

The mixing intensity samples in Section 3.2.1 and non-dried, ultrasonicated CNF/xanthan samples, diluted to 0.03 wt%, were tested. They were put in 6 mL polytop vials. Photos were taken in 30 min time increments and quantitatively assessed to infer the degree of sedimentation with time.

3.3.14 Mechanical testing

Tensile testing was done on all TPS samples using an Instron 5966 universal testing system. The methodology is in accordance with the ASTM D882-18 standard. The grip separation rate was 50 mm/min with a grip separation length of 100 mm. The pure TPS film strip size was 20.0 mm × 125 mm and the reinforced films were 16.4 mm × 125 mm. The thickness was measured at three points and the average was taken. Average film thickness was ≈210 µm. Five strips of each sample were tested. All samples tested were incubated for 10 d – 14 d.

The tensile values of both the neat TPS and the reinforced TPS were fitted to a quadratic formula shown in Equation 18

$$Z = aX + bY + cXY + dX^2 + eY^2 \tag{18}$$

where X and Y refer to glycerol and humidity for neat TPS and CNF and xanthan for reinforced TPS. All lower case Roman letters are the coefficients for each term. Z is either of the three tensile properties.

3.3.15 Thermo gravimetric analysis

Thermo gravimetric analysis (TGA) was done using a SDT Q600 Simultaneous TGA/DSC (TA instruments). The samples analysed was the neat TPS, 2.5 phs xanthan TPS sample, 5 phs CNF TPS, and the 2.5 phs xanthan + 5 phs CNF TPS sample. The samples were placed in alumina pans and heated from room temperature to 800 °C in N_2 at a heating rate of 10 °C/min.

3.3.16 Statistical analysis

All statistical tests were done either with Scipy's `stats` module or using the `statsmodels` package in python (Virtanen *et al.* 2020; Seabold & Perktold, 2010). The `ols` function from `statsmodels` was used for ANOVA analysis and linear regression.

4 Results and discussion

4.1 Characterisation of native starch

The iodine test estimated the starch to have an amylose content of 23.34±0.55%. This is similar to the value reported by Nwokocha *et al.* (2011) for yellow amura starch. Table 13 shows the gelatinisation temperature of the starch determined by the DSC. The range is quite wide; this is probably due to the fast heating rate. Nonetheless, the values are within the range for yellow amura starch (Nwokocha *et al.* 2011). Figure 12 shows the XRD scan of the pure starch. The strong peaks at 15.1°, 17.1° and 23.0° and the weak one at 28.9° indicate the starch crystalline structure is type A (Van Soest *et al.* 1996d; Van Soest & Vliegenthart, 1997). Yellow amura starch was also found to be type A (Nwokocha *et al.* 2011). The relative crystallinity is 22.06 %, which is lower than expected for native starch. Since the starch was milled, it is proposed that this had decreased the relative crystallinity.

Table 13: Gelatinisation temperature range for amura starch.

T_o (°C)	T_p (°C)	T_c (°C)
68.90	73.75	79.46

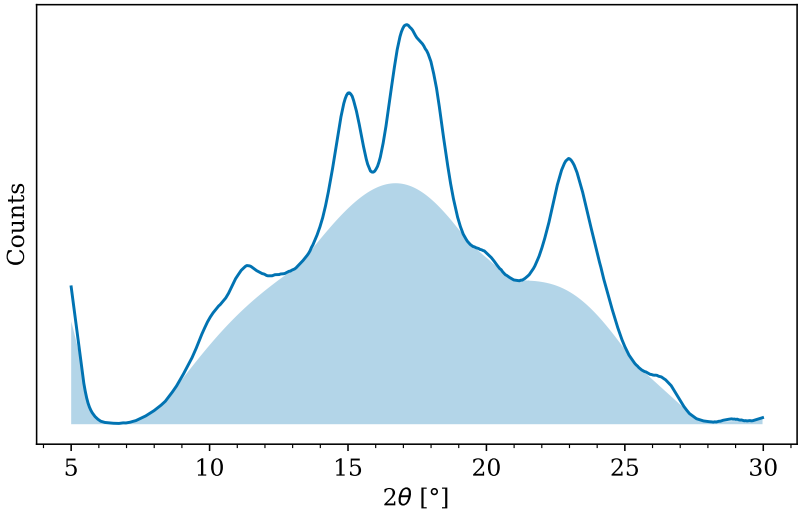

Figure 12: XRD scan of pure starch with amorphous region.

Figure 13 shows the FTIR bands of the pure amura starch. The type of bonds associated with each peak are in Table 14. The 3 crystalline types of starch had been shown to have their own unique spectra (Pozo *et al.* 2018). Type A starch had a higher peak at 3300 cm^{-1} and a well-resolved peak at 1022 cm^{-1}. The band at 1022 cm^{-1} in Figure 13 does not have a clear peak, but there is a slight bump, which was absent in the spectra of B and C starches. The peaks between 1500 cm^{-1} – 1600 cm^{-1} are odd, as the literature does not describe them being there at all. What the cause of the peaks is, is unknown.

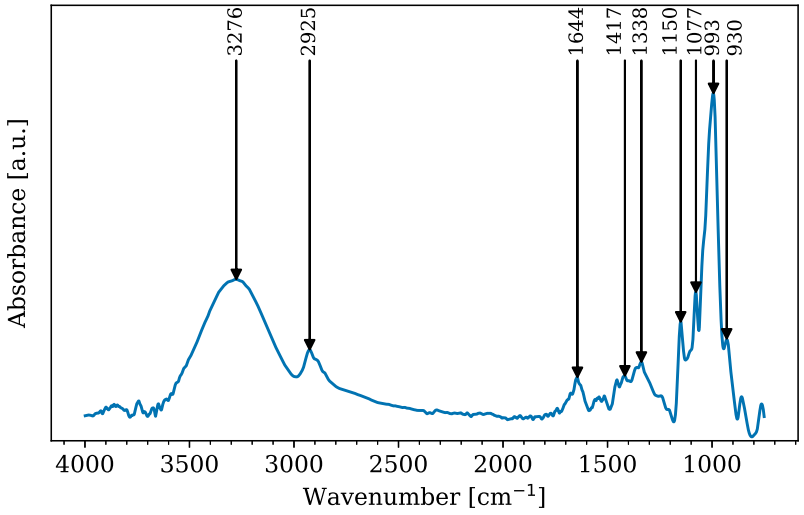

Figure 13: FTIR scan, with labels of peaks, for pure amura starch.

Table 14: FTIR spectra of starch with corresponding bonds. (Wiercigroch *et al.* 2017; Galat, 1980; Cael, Koenig & Blackwell, 1975).

Band	Wavenumber (cm^{-1})	Type of bond
O–H	3276	Stretching
C–H	2925	Stretching
H_2O	1644	Bound water
C–H	1417	Bending
O–C–H, CH_2	1338	Bending
C–O, C–C	1150	Stretching
C–O	1077	Stretching
C–O–H solvated	993	Stretching
C–O–C	930	Stretching

4.2 Characterisation of neat TPS

Figure 14 shows the FTIR spectra of the pure thermoplastic starch, and more specifically of sample Mg35 (Table 10a). This was taken after 14 days of conditioning. The spectra are very similar to that of pure starch. The only major difference is that the TPS has no peaks in the 1500 cm^{-1} – 1600 cm^{-1} range. There are some peak shifts that are observed, though they are minor. For instance, the 3276 cm^{-1} peak shifted to 3282 cm^{-1}. This suggests that the newly formed hydrogen bonds between glycerol and starch are weaker than those between the starch itself. The shift in the 930 cm^{-1} peak, which is the glycosidic peak, suggests a decrease in glycosidic bonds due to the thermal processing. This peak shift tends to be much larger when the starch is extruded and when the native starch is more unrefined (Paluch *et al.* 2022). The TPS spectra at different humidities and glycerol levels did not show any significant differences.

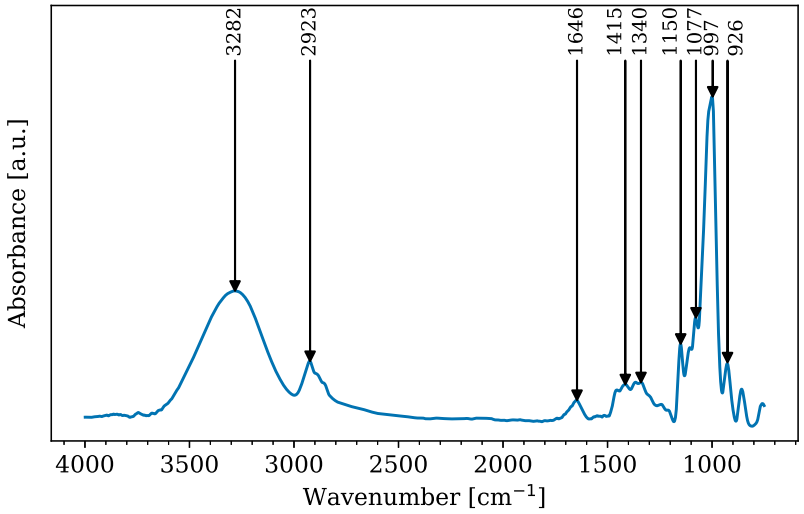

Figure 14: FTIR spectra of pure TPS with 35 phs glycerol and stored at 54 % relative humidity (Sample Mg35).

Table 15 shows how the crystallinity of TPS was influenced by storage humidity, glycerol concentration, and time. There are some trends to note. The samples are still highly amorphous at day four. Only Na35 and Na40 showed any significant retrogradation. This is due to the relatively high storage humidity and high glycerol content of Na35 and Na40, allowing for more chain mobility. This causes faster recrystallisation. All the samples have retrograded significantly at day 14. The difference between K and Mg samples is at day 14 more noticeable. The retrogradation increased with increasing humidity levels. The trend with glycerol is not as noticeable. The samples with 30 phs glycerol showed less crystallinity. The T_g of the 30 phs samples is very near room temperature, thus the chain mobility is very limited and retrogradation stunted.

The change in crystallinity over time is clearly illustrated in Figure 15. Figure 15a has a very

Table 15: Relative crystallinity (%) of retrograded TPS with various glycerol levels and storage humidities.

Glycerol (phs)	Day	Humidity		
		K (43 %)	Mg (53 %)	Na (75 %)
30	4	4.58	3.76	4.37
	14	8.11	8.12	10.36
35	4	3.90	4.14	8.05
	14	8.33	9.73	10.85
40	4	5.19	4.61	6.59
	14	7.87	8.79	11.81

large amorphous region, whereas Figure 15b has clearly defined crystal peaks. The peaks of 16.9°, 19.6° and 21.7° are the FTIR spectra of the V_H crystals that form after starch gelatinisation (Van Soest *et al.* 1996d; Van Soest & Vliegenthart, 1997).

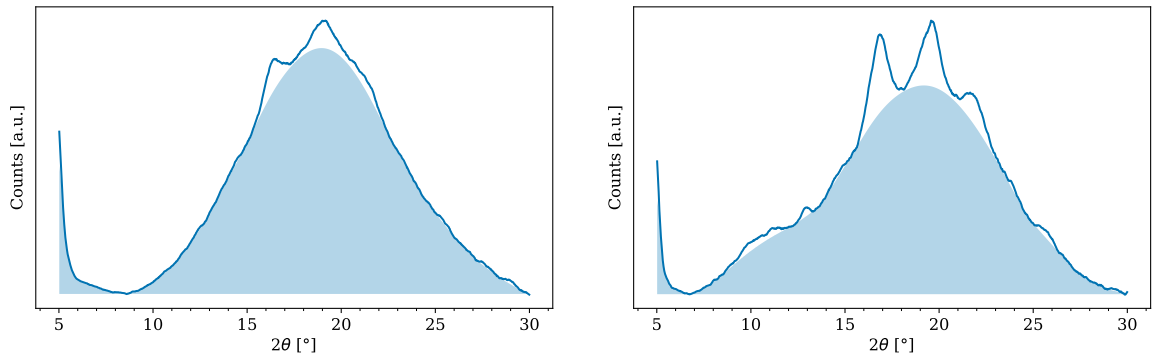

(a) Day 4.

(b) Day 14.

Figure 15: XRD spectra of TPS with 35 % glycerol stored at 54 % RH on 2 different days.

The influence of glycerol and humidity on the TPS's T_g is shown in Table 16. The influence of glycerol is as expected, with higher glycerol values meaning lower T_g. Higher humidity also suggests lower T_g, except in the case of Na35, which shows a slight deviation. Na40 is unfilled due to the DMA not returning sensible data despite 3 attempts. It is expected that the high moisture content of the Na samples might have negatively influenced the data collection.

Table 17 shows the water vapour permeability results of the amura TPS films. Glycerol and humidity both increase the permeability of the TPS films to water vapour. This is to be expected, as glycerol is hygroscopic and higher humidity means a higher partial pressure to force vapour through. The values are on the low side in comparison to most research. It might be due to most papers only doing the analysis for 24 h (Mali *et al.* 2006). Some research that extended the analysis time got values more similar to the ones observed (Othman *et al.* 2021), but others

Table 16: Estimate for each TPS sample's T_g (°C) at two frequencies based on the peak tan δ.

Glycerol (phs)	Frequency (Hz)	Humidity		
		K (43 %)	Mg (53 %)	Na (75 %)
30	1	47.9	38.1	19.9
	10	49.4	43.1	28.3
35	1	35.5	21.3	23.1
	10	38.7	28.8	33.8
40	1	29.7	11.1	–
	10	29.9	22.7	–

also found values that were higher (Talja *et al.* 2007).

Table 17: WVP (g m^{-1} d^{-1} kPa^{-1}) of amura TPS films with various glycerol levels and storage humidities.

Glycerol (phs)	Humidity		
	K (43 %)	Mg (53 %)	Na (75 %)
30	4.93×10^{-5}	6.74×10^{-5}	1.43×10^{-4}
35	9.06×10^{-5}	1.34×10^{-4}	1.74×10^{-4}
40	1.17×10^{-4}	2.23×10^{-4}	3.94×10^{-4}

4.3 Mechanical properties of neat TPS.

The quadratic regressions of Equation 18 on the tensile properties of the pure TPS films are shown in Table 18. The format of the Equation is repeated below. The response surface of the significant terms is shown in Figure 16. Note that the glycerol concentrations and the humidities were all normalised to values between -1 and 1. For instance, 30 phs glycerol represents -1, 35 phs represents 0, and 40 phs represents 1.

$$\text{Tensile} = \text{Intercept} + \text{Glycerol} + \text{Humidity} + \text{Glycerol} \times \text{Humidity} + \text{Glycerol}^2 + \text{Humidity}^2$$

All terms, except the linear Glycerol term, show significant effects on the tensile strength. The strong quadratic terms, which are both negative, suggest a maximum is present, resulting in

a smooth hill shape. This can be seen in Figure 16a. The central peak is an abnormality and correlates with the crystallinity results from Table 15, where Mg35, which is the central sample, showed a higher-than-expected crystallinity.

The modulus has a significant linear humidity and quadratic glycerol term. This implies a rising ridge shape for the response surface, which can be seen in Figure 16b. Therefore, the maximum is found in the centre of the glycerol axis and at the lower end of the humidity axis.

Though most literature works found that higher glycerol levels imply lower strength and stiffness, unexpected peaks are not unheard of. Bui & Son (2018) reported a similar maximum at 35 phs glycerol at a humidity of 50 %. Bui & Son (2018) postulated that there was a low starch phase that acts as a cross-linking agent. The secondary phase was indicated by DSC thermograms. Note that the authors of this work used a high amylose starch. The other possibility is that the combination of glycerol, humidity, and timing is optimal for amylose and intermolecular-amylopectin recrystallisation for this starch. This would allow for maximal tensile properties.

The elongation has only significant linear terms, with glycerol and humidity inversely correlated with elongation. This might sound counter-intuitive and can only be addressed when also looking at the large, positive interaction term, showcased in Figure 16c. Elongation increases when both glycerol and humidity are low or high but decreases when one is high and the other low. Low glycerol and humidity will cause low retrogradation, allowing for a more amorphous polymer. High glycerol leads to phase separation, making the polymer more fragile. The high humidity might offset this by making the starch phase act more like the glycerol phase. When the humidity is high but glycerol is low, one can still expect some substantial retrogradation to occur, causing stress points in the polymer.

Table 18: Quadratic regression coefficients to all tensile response variables of pure TPS.

	Tensile strength		Tensile modulus		Elongation	
	coef (MPa)	p	coef (MPa)	p	coef (%)	p
Intercept	4.60 ± 0.33	0.00	129 ± 24	0.00	48.27 ± 8.49	0.00
Humidity	-0.31 ± 0.16	0.00	-35 ± 12	0.00	-7.24 ± 4.08	0.00
Glycerol	0.02 ± 0.16	0.85	-10 ± 12	0.09	-4.46 ± 4.13	0.04
Humidity:Glycerol	-0.19 ± 0.19	0.05	-17 ± 14	0.02	9.55 ± 4.87	0.00
Humidity^2	-0.47 ± 0.33	0.01	20 ± 24	0.11	-0.32 ± 8.51	0.94
Glycerol^2	-0.83 ± 0.27	0.00	-53 ± 20	0.00	3.37 ± 7.06	0.36

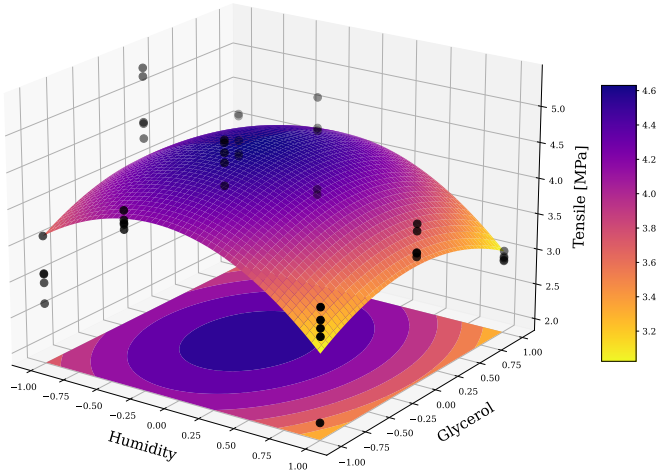

(a) Strength.

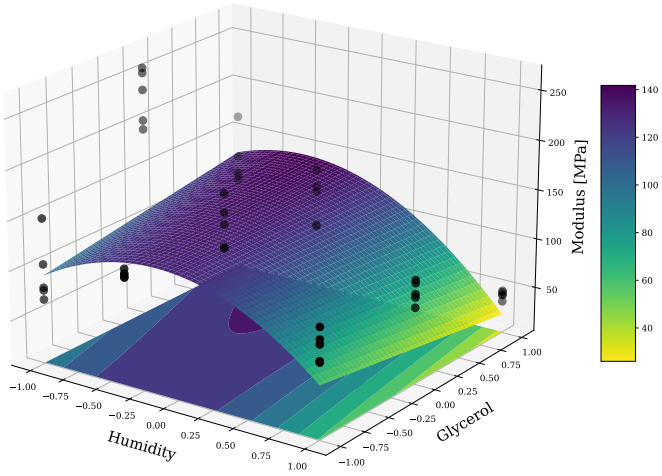

(b) Modulus.

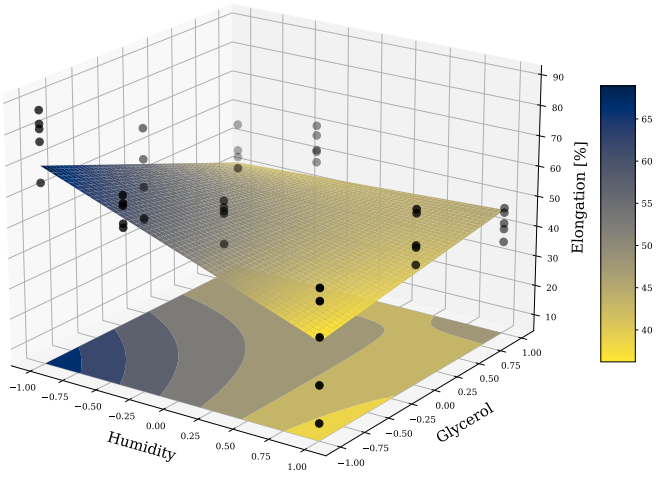

(c) Elongation.

Figure 16: Response surface plots, with data points, of the significant terms for each TPS tensile response variable.

4.4 Xanthan as capping agent for CNFs

4.4.1 FTIR

Figure 17a and Table 19a show the FTIR spectra, with the bond allocations, of the CNF. The peaks of 1158 cm^{-1} and 900 cm^{-1}, and the absence of a peak at 1111 cm^{-1}, suggest the cellulose is mostly amorphous cellulose (Nelson & O'Connor, 1964). This is expected due to the amorphous regions in CNFs.

Xanthan has many carboxyl groups, and this is shown in Figure 17b and Table 19b. The very strong peak at 1603 cm^{-1} and the moderate one at 1707 cm^{-1} are mainly from the carboxyl units of the acetyl group (Pawlicka *et al.* 2019).

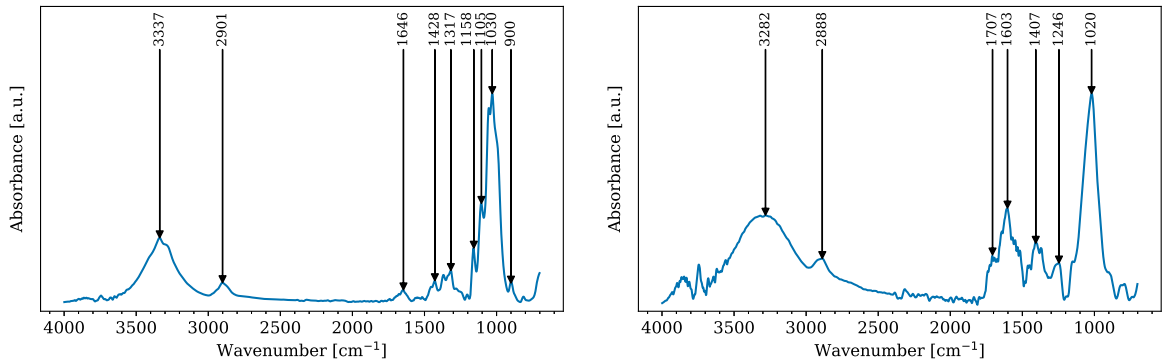

(a) CNF.

(b) Xanthan.

Figure 17: FTIR of CNF and xanthan gum with wavenumbers of notable bands.

Table 19: FTIR bands of CNF and xanthan gum with corresponding bonds.

(a) NC (Nelson & O'Connor, 1964).

Band	Wavenumber (cm^{-1})	Type of bond
O–H	3337	Stretching
C–H	2901	Stretching
H_2O	1646	Bound water
CH_2	1428	Scissoring
O–C–H	1317	Bending
C–O–C	1158	Stretching
C–O	1030	Stretching
C_1	900	Vibration

(b) Xanthan (Pawlicka *et al.* 2019).

Band	Wavenumber (cm^{-1})	Type of bond
O–H	3282	Stretching
C–H	2888	Stretching
COOR	1707	Stretching
C=O	1603	Stretching
C=O	1407	Strecthing
O–C–H	1246	Bending
C–O	1020	Stretching

Figure 18 shows how the FTIR spectra change with the addition of xanthan to CNF. The spectra change drastically at 25 % xanthan addition, with the carboxyl bonds becoming very prominent.

These peaks are not so visible in the 15 % xanthan sample, which looks identical to the CNF spectra. The high amount of scattering that is visible with some of the samples makes it hard to draw any conclusions regarding peak shifts. It does appear as if the C=O peaks shift more to the left, which could be due to the linking between xanthan and CNF.

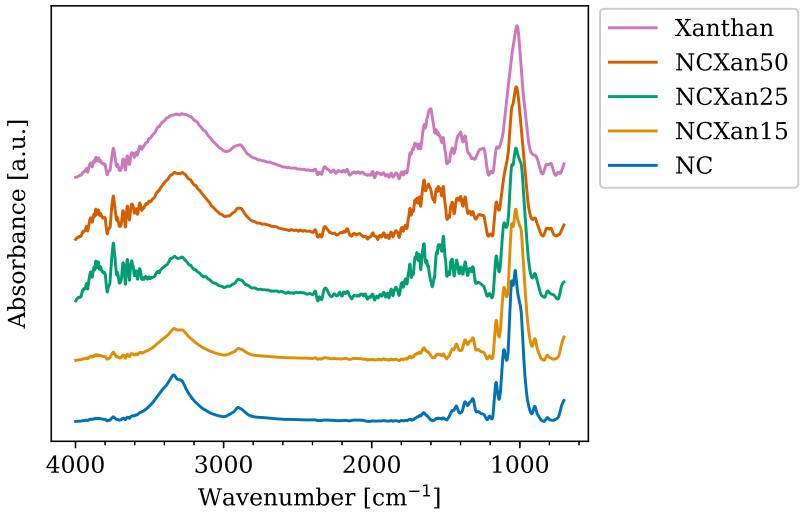

Figure 18: FTIR spectra of CNF/xanthan at various ratios.

4.4.2 TEM

The TEM images in Figure 19 to Figure 21 are of completely dried CNFs and its mixtures with xanthan. Insight is given on the structure that is trying to be redispersed. Figure 19 shows that the pure cellulose fibres agglomerate aggressively and in a zipper-like manner. This is hornification. The addition of 15 % xanthan, shown in Figure 20, displays some marked improvement in the agglomeration, but it is still visible. Nearly all the agglomeration has disappeared with 50 % xanthan addition, as shown in Figure 21. This proves that, with enough xanthan addition, the CNFs can be kept apart even in the dried state. Using pixel measurement, the estimated individual CNF fibre is estimated to be 10 nm – 18 nm in width.

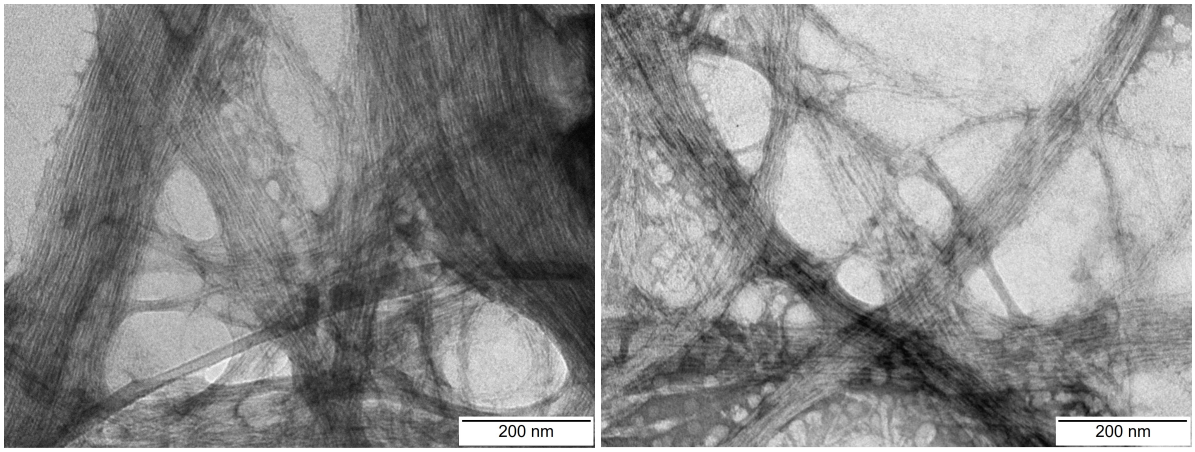

Figure 19: TEM images of pure CNF.

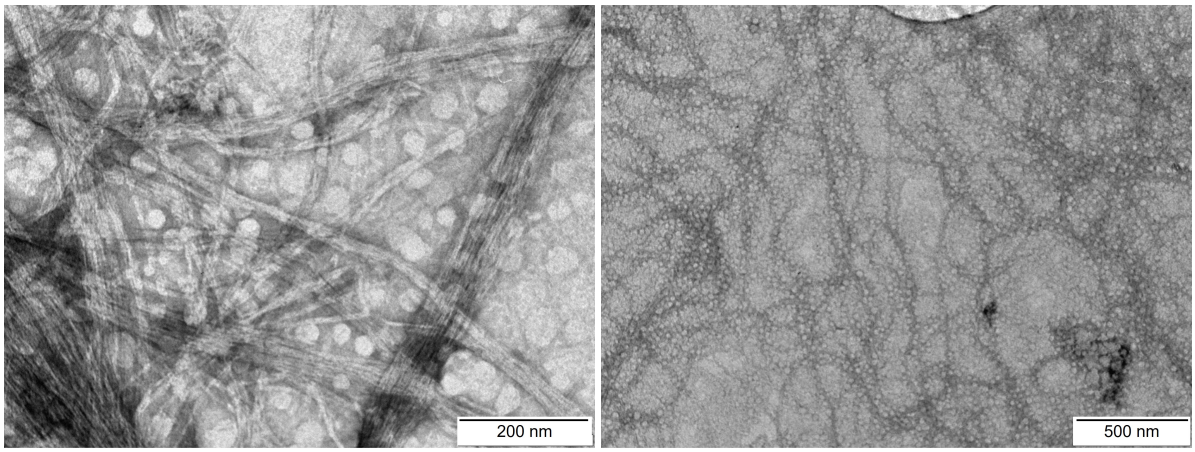

Figure 20: TEM images of CNF with 15 % xanthan.

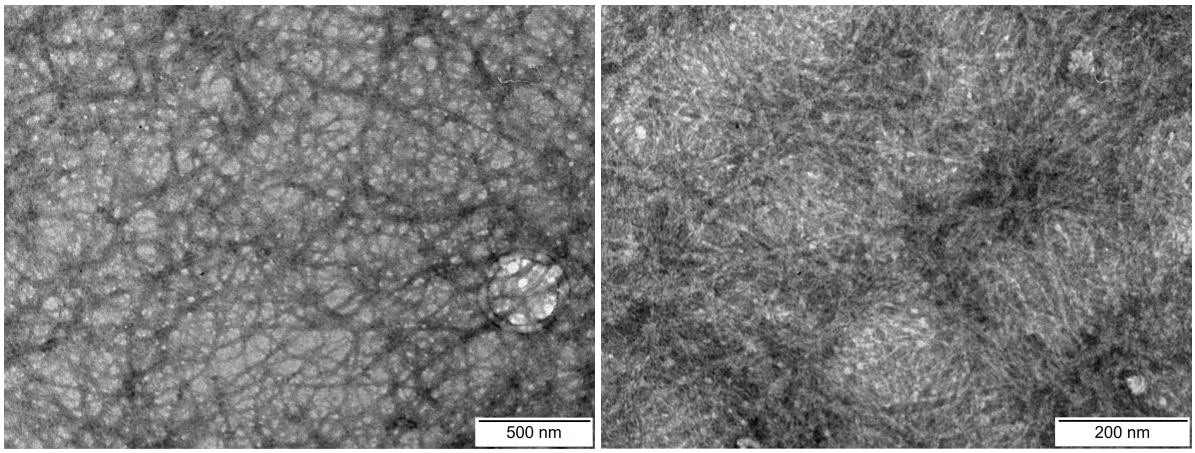

Figure 21: TEM images of CNF with 50 % xanthan.

4.4.3 Zeta potential

The zeta potential, shown in Table 20, shows the mean of each sample with the 95 % confidence interval. The dried-then-redispersed samples all show an increase in zeta potential. A Welch's t-test, which assumes unequal variance, was done on the dried-then-redispersed pure NC vs. non-dried pure NC and returned a p-value = 0.064. This shows the difference is not significant if 5 % significance is required. Bartlett's test confirmed that the assumption of unequal variance was adequate. The effect of xanthan at 15 % addition is much larger in the dried-then-redispersed samples than in the non-dried samples.

Table 20: Effect of drying and xanthan addition on CNFs zeta potential.

Dried	Xanthan (%)	Zeta potential (mV)
Yes	0	-9.92 ± 0.85
	15	-18.78 ± 1.35
	25	-22.00 ± 2.03
	50	-22.22 ± 1.32
No	0	-7.11 ± 2.50
	15	-12.79 ± 0.99
	25	-13.48 ± 1.13
	50	-18.58 ± 1.52

The increase in the zeta potential from 15 % – 50 % xanthan in the dried-then-redispersed samples is minor in comparison with the non-dried samples. A two-sided t-test revealed a p-value of 0.86 for the dried 25% and 50% samples. One can infer the two samples are similar. These results indicate that the xanthan adheres, or interacts in some manner, to the surface of the CNF once dried, but not when not dried. The adherence, if true, is not removed by the ultrasonication. The ultrasonication might even be the cause. Another possible hypothesis is sonochemistry, where ultrasonication creates reactive groups on the surface, which could alter the surface charge.

4.4.4 Viscosity

Figure 22 shows the shear thinning behaviour of pure NC and NC with xanthan, with the values of the dried-then-redispersed and non-dried samples averaged. The shear thinning behaviour is linear when shown on a log-log plot. This implies that the power law model of Equation 8 is suitable. The translucent bands around the lines represent 1 sd (standard deviation) from the mean. This represents the variance of the results from the three repeats. The pure CNF

samples, or Xan0, show considerably more variance than the rest, implying that the rheological properties are not well retained. All the samples containing xanthan have smaller variances.

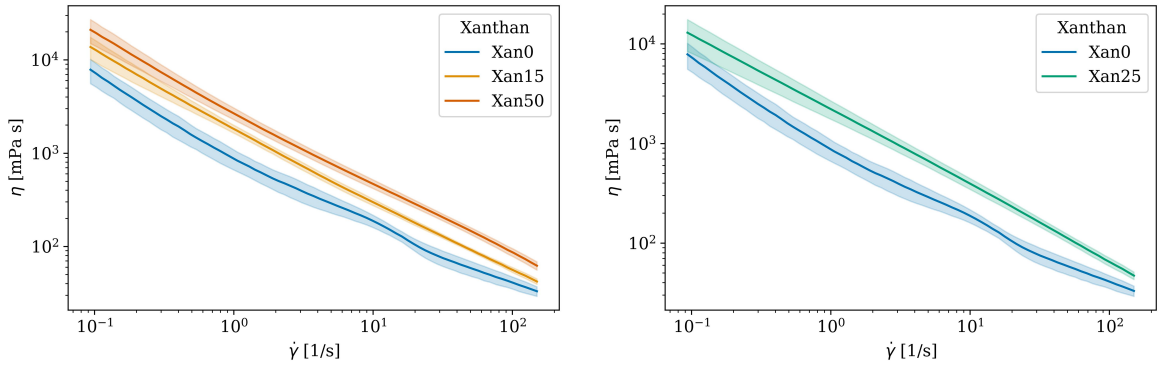

(a) 0 %, 15 % and 50 % Xanthan addition.

(b) 0 % and 25 % Xanthan addition.

Figure 22: Viscosity vs shear rate plots of CNF/xanthan suspensions.

Figure 23 gives the linear fit of one of the repeats for both dried-then-redispersed and non-dried, with the linear fit done on the log transformation of the data according to Equation 9. There is considerable variation between the previously dried, pure CNF dispersion and the non-dried one, with much less difference in the other samples. The values of $\ln K$ and $n-1$ were obtained by fitting the values from $10^0\,s^{-1}$ – $10^2\,s^{-1}$ to Equation 10, and are shown in Table 21. The coefficients are shown with their 95 % confidence interval.

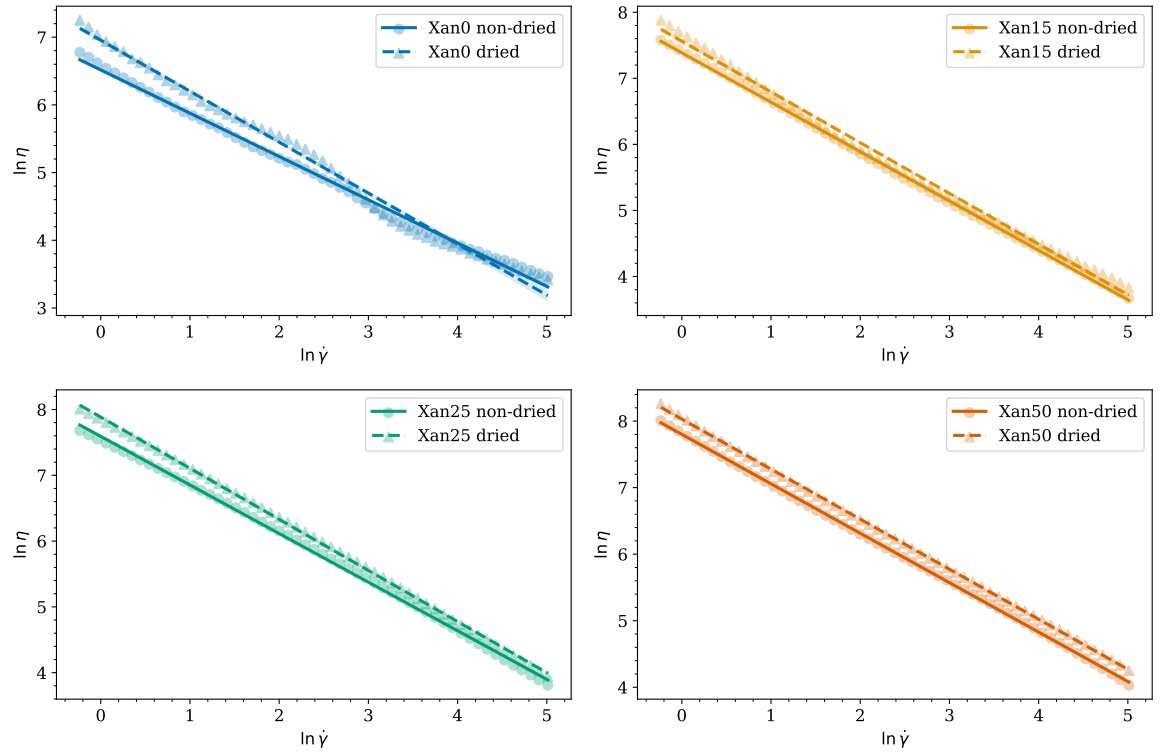

Figure 23: Linear fit of shear thinning behaviour of both previously dried and non-dried suspensions.

Table 21: Coefficients for a least-squares linear fit of Equation 10 to the viscosity data.

Coeff.	Xan0	Xan15	Xan25	Xan50
$\ln K$	6.920 ± 0.037	7.500 ± 0.018	7.856 ± 0.020	7.952 ± 0.016
α	-0.419 ± 0.052	-0.093 ± 0.025	-0.284 ± 0.028	-0.200 ± 0.022
$n-1$	-0.696 ± 0.013	-0.751 ± 0.006	-0.782 ± 0.007	-0.744 ± 0.005
β	0.059 ± 0.018	0.002 ± 0.009	0.033 ± 0.010	0.015 ± 0.008

All the α values are negative, showing that the viscosity is higher for previously dried dispersions. Nearly all the samples differ significantly between non-dried and previously dried dispersions, with almost all coefficients having p-values of 0.000. The only coefficient that did not is the β of Xan15, which is very near 0, and has a p-value of 0.688. This implies the difference in slopes between non-dried and dried are too small to say they are different. All β and α values are smaller for samples with xanthan than without. This suggests that the inclusion of xanthan allows more of the rheological properties to be retained after drying. One can thus conclude that xanthan gum lowers agglomeration to a significant degree.

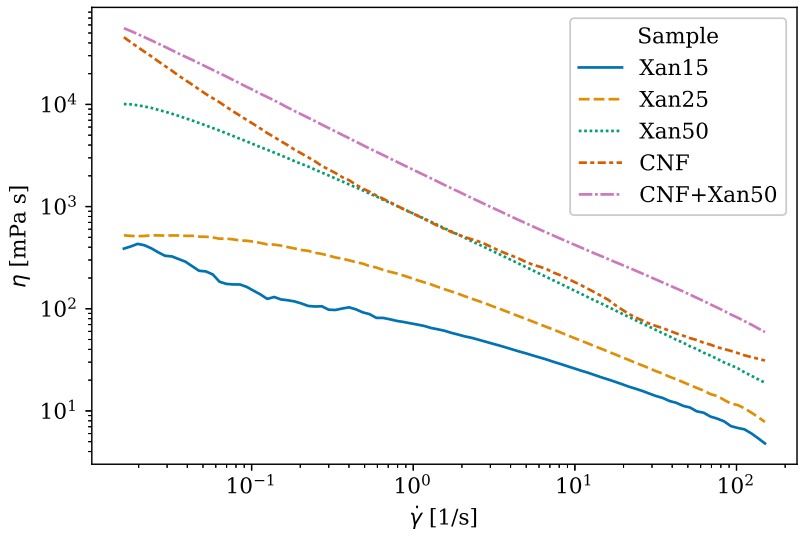

Figure 24: Viscosity of pure xanthan compared to CNF and CNF mixture.

Figure 24 and Table 22 both show information on the shear thinning behaviour of pure xanthan at the same concentrations as those in the CNF mixtures. The rheometer used is not well suited to measure low viscosities at very low shear rates; thus the jagged results for the 15 % xanthan solution. The Newtonian plateau that xanthan exhibits in the 25 % xanthan sample is visible. There is a very sharp increase in viscosity with the addition of xanthan. The K is on a logarithmic scale, thus a small increase in $\ln K$ means a very large increase in K itself. The increase in CNF viscosity when adding 15 % xanthan does not make clear sense when looking at the low viscosity of pure xanthan at the same concentration. A possible explanation for this is that the

xanthan gum does not gel at the 15 % concentration, but once added with the CNF it creates a gel structure, drastically increasing the viscosity. This is quite possible since xanthan was shown to have rheological interaction with other hydrocolloids (BeMiller, 2019: 264–265).

Table 22: Power law coefficients of Equation 9 for pure xanthan samples.

Xanthan (%)	$n-1$	$\ln K$
15	-0.523	4.404
25	-0.633	5.368
50	-0.760	6.761

4.4.5 SEM

Non-dried, ultrasonicated dispersion

Figures 25–29 show non-dried samples that were ultrasonicated. This is to illustrate the native state of the nanocellulose and the effect xanthan has on it. Note that the large crystals present in the figures are KNO_3 crystals. This is due to the fact that these samples are the same as those used for the zeta potential measurements.

Figure 25 shows CNFs in their native state. The fibres are well dispersed with minimal agglomeration. Pure xanthan is shown in Figure 26. This is, as far as we know, the first images of xanthan gum in its fibrous form. One will note it is quite similar in appearance to CNF, with the smoothness of the xanthan fibres being the only noticeable difference. What is also incredible is the rectilinear orientation of the xanthan fibres. This is likely due to the long persistence length of xanthan gum and gives insight into how xanthan fibres orient themselves within suspensions.

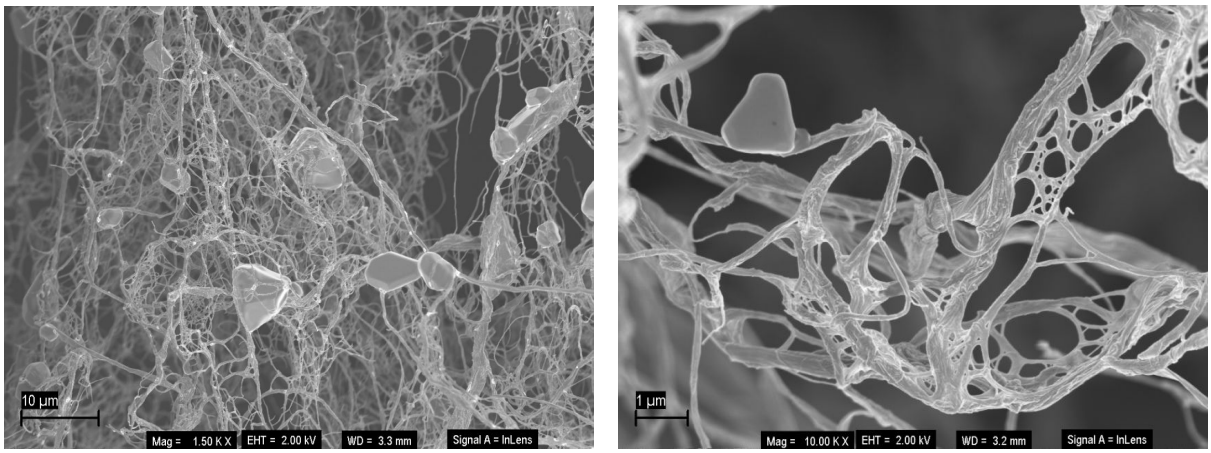

(a) 1500 times magnification **(b)** 10000 times magnification

Figure 25: SEM of ultrasonicated non-dried pure nanocellulose.

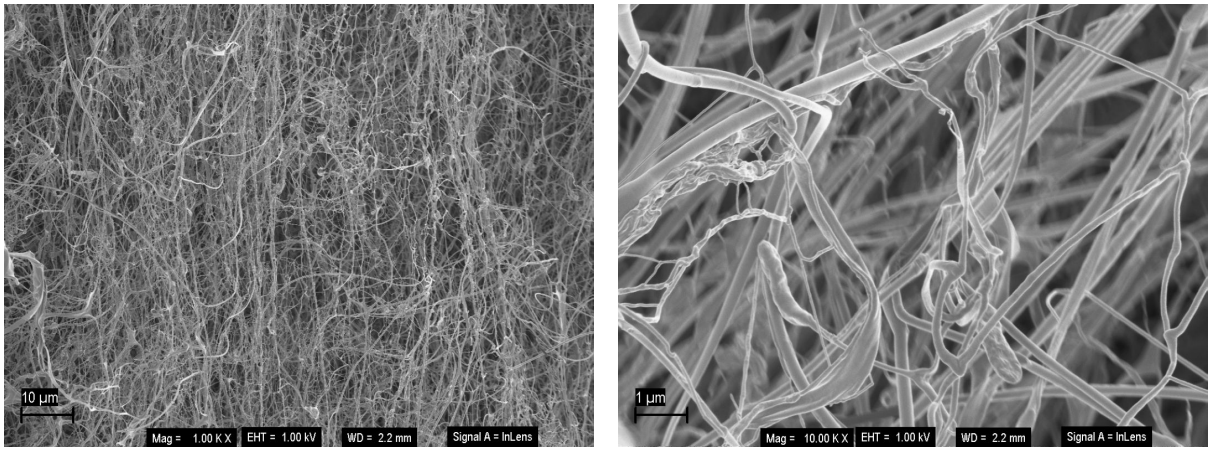

(a) 1000 times magnification **(b)** 10000 times magnification

Figure 26: SEM of pure xanthan gum.

Figure 27, Figure 28, and Figure 29 show how increasing the xanthan concentration relative to the CNF affects the structure. A large amount of entanglement is noticeable; not agglomeration per se, but interweaving between the fibres. It is suspected that the xanthan gum and CNF interlaces with one another. This is most prominent in the 50 % xanthan sample, Figure 29, where it appears as if the fibres are being glued together. This alludes to the interaction effects seen with xanthan gum and other hydrocolloids. The fibres vary in size. The CNFs were estimated to be between 75 nm – 300 nm in size, with the majority being on the lower end at about 125 nm – 150 nm. The size was estimated using pixel measurements of the images.

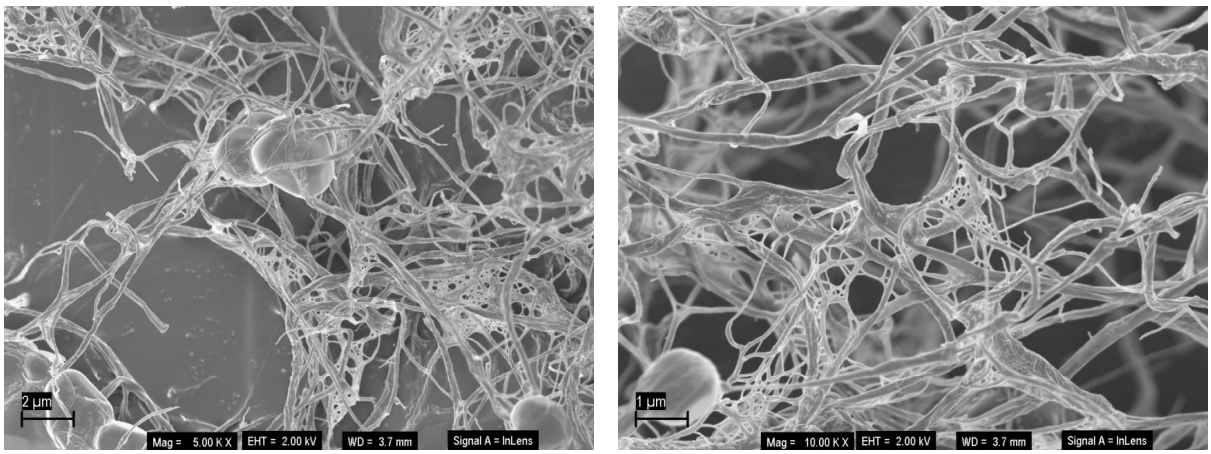

(a) 5000 times magnification **(b)** 10000 times magnification

Figure 27: SEM of ultrasonicated non-dried nanocellulose with 15 % xanthan.

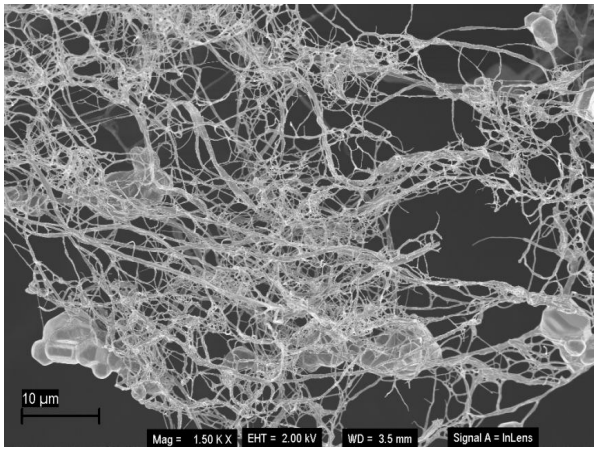

(a) 1500 times magnification

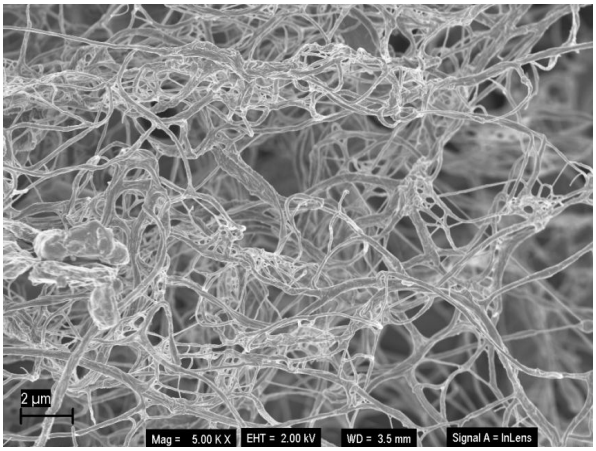

(b) 5000 times magnification

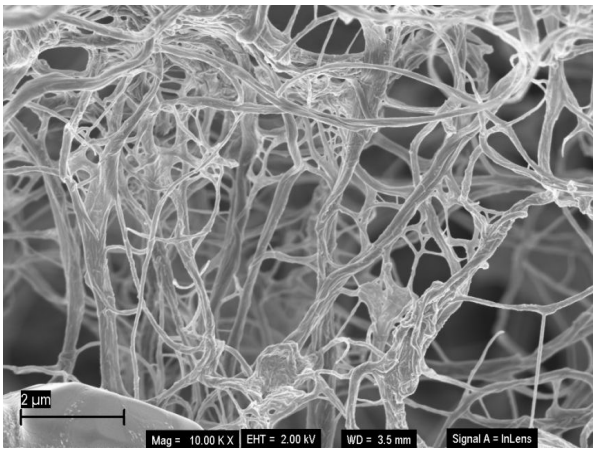

(c) 10000 times magnification

Figure 28: SEM of ultrasonicated non-dried nanocellulose with 25 % xanthan.

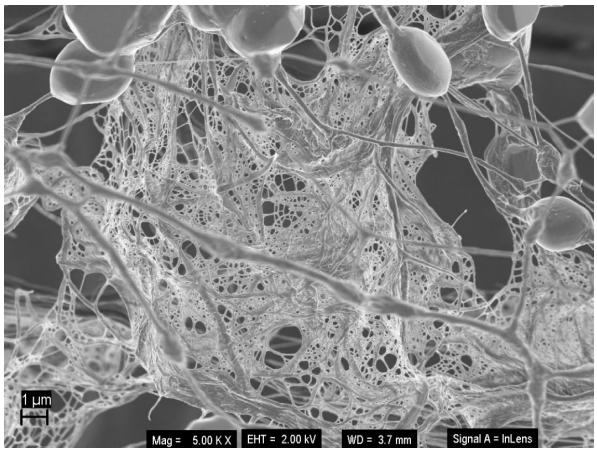

(a) 5000 times magnification

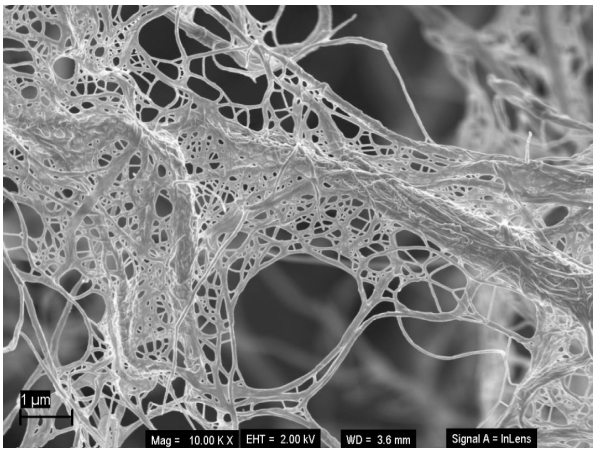

(b) 10000 times magnification

Figure 29: SEM of ultrasonicated non-dried nanocellulose with 50 % xanthan.

Dried samples redispersed with ultrasonication.

Figure 30 proves that the ultrasonication is intense enough to redisperse the dried NC fibres.

Notice the broken points on the fibres. It is suspected that ultrasonication, being such a harsh redispersion method, broke the fibres at the interlinking points. This phenomenon could influence the characteristics of the CNFs, though to what extent is not certain.

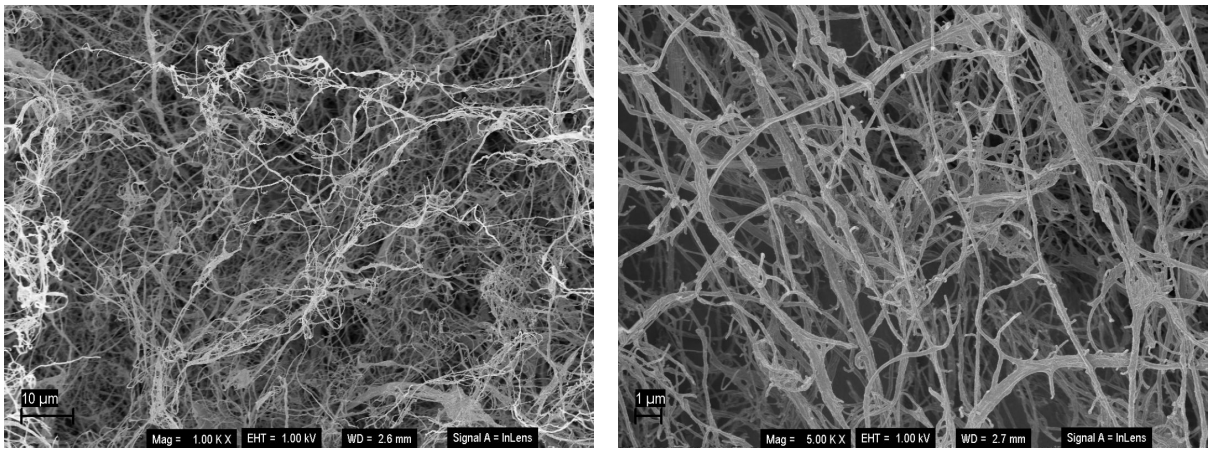

(a) 1000 times magnification **(b)** 5000 times magnification

Figure 30: SEM of ultrasonicated dried, pure nanocellulose.

Dried samples redispersed with shear mixing.

The following figures are of the dried samples redispersed till B intensity, as discussed in Section 3.2.1.

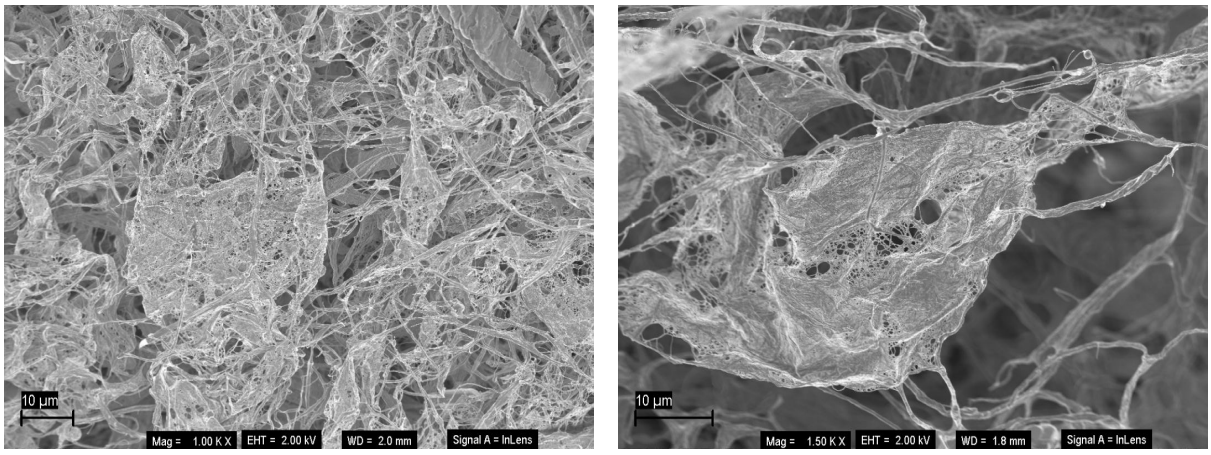

(a) 1000 times magnification. **(b)** 1500 times magnification.

Figure 31: SEM of mechanically mixed sample of pure nanocellulose.

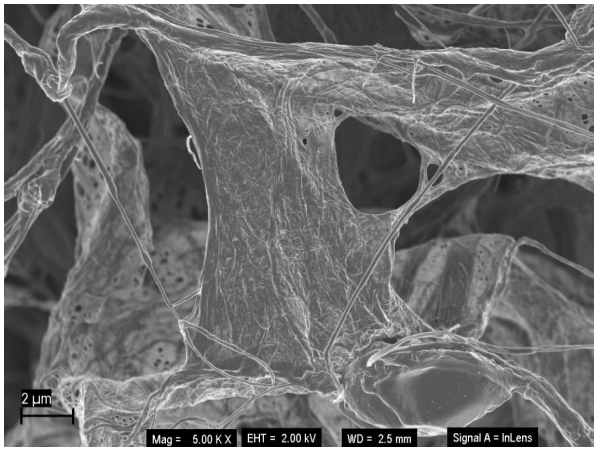

(c) 5000 times magnification.

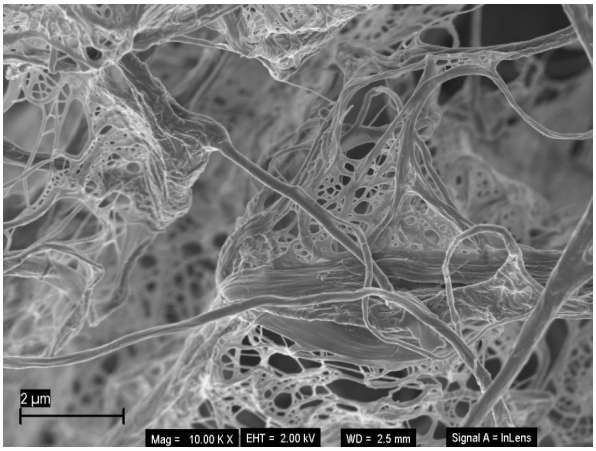

(d) 10000 times magnification.

Figure 31: SEM of mechanically mixed sample of pure nanocellulose.

In Figure 31, extreme agglomeration is apparent in pure, dried and redispersed nanocellulose. The high-shear mixing is ineffective at breaking the agglomerates. Even at ×1000 magnification, the agglomerates are clearly visible. This also speaks to the intensity of ultrasonication. These images support the trends seen in the turbidity results shown in Figures 41a and 41b.

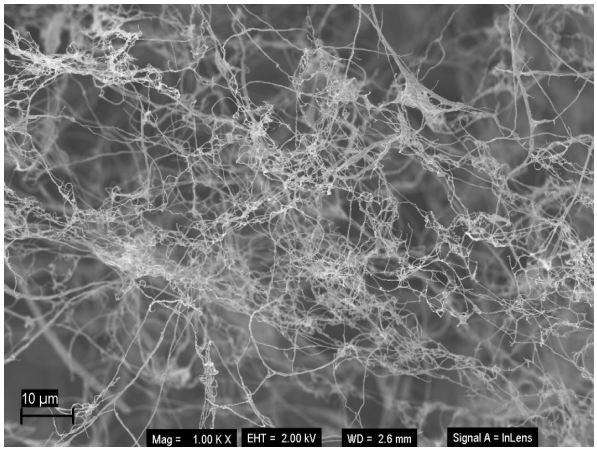

(a) 1000 times magnification

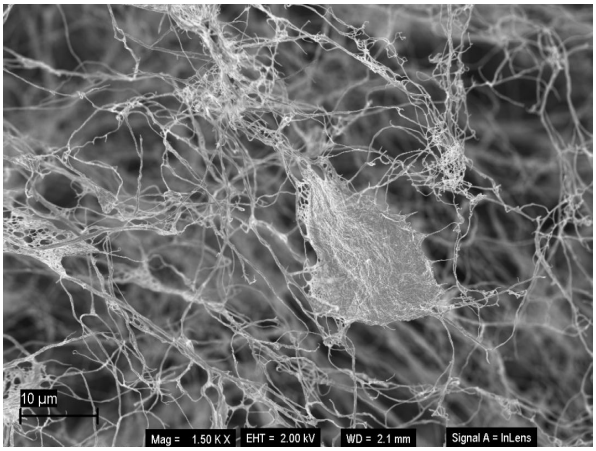

(b) 1500 times magnification

Figure 32: SEM of mechanically mixed sample of nanocellulose with 15 % xanthan.

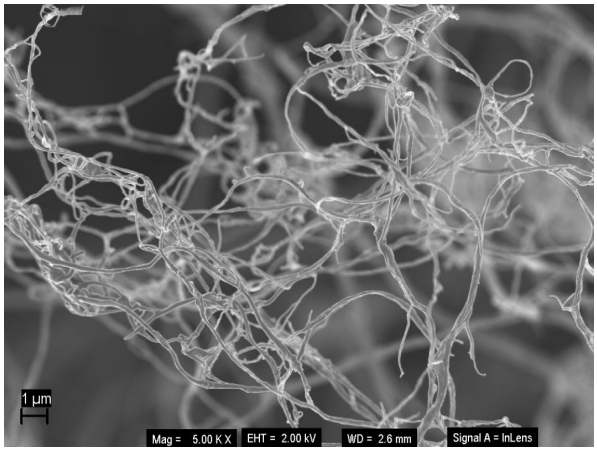

(c) 5000 times magnification

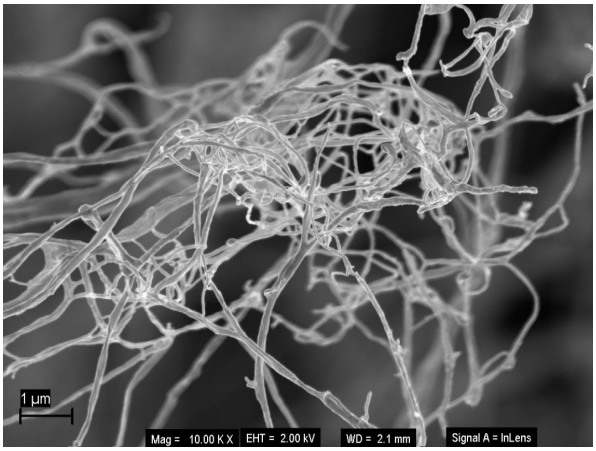

(d) 10000 times magnification

Figure 32: SEM of mechanically mixed sample of nanocellulose with 15 % xanthan.

Figure 32 shows marked improvement in the redispersion of nanocellulose, supporting the hypothesis that xanthan is effective at reducing interfibril agglomeration. Some agglomerates are still visible (Figure 32b) but the degree of agglomeration is considerably less. It also seems as if the fibres are less entangled.

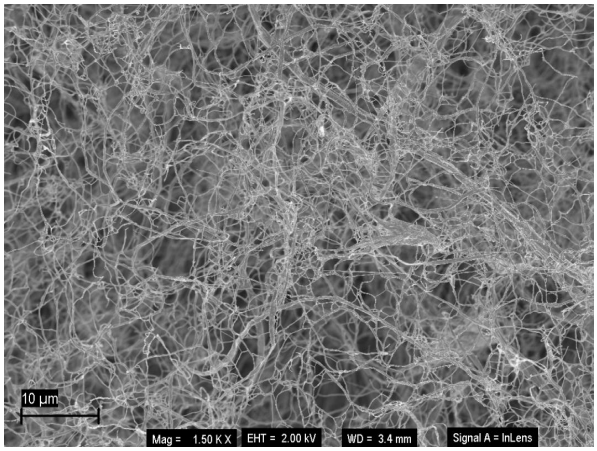

(a) 1500 times magnification

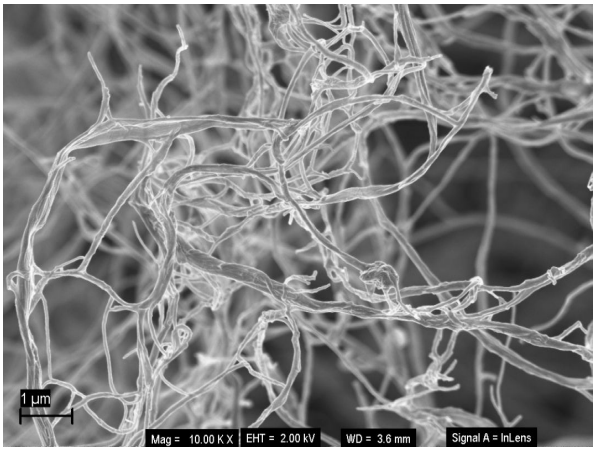

(b) 10000 times magnification

Figure 33: SEM of mechanically mixed sample of nanocellulose with 25 % xanthan.

The addition of 25 % xanthan proved to give the best redispersion, as shown by Figure 33. No large agglomerates are visible, supporting the hypothesis that xanthan can allow effective redispersion of nanocellulose with mechanical mixing alone. The Figures show that one can redisperse the CNFs back to individual fibre form. This also supports the turbidity results, shown in Figures 41a and 41b, where X25 seemed to have the best results.

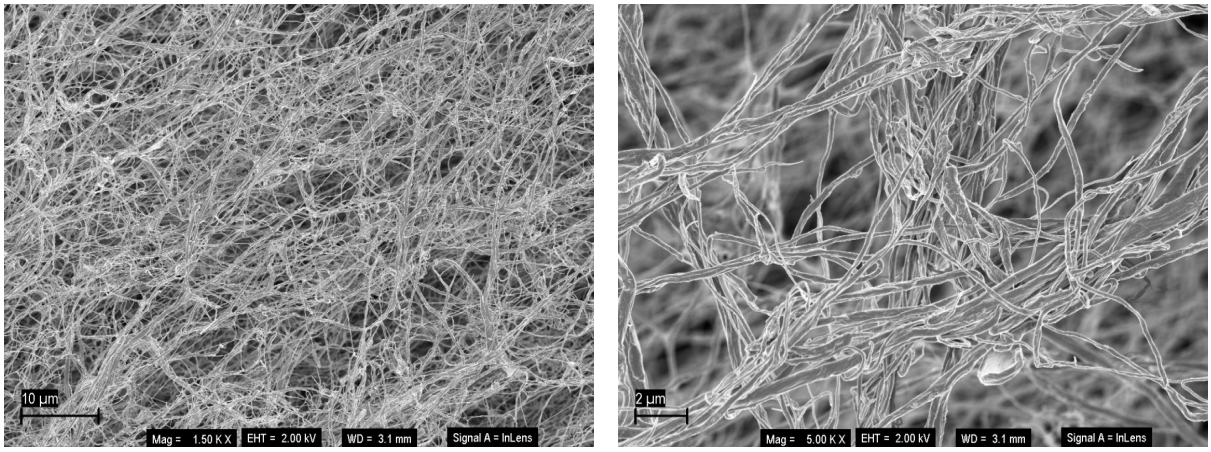

(a) 1500 times magnification **(b)** 5000 times magnification

Figure 34: SEM of mechanically mixed sample of nanocellulose with 50 % xanthan.

The entanglement is once again visible at 50 % xanthan addition. Figure 34 shows that, though redispersion is appreciable, the same observation of fibre bundling is apparent as shown in Figure 29.

These images provide undeniable evidence that xanthan gum addition is effective at limiting agglomeration between CNFs. Xanthan gum allows full redispersion of previously dried CNFs with shear mixing alone, even to the same extent as ultrasonication.

4.4.6 Turbidity

The turbidity tests concern the change in absorbance/turbidity with wavelength due to the diameter of the fibres. Figure 35 shows the relationship between τ, the turbidity, and λ, the wavelength, on a log-log scale. There is a strong linear relationship. Note also the increase in the width of the bands, which represent 1 sd, as the wavelength increases. This implies that a log transformation may not be the best transformation for the data. The slope of this line is -1.64, a far cry from the -3 one would expect if Equation 11 was true. Figure 36 further illustrates that Equation 11 is inappropriate, as the correlation between τ and $1/\lambda^3$ is not linear.

Figure 37 shows that Equation 12 is more appropriate, as the correlation between $1/\lambda^2$ and $c/(\tau\lambda^3)$ is nearly linear, with little increase in variance across the range. This implies that the μ is quite large. This stands in contrast with Figure 38, where Equation 13 does not show a linear relationship, nor a constant variance. This brings the applicability of Equation 13 into question.

Figure 39 and Figure 40 show the size parameters determined via the Carr-Herman equation, Equation 12, and the Yeromonahos equation, Equation 13, respectively. The error bars in the figures show the 95 % confidence interval. The SEM images in Section 4.4.5 show that the

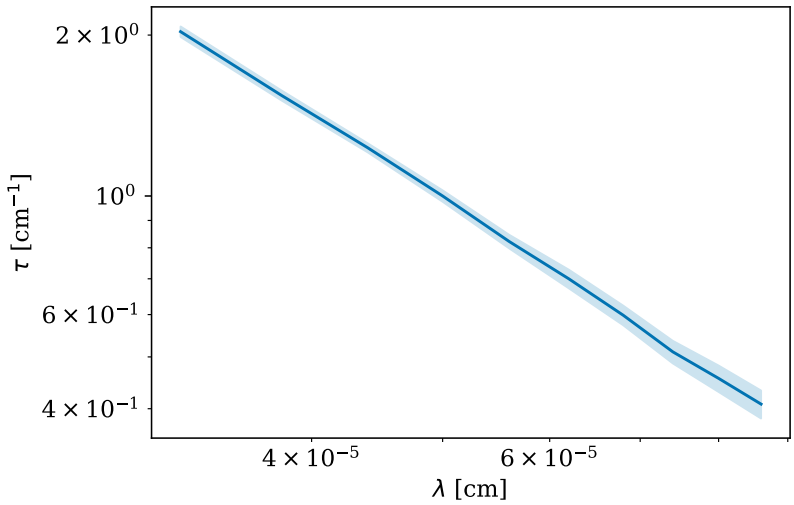

Figure 35: Log-log plot showing the relationship between τ and λ of a pure CNF sample.

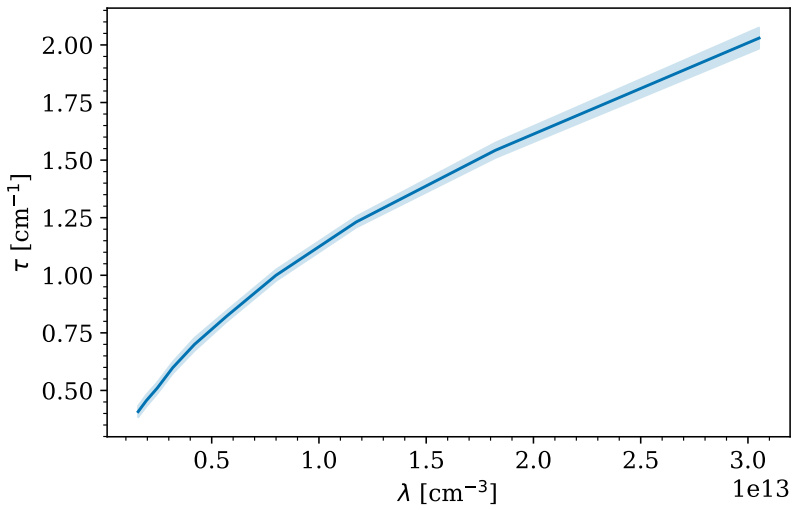

Figure 36: Visual representation of the curve used for Equation 11 done on a pure CNF sample.

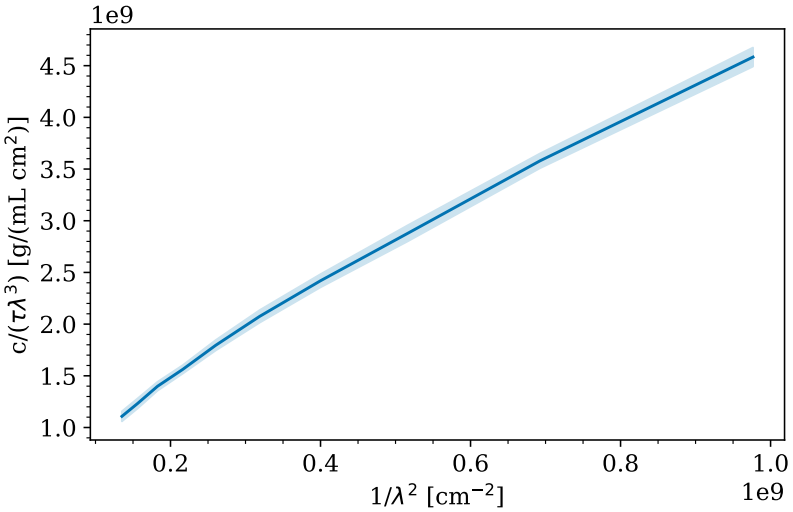

Figure 37: Visual representation of the curve used to fit Equation 12 of Carr & Hermans (1978), done a pure CNF sample.

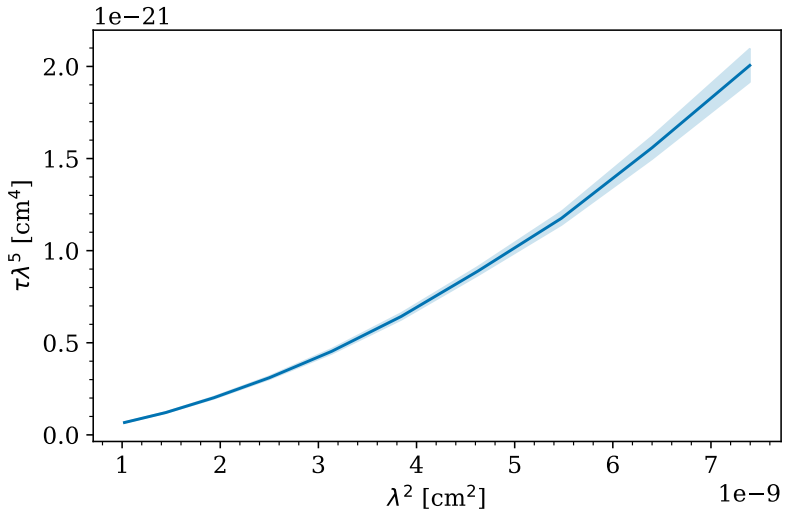

Figure 38: Visual representation of curve used to fit Equation 13 of Yeromonahos, Polack & Caton (2010), done a pure CNF sample.

assumption that $d << \lambda$ is not appropriate, as the majority of the fibres have diameters larger than 100 nm. The Yeromonahos equation should thus, in theory, be the most accurate equation. The linear correlation observed with the Carr-Herman equation might just be coincidental.

The Yeromonahos equation indeed does give the most accurate d estimation, if the SEM images are representative of the general samples. The Carr-Herman equation places the d around 260 nm. The Yeromonahos equation places it at 147 nm, much closer to that observed in the SEM images. There is a general trend that the d increases with xanthan addition. The entanglement phenomena could be to blame for that, creating bundles that seem like large fibres. The μ increases with xanthan addition, but then suddenly drops at X50. The confidence interval is very large for the X50 sample, so the drop is not that significant. More accurate sizing needs to be done, such as with atomic force microscopy, to confirm the accuracy of this method.

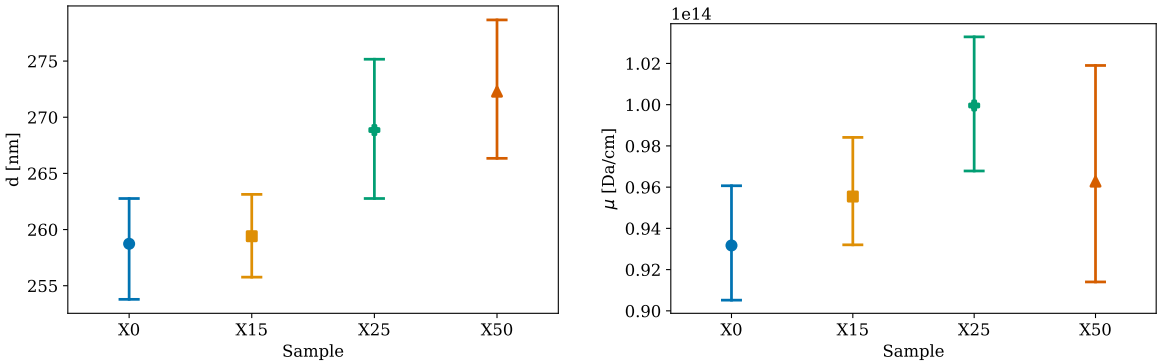

(a) Carr-Herman d.

(b) Carr Herman μ.

Figure 39: Size parameter estimates of non-dried, ultrasonicated estimated with the Carr-Herman equation (Equation 12).

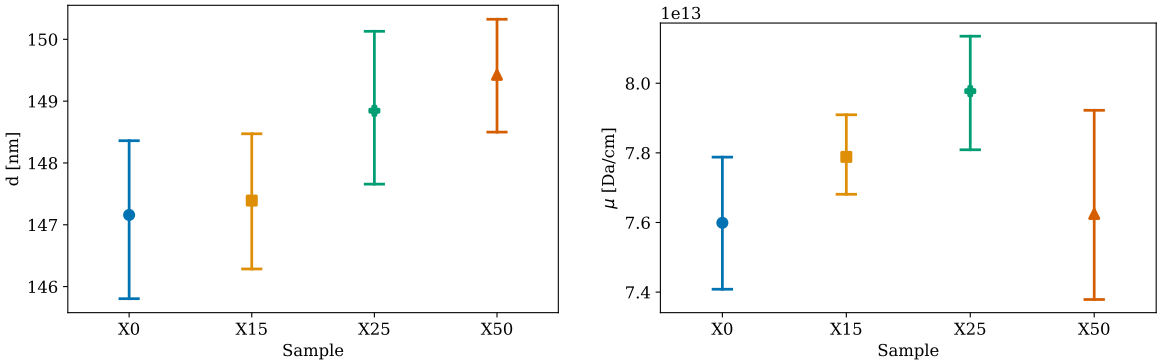

(a) Yeromonahos d.

(b) Yeromonahos μ.

Figure 40: Size parameter estimates of non-dried, ultrasonicated samples done with the Yeromonahos equation (Equation 13).

Figure 41 and Figure 42 show the change in size parameters with mixing intensity using the Carr-Herman equation and the Yeromonahos equation, respectively. The estimated size param-

eters for the X0 samples show a marked decrease going from L to U in all the figures. This supports Equation 3; the particle size decreases as the mechanical energy applied increases. All samples with xanthan show much lower size parameters at low shear rates. This suggests that xanthan gum limits the interfibril bonds between CNFs; thus less shear force is required to separate the fibres.

X0's d starts at 154.9 nm for L and ends at 147.4 nm for U according to the Yeromonahos equation (Figure 42a). The X15 sample in comparison goes from 149.2 nm (L) to 147.5 nm (U). The shift in sample X15 is almost negligible and is probably due to small amounts of CNFs that were in close proximity that could then agglomerate. X0 shows a considerable decrease. The estimated d of X25 sample for B and U is 147.0 nm, exactly the same, whereas there is a clear difference when looking at X0, with its B sample's d being 149.0 nm. This suggests that when one adds xanthan similar degrees of particle separation can be achieved via shear mixing than with ultrasonication. The same does not hold true when xanthan is absent.

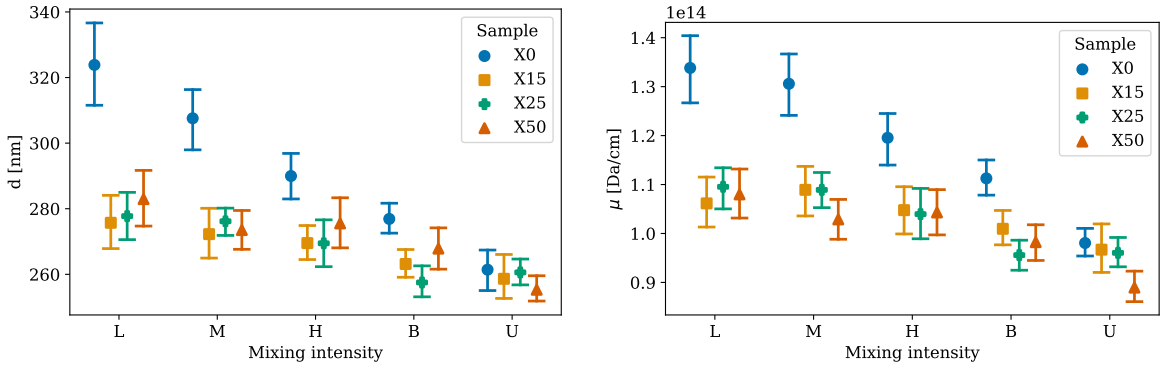

(a) **(b)**

Figure 41: Size parameters determined using Carr-Herman (Equation 12).

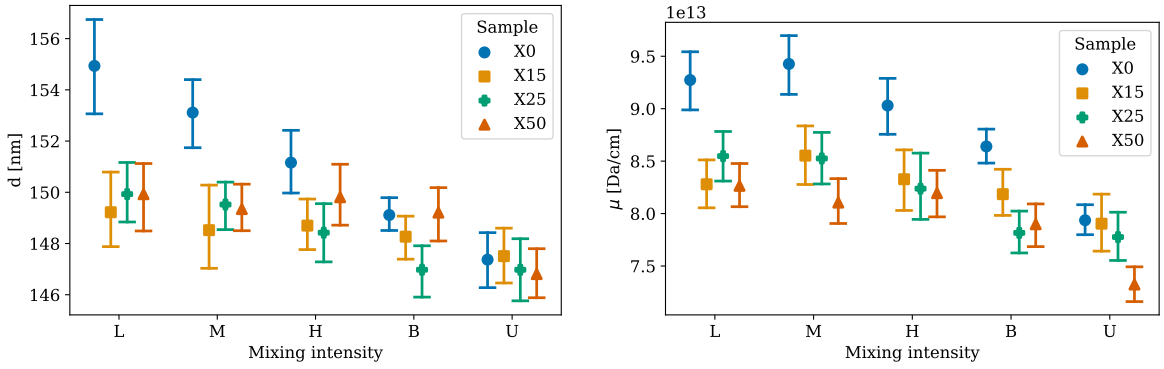

(a) **(b)**

Figure 42: Size parameters determined using the Yeromonahos equation (Equation 13).

The μ value estimates of the Yeromonahos equation do seem quite questionable, following a less clear trend than its counterpart, the Carr-Herman equation. If the assumption that the fibres

are cylinders is true, one would expect $d^2 \propto \mu$. Figure 43 is a scatter plot with a linear fit of sample X15's d^2 and μ. The bands indicate the 95 % confidence interval. Figure 43a is done using the Carr-Herman equation and has a strong linear correlation between d^2 and μ. This is not true for the Yeromonahos equation, as shown in Figure 43b, where the variance is much larger. The R^2 for the Carr-Herman equation is 0.817, whereas for the Yeromonahos equation, it is 0.396. This does bring into question the validity of the Yeromonahos equation.

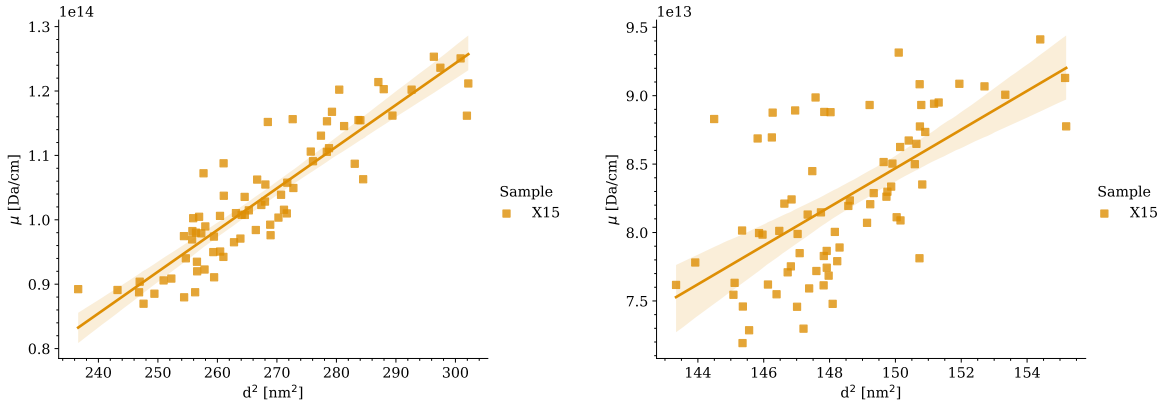

(a) Carr-Herman **(b)** Yeromonahos

Figure 43: Linear fits of d vs μ of both models.

The assumption that all the particulates are infinitely long cylinders is not valid. The X0–B sample, shown in Figure 31, are more like large plates, not fibres. The size parameters' accuracy are thus questionable. Nonetheless, the method does prove promising for estimating difference in the degree of agglomeration.

4.4.7 Specific surface area

Previous works used the original Langmuir adsorption isotherm (Equation 14) to determine $q_{\max}$. Figure 44 and Table 23 illustrate the non-linear curve-fitting of the Langmuir isotherm (Equation 14) to the adsorption data of the dried-then-redispersed and non-dried samples. One will note that in Figure 44a and Figure 44b that the original Langmuir isotherm does not fit the data well, plateauing too early. This brings to question the suitability of the Langmuir isotherm for modelling the adsorption of Congo red onto nanocellulose. Freundlich (Equation 15), shown in Figure 44c and Figure 44d, shows quite a good fit, suggesting that the surface of the CNF and xanthan might be heterogeneous. Freundlich, unfortunately, is an empirical equation, and thus offers no further information.

The best results are obtained using the modified Langmuir isotherm (Equation 16), shown in Figure 44e and Figure 44f. This is to be expected as it has an extra parameter to fit, increasing its variance. Table 23b shows the coefficients determined by the bootstrap method for Equation 16.

None of the q_H terms has a p-value above 0.04, suggesting that the q_H terms are significant. The k-fold cross-validation results are shown in Table 24. For all the samples, except those with 50 % xanthan, the RMSE is considerably less, implying that the hydrophobic term does not cause over-fitting. The difference in RMSE decreases with increasing xanthan concentrations, suggesting that xanthan gum's effect on the adsorption is not well captured by the modified Langmuir model.

Investigating the parameters revealed an interesting quirk. The modified Langmuir tended to overestimate the $q_{\max}$ values for certain fits where it was visually obvious they should be lower than reported. It was decided to investigate the significance of the K_L term. If one were to assume that the adsorption-desorption kinetics for all samples are the same, which they nearly are, one can correct for the $q_{\max}$ value discrepancy, allowing for a more realistic fit. The results are shown Figure 44g and Figure 44h. The fixed K_L-model is referred to as LangmuirK. Table 23 reveals that fixing the K_L for all the fits does not influence the accuracy of the regression by much. It was thus concluded that fixing the K_L values as equal for all regressions, thus decreasing the variance, is a worthwhile trade-off for the increase in robustness.

Table 26 shows the estimated specific surface area of the fits and reveals two things: the specific surface area decreases with increasing xanthan concentration, and there is no noticeable difference between the dry and wet samples. These samples were, unfortunately, all ultrasonicated. This explains why all the SSAs are the same. A test was then done on all the samples made in Section 3.2.1, and the results revealed nothing conclusive. The differences between mixing intensities had no discernible pattern. The theory is that the long incubation could be at fault. The samples were left for ≈24 h, as time constraints prevented the test from being done on the same day. The works on which the test is based used a time horizon of 6 h. It could be possible that kinetics are at play, as the SSA revealed by our study is considerably higher than that of the other papers. The SSA found of the pure CNF is on the high end, but such high values have been reported by other authors, with values of 430 $m^2\,g^{-1}$ and 386 $m^2\,g^{-1}$ reported (Ketola *et al.* 2019; Moser, Henriksson & Lindström, 2016). Kwak *et al.* (2019) reported a SSA of 251 $m^2\,g^{-1}$ for CNFs using Congo red adsorption with the Langmuir adsorption isotherm.

Despite the unfortunate shortfall of the test, at least an interesting observation was made regarding the appropriate adsorption isotherm . It is not certain whether Congo red is a suitable test to assess the degree of agglomeration and redispersion. If the test were to be used, the author would suggest to rather do a kinetic study.

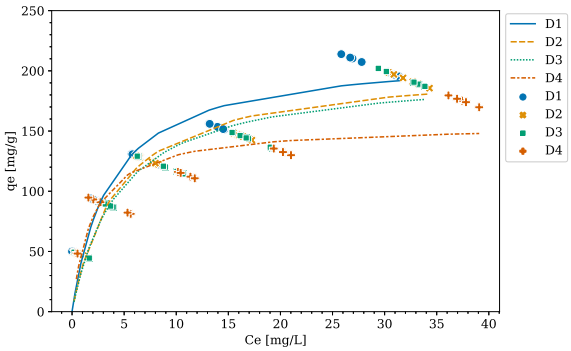

(a) Langmuir D

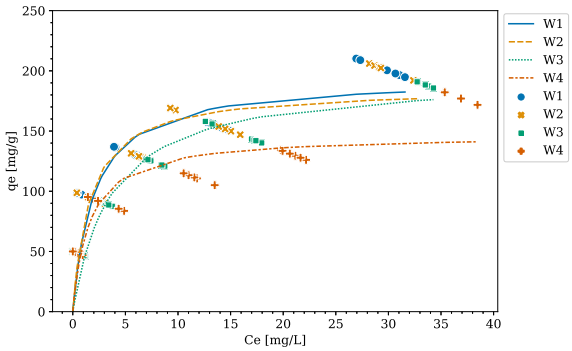

(b) Langmuir W

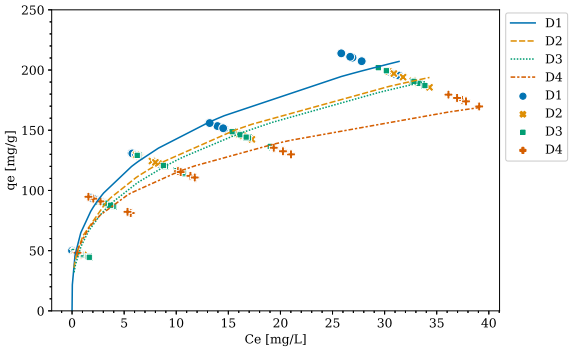

(c) Freund D

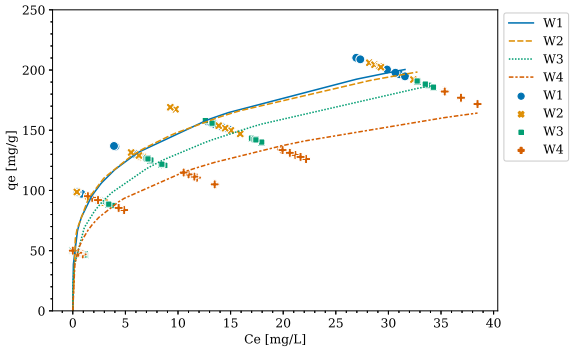

(d) Freund W

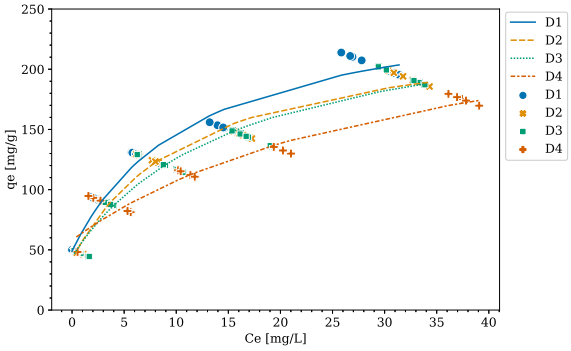

(e) Langmuir2 D

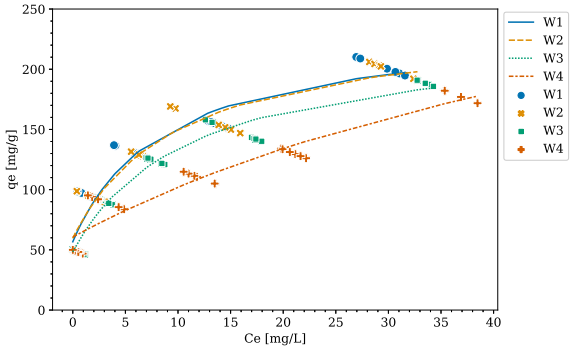

(f) Langmuir2 W

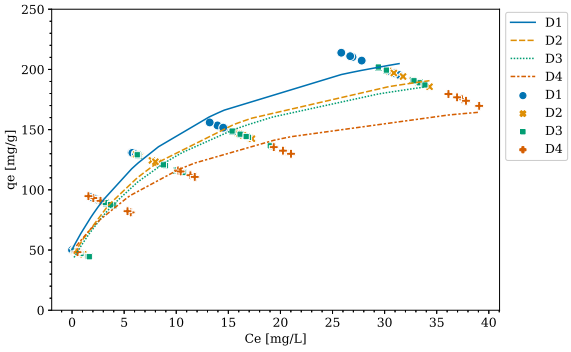

(g) LangmuirK D

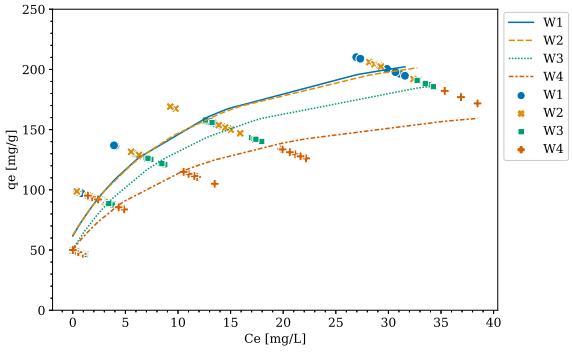

(h) LangmuirK W

Figure 44: Regressions of various adsorption models on the Congo red adsorption results.

Table 23: Coefficients for Langmuir and Langmuir2 with their standard deviation determined through bootstrapping.

(a) Langmuir coefficients.

	D1		D2		D3		D4	
	mean	sd	mean	sd	mean	sd	mean	sd
q_{max}	214.1	10.4	202.6	9.2	199.2	11.8	158.7	14.2
K	0.278	0.047	0.238	0.043	0.229	0.053	0.514	0.208
	W1		W2		W3		W4	
	mean	sd	mean	sd	mean	sd	mean	
q_{max}	193.5	12.4	186.0	17.8	194.6	8.3	149.2	13.2
K	0.563	0.243	0.884	0.585	0.279	0.047	0.642	0.221

(b) Langmuir2 coefficients.

	D1		D2		D3		D4	
	mean	sd	mean	sd	mean	sd	mean	sd
q_H	49.1	4.9	41.5	4.4	44.1	7.1	58.0	7.4
q_{max}	214.0	17.2	197.7	11.8	215.5	29.7	230.1	55.6
K	0.087	0.019	0.089	0.018	0.068	0.027	0.033	0.030
	W1		W2		W3		W4	
	mean	sd	mean	sd	mean	sd	mean	sd
q_H	57.1	7.4	59.9	6.7	48.3	4.5	59.9	7.5
q_{max}	181.1	14.4	182.8	15.0	179.9	8.9	343.7	113.5
K	0.117	0.034	0.101	0.028	0.092	0.015	0.026	0.069

Table 24: RMSE of k-fold cross validation for Langmuir and Langmuir2 for each sample.

Sample	D1	D2	D3	D4	W1	W2	W3	W4
Langmuir	21.5	24.3	26.3	34.5	23.8	26.5	24.2	38.9
Langmuir2	13.0	17.2	20.5	34.3	11.8	11.7	16.9	37.5

Table 25: Sum squared error of Langmuir2 with the K varied and Langmuir2 if the K is fixed for all fits.

Sample	D1	D2	D3	D4	W1	W2	W3	W4
Langmuir2	3764.0	2636.0	5046.0	3411.0	5552.0	6083.0	3097.0	4568.0
LangmuirK	3785.0	2669.0	5108.0	4362.0	5896.0	6242.0	3157.0	6131.0

Table 26: Total specific surface area of each sample calculated of the sum of q_H and $q_{\max}$ of LangmuirK.

Sample	D1	D2	D3	D4	W1	W2	W3	W4
SSA ($m^2\ g^{-1}$)	400.8	367.3	359.2	302.9	387.8	382.7	354.5	292.6

4.4.8 Sedimentation

Sedimentation tests were done to assess the colloidal stability of the CNF/xanthan dispersions at various mixing intensities, shown in Figures 45–49. The impact of different mixing intensities on pure nanocellulose is shown in Figures 45a–45d. The L and M samples sediment very early on, with the L sample showing more condensed sediment. H and B show sedimentation after 1 h, with H showing a clearer bed than B. After a full day, all samples have sedimented. This shows that pure, dried CNF is not colloidally stable when redispersed, no matter the method.

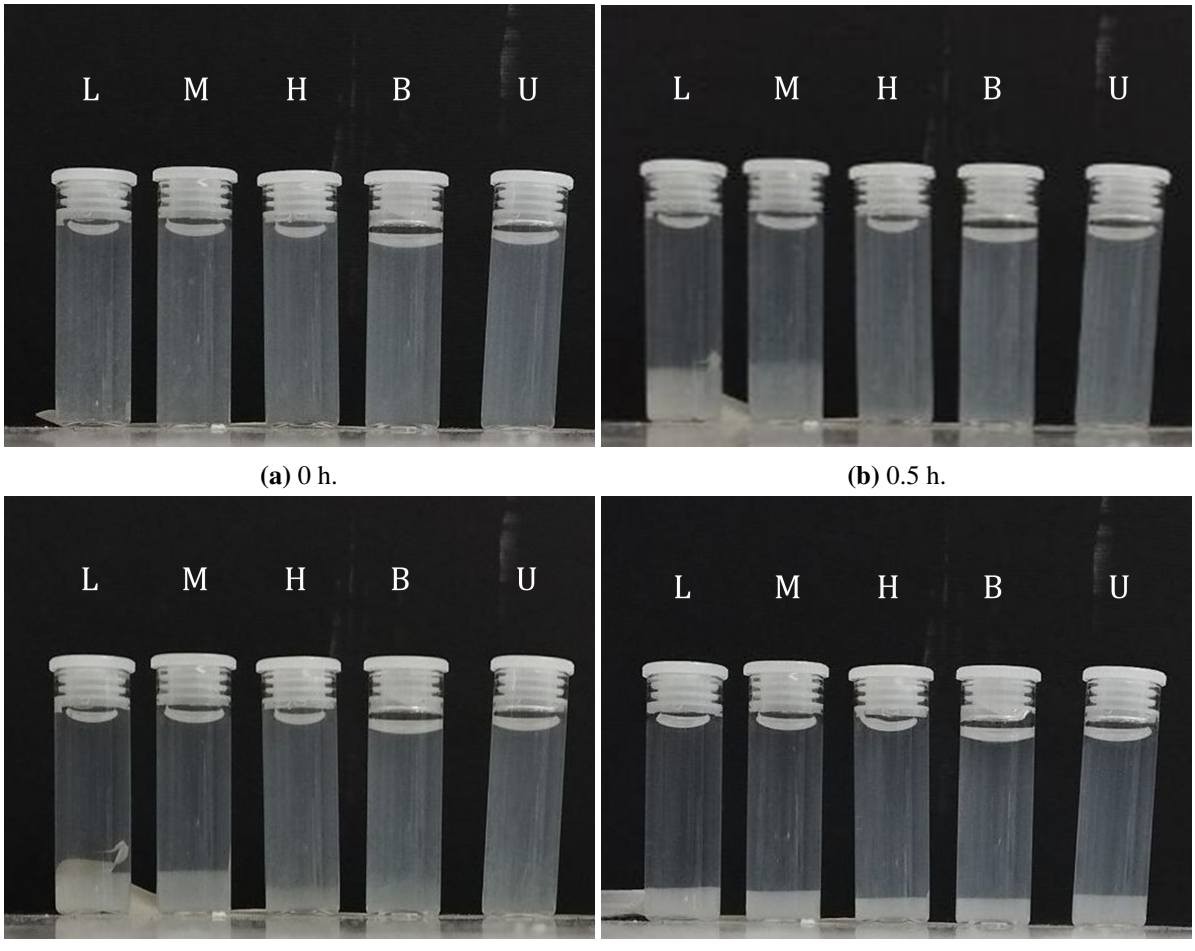

(a) 0 h. **(b)** 0.5 h.

(c) 1 h **(d)** 24 h.

Figure 45: Sedimentation analysis of pure, dried CNF samples with various mixing intensities.

The addition of xanthan has a marked effect. Only X15-L shows early sedimentation, as shown in Figures 46a–46c. The other X15 samples only showed very slight sedimentation after a full

day. The X25 samples, Figures 47a– 47c, and X50 samples, Figures 48a– 48b, showed no significant change after 24 h.

There are two causes for this: the higher ease of particle redispersion with xanthan, as shown in Section 4.4.6, and the higher zeta potential due to xanthan gum addition, as shown in Section 4.4.3. Larger particles tend to sediment more readily, as they have a lower aspect ratio and thus less relative interaction with other molecules to make a stable suspension. The higher the surface charge, and the higher the interaction surface, the more difficult it is for particles to agglomerate, as postulated by the DLVO theory.

These results bring to light a recurring theme, that there is some interaction occurring with the xanthan and CNF upon drying. The close proximity during drying could allow xanthan to become like a surfactant. The xanthan could then coat the CNF and give it a much higher surface charge.

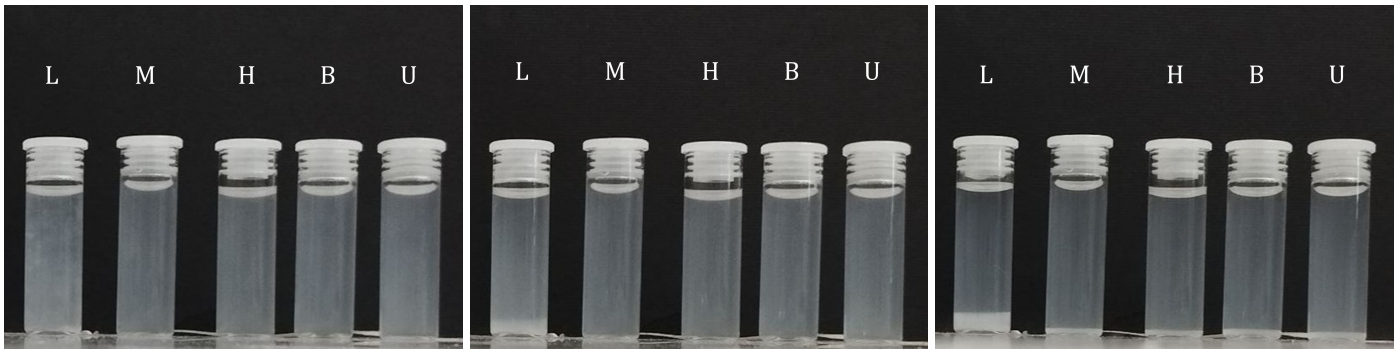

(a) 0 h. **(b)** 1.5 h. **(c)** 24 h.

Figure 46: Sedimentation analysis of X15 samples with various mixing intensities.

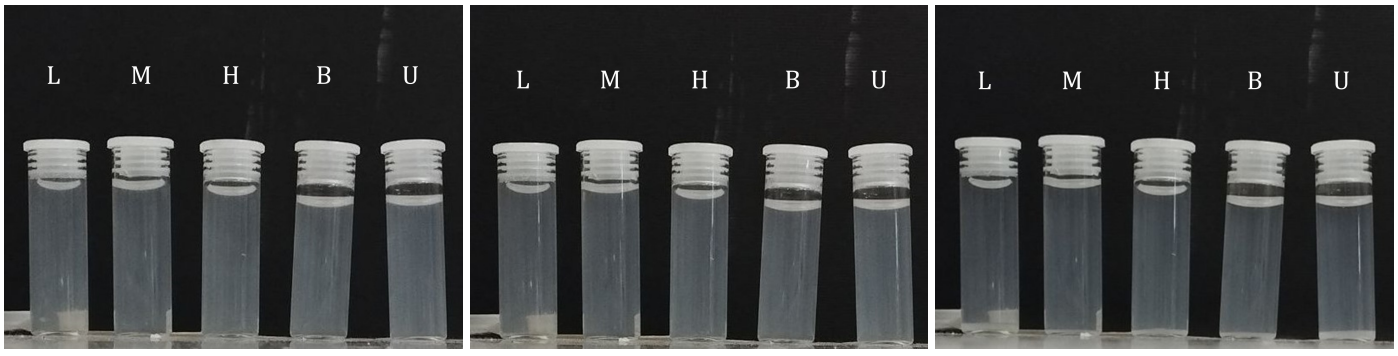

(a) 0 h. **(b)** 1.5 h. **(c)** 24 h.

Figure 47: Sedimentation analysis of X25 samples with various mixing intensities.

The non-dried, ultrasonically dispersed samples clearly show the distinction between adding xanthan and not adding xanthan. Figures 49a–49c show that the addition of xanthan reduces the tendency to sediment. The fact that all the non-dried dispersions sedimented after a day is interesting to note. This supports the observation that the previously dried dispersions had higher zeta potentials than the non-dried dispersions.

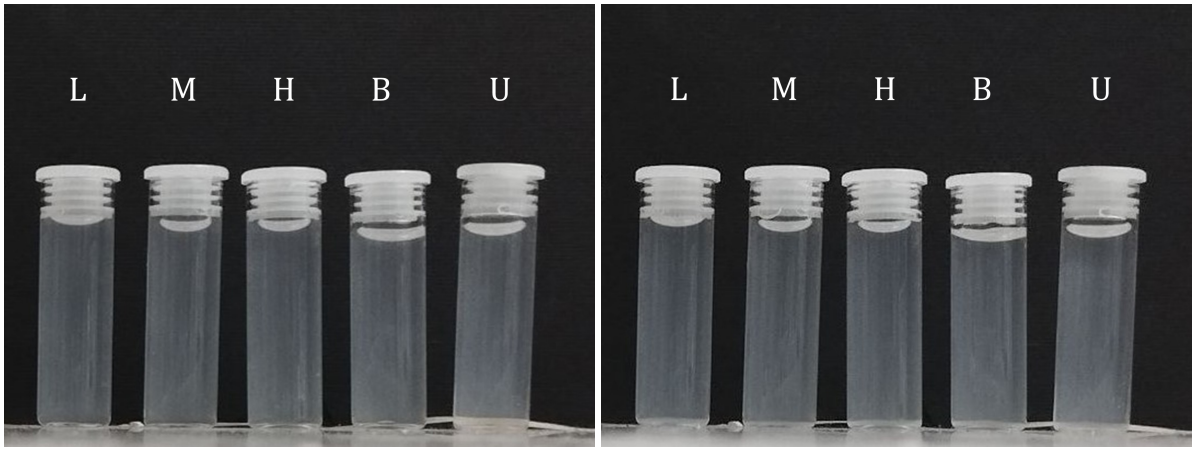

(a) 0 h. **(b)** 24 h.

Figure 48: Sedimentation analysis of X50 samples with various mixing intensities.

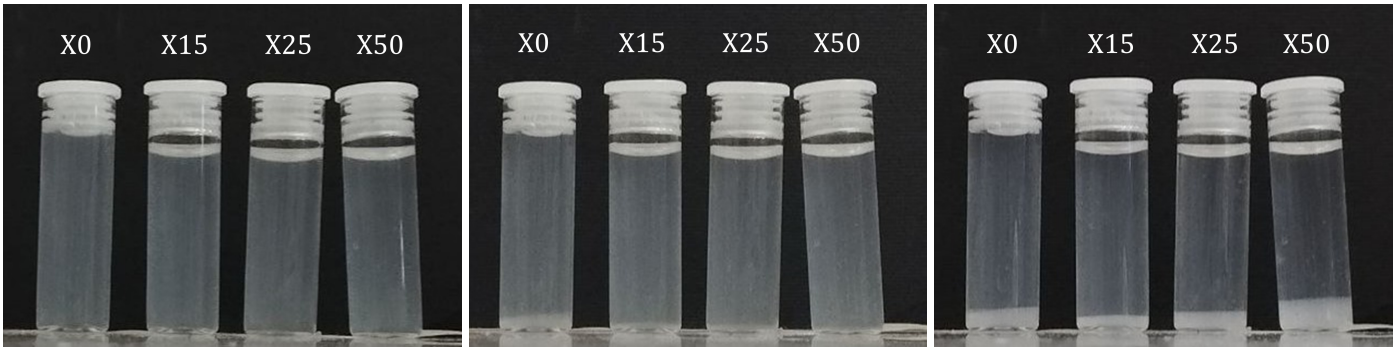

(a) 0 h. **(b)** 4 h. **(c)** 24 h.

Figure 49: Sedimentation analysis of non-dried samples with various mixing intensities.

4.5 Reinforcement of TPS with CNF/xanthan.

The stress vs. strain plots are shown in Figure 50. Note that the pure TPS was produced using the double-casting method as well. It is to ensure that the comparison between neat pure TPS and reinforced TPS is not affected by the casting method. It is surprising to see the double-casted pure TPS is stronger than any TPS sample that was single-casted (Table 18). This is an unexpected result, as one would expect the possible thermal degradation to lower the molecular mass of the polymer, weakening it. The average tensile strength, modulus and elongation for pure TPS, double-casted, are 5.4 MPa, 0.31 GPa, and 56.4 %, respectively.

The two TPS samples with only xanthan added are included in Table 12. At 1.25 phs (Low) addition, xanthan has a negligible impact on the TPS. With 2.5 phs xanthan addition (High), the effect is very noticeable, with a large decrease in elongation and an increase in tensile strength. The high xanthan TPS sample exhibited an average tensile strength, modulus and elongation of 9.6 MPa, 0.61 GPa, and 19.9 %, respectively. This alludes to a continuous network forming once there is enough xanthan, where the xanthan fibres can effectively interlink within the polymer matrix.

The NC sample in Figure 50 refers to the TPS with 5 phs non-dried CNF (+1). The tensile strength and increase in stiffness is significant, and is higher than all literature values at 5 phs addition shown in Figure 7. The NCXan sample in Figure 50 refers to the strongest sample in Table 28, the dried +1 CNF with 25 % xanthan. This sample shows a remarkable tensile strength of 23.0 MPa.

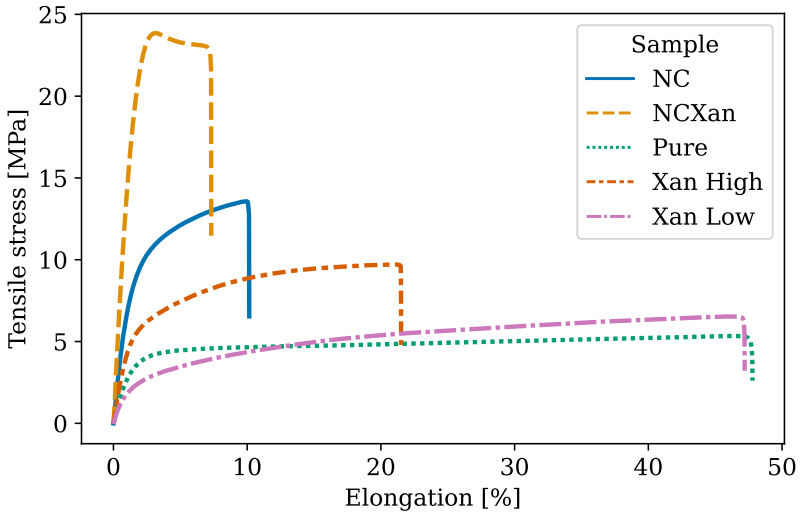

Figure 50: Stress-strain curves for pure, xanthan, CNF, and CNF/xanthan TPS samples with 30 phs glycerol stored at 54 % RH for 10 d – 14 d.

4.5.1 CCF results

Table 27 shows the results of the quadratic fit (Equation 18) of the CCF design laid out in Table 11. The Equation represented is shown below. The tensile strength shows a positive linear relationship with both CNF and xanthan. The quadratic terms are small and insignificant. CNF has the largest effect on tensile strength. There is a strong interaction term between the CNF and xanthan, showing synergism. An explanation for this relatively large interaction term is the highly interlaced network that forms when xanthan is added to CNF. The SEM images of pure xanthan and pure CNF, shown in the images in Figures 25 and 26, do not exhibit nearly as interlaced networks as when CNF and xanthan are combined, as shown in the images in Figures 27 and 28. The webbed network can allow for all the fibres to be interlaced within the matrix, allowing for stronger reinforcement as fibres act as one continuous phase.

$$\text{Tensile} = \text{Intercept} + \text{CNF} + \text{Xan} + \text{CNF} \times \text{Xan} + \text{CNF}^2 + \text{Xan}^2$$

Only the CNF term has more than 95 % significance for the tensile modulus. All other terms are small and insignificant. There is nearly no curvature to be found. As expected, CNF increases the stiffness of the polymer. All other terms, though small and statistically insignificant, are positive. This suggests that xanthan does contribute to the stiffness but more tests are needed for confirmation.

CNF has a strong effect on the elongation of the TPS, both in the linear and quadratic terms. The terms are negative, showing that CNF addition, especially at high loadings, decreases the elongation. One can note that the linear and quadratic CNF terms are of similar magnitude. This shows that the effect of CNF on elongation is actually very small at low loadings, but high at high loadings. Xanthan does not show any significant effects on the elongation. It is expected for CNF to decrease the elongation as it increases strength and stiffness.

Table 27: Quadratic fit of CCF design for all tensile response variables on 30 phs glycerol TPS stored at 54 % RH for 10 d – 14 d.

	Tensile strength		Tensile modulus		Elongation	
	coef (MPa)	p	coef (MPa)	p	coef (%)	p
Intercept	16.15 ± 0.94	0.00	1065 ± 97	0.00	7.79 ± 1.10	0.00
CNF	1.67 ± 0.65	0.00	146 ± 66	0.00	−1.41 ± 0.74	0.00
Xan	0.78 ± 0.65	0.02	33 ± 66	0.33	−0.50 ± 0.74	0.20
CNF:Xan	1.04 ± 0.78	0.01	62 ± 81	0.14	0.70 ± 0.92	0.14
Xan^2	0.75 ± 1.04	0.16	76 ± 106	0.17	0.16 ± 1.20	0.80
CNF^2	0.18 ± 1.04	0.73	45 ± 106	0.41	−1.25 ± 1.20	0.05

Figure 51 gives a visual representation of the fits done in Table 27, showing both the response curve and contour plots. The response curves are only of the terms that were at least 95 % significant. The interaction term from the tensile strength gives Figure 51a some curvature, as can be seen in the contour plot. One can note the interaction term by looking at the near linear lines at low NC loading and how they become more curved at higher loadings. NC, as the major driver of the tensile strength, is also noticeable by the steeper slope along its axis.

The modulus is only significantly influenced by the CNF linear term. Thus the surface curve is very simplistic. The elongation is also only affected by the CNF. The curvature is very clear. The large dark shade on the contour plot, Figure 51b, shows the range at low CNF loadings where the linear and quadratic terms nearly cancel each other out, causing the plateau.

4.5.2 TPS reinforced with dried vs. non-dried CNF/xanthan dispersions.

Table 28 shows the mean tensile values of the TPS reinforced with previously dried or non-dried CNF/xanthan dispersions with the 95 % confidence interval. The trend of the data is not very clear, but there are some general observations. There does seem to be a difference between TPS reinforced with previously dried dispersions and non-dried dispersions, with previously dried showing, surprisingly, stronger values. The pure CNF samples do not show much difference. The SEM images in Figure 31 give a possible explanation. The CNFs are agglomerated but still have a porous, interlaced structure. Starch is highly compatible with cellulose, and thus the pores could be filled by the gelatinised starch, still allowing for significant reinforcement. If one were to use a less compatible polymer, there might be more of a difference noticed with the reinforcement ability. These results still show that xanthan is a beneficial addition to the nanocellulose and that previously dried CNF/xanthan still has appreciable reinforcement qualities. The best example of this is the dried +1 CNF TPS sample with 25 % xanthan. It poses the highest strength and stiffness of any sample, higher than any sample referenced in Figure 7.

The elongation reduces drastically at the +1 CNF loadings with 25 % or 50 % xanthan. The same can be said for the −1 CNF 50 % xanthan sample. This could allude to the interlaced network theory, that once one has enough of the fibres dispersed, they will create a continuous network. This network will be much less elastic than the TPS and will fail at a lower strain. Only once sufficient amounts of CNF and xanthan are present in the matrix, and a continuous network formed, can this shortened form of failure occur. The +1, 25 % xanthan sample even shows lower strain than the 50 % one. This could be due to the xanthan amount becoming too high, creating a separate xanthan phase that is weaker than the CNF/xanthan network.

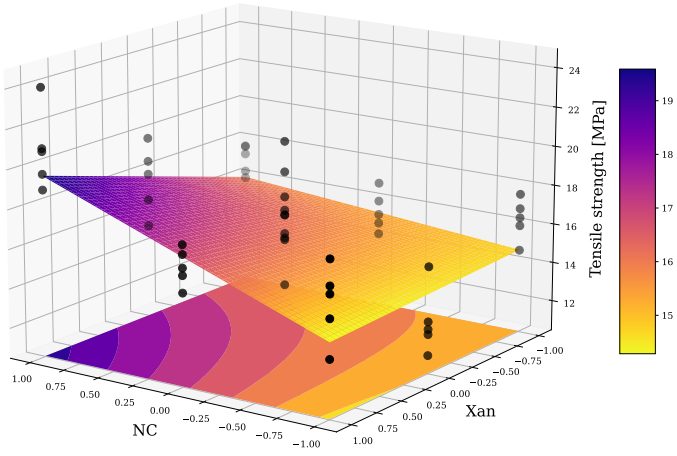

(a) Strength.

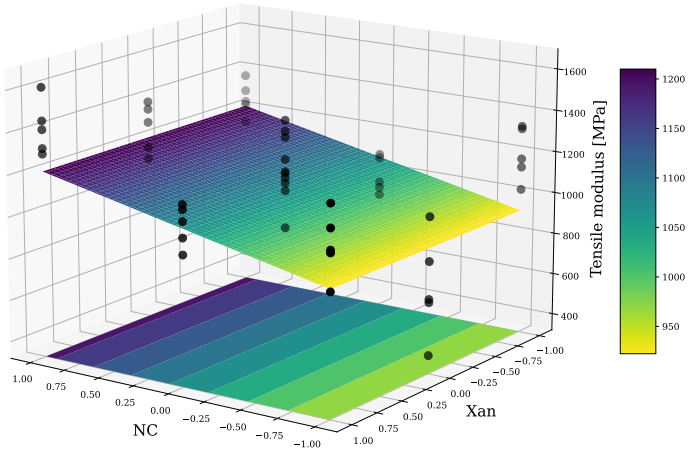

(b) Modulus.

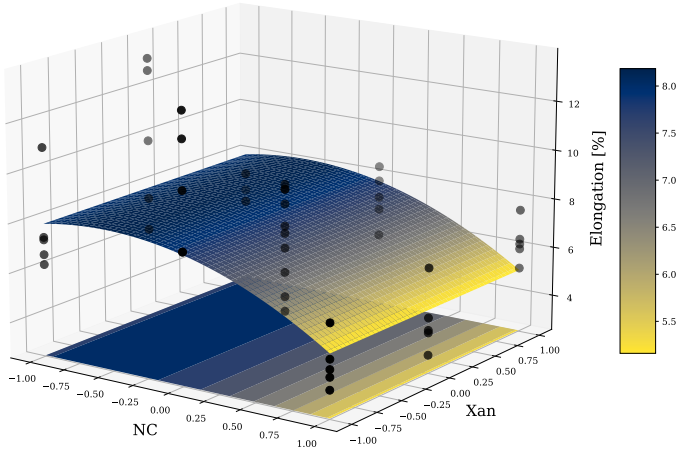

(c) Elongation.

Figure 51: Response surface plots of the CCF design with quadratic model and data points.

Table 28: Tensile properties of 30 phs glycerol TPS stored at 54 % RH for 10 d – 14 d reinforced with non-dried or dried CNF and xanthan at different concentrations.

CNF	Xan (%)	Non-dried			Dried		
		Strength (MPa)	Modulus (GPa)	Elongation (%)	Strength (MPa)	Modulus (GPa)	Elongation (%)
-1	0	8.3 ± 0.5	0.44 ± 0.09	24.6 ± 2.7	10.5 ± 1.2	0.76 ± 0.08	12.2 ± 2.1
	15	9.2 ± 0.7	0.61 ± 0.07	17.0 ± 3.0	12.4 ± 0.5	0.87 ± 0.04	14.6 ± 1.5
	25	15.3 ± 0.6	1.05 ± 0.03	10.8 ± 1.5	11.8 ± 1.1	0.82 ± 0.09	13.0 ± 2.0
	50	16.3 ± 0.9	1.19 ± 0.11	7.7 ± 1.6	14.3 ± 1.1	1.01 ± 0.13	9.4 ± 1.4
+1	0	14.3 ± 2.9	1.04 ± 0.32	9.1 ± 2.1	15.3 ± 1.0	1.03 ± 0.06	11.0 ± 1.7
	15	12.9 ± 1.7	0.94 ± 0.18	14.3 ± 2.5	19.4 ± 2.1	1.31 ± 0.16	9.5 ± 2.3
	25	17.0 ± 0.7	1.25 ± 0.08	4.7 ± 0.9	23.0 ± 0.7	1.48 ± 0.07	7.0 ± 0.8
	50	20.9 ± 1.7	1.42 ± 0.11	6.3 ± 0.8	19.4 ± 1.3	1.46 ± 0.15	7.9 ± 0.7

4.5.3 TGA

The influence of CNF and xanthan on the thermal stability of the TPS films is shown in Figure 52. CNF (NC) does show to improve the thermal stability of the TPS slightly, showing a later derivative peak and generally higher residual mass. It is interesting to note that xanthan-containing samples seem to be less thermally stable than the pure TPS, with them having a lower peak derivative temperature. This is observed even if CNF is present or not. The effect is minor though and the increase and decrease in thermal stability is mostly negligible.

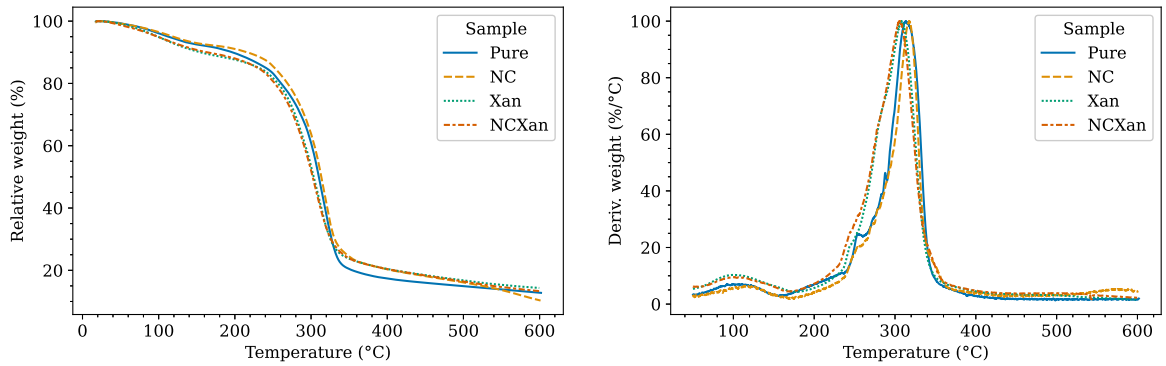

(a) Mass change with temperature.

(b) Derivative of mass change.

Figure 52: Influence of CNF (NC) and xanthan on the thermal stability of amura TPS with 30 phs glycerol stored at 54 % humidity.

5 Conclusions

The native amura starch proved to have an A-type crystallinity similar to yellow amura starch. The amura-based TPS has retrogradation, permeability, and tensile behaviour similar to other starches reported in the literature. A quadratic fit of the tensile strength data, with glycerol and humidity as the independent variables, shows a maximum at 35 wt% glycerol and 53 % – 54 % relative humidity. Amura starch is thus a suitable source for TPS.

Analyses of the rheology, turbidity, and colloidal stability of previously dried and non-dried CNF/xanthan dispersions, as well as their SEM/TEM images, prove that xanthan is effective at limiting hornification. The rheology of previously dried and non-dried neat CNF dispersions is very divergent. When 15 wt% xanthan is added, no difference between the shear thinning slopes of the previously dried and non-dried dispersions can be observed. Turbidity measurements allowed for fibre diameter estimation using the Yeromonahos equation. It proves that, with the addition of xanthan, one can redisperse the CNFs to their original size. Neat CNFs have an estimated diameter of 149.0 nm and 147.4 nm when high-shear mixed and ultrasonicated, respectively. CNFs with 25 wt% xanthan have an estimated diameter of 147.0 nm for both shear mixing and ultrasonication. The Carr-Herman equation, the predecessor of the Yeromonahos equation, overestimates the diameter size but gives a similar trend.

SEM imaging of freeze-dried CNF/xanthan dispersions confirms the observations made with the turbidity measurements. The majority of ultrasonicated CNF fibres have a diameter in the range of 125 nm – 150 nm. Ultrasonication is required to redisperse the pure dried CNFs to their original size. Large agglomerates are evident in previously dried, neat CNF dispersions that are only shear mixed. CNF dispersions with 25 wt% xanthan added, whether previously dried and shear mixed, or non-dried and ultrasonicated, are indistinguishable. The images also show that a highly interlaced network forms when xanthan is added to CNFs.

Zeta potential measurement showed that drying and xanthan addition both increased the surface charge of the fibres. This is reflected in the sedimentation tests, where dispersions made from non-dried samples and pure, dried CNFs sedimented within a day. Solutions containing previously dried CNFs with xanthan, in contrast, sedimented little or not at all. Samples with xanthan show colloidal stability even with low-shear mixing, supporting the previous findings.

The SSA measurements provided little insight into the agglomeration but did provide information for the appropriate adsorption isotherm. The modified Langmuir model, tested with k-fold cross-validation, has a RMSE of 13.0, compared to 21.5 for the original Langmuir. This proves that the modified Langmuir is a more adequate model.

The influence of xanthan gum and CNF on the tensile properties of TPS was modelled using a

quadratic fit done on a central composite design. The quadratic fit reveals a significant, positive interaction term between CNF and xanthan regarding the tensile strength, implying synergism between the two. The synergistic effect can be explained as the formation of a highly interlaced, continuous network within the polymer matrix. The addition of 1.25 phs xanthan to the TPS, no CNF added, shows no marked improvement, whereas with 2.5 phs addition the tensile strength improves from 5.4 MPa to 9.6 MPa. There is no noticeable difference between TPS reinforced with comparable amounts of previously dried or non-dried CNF dispersions, with or without xanthan addition. It is postulated that the high compatibility between CNF and TPS is the cause for the small differences. TPS reinforced with 5 phs previously dried CNF containing 25 wt% xanthan, relative to the CNF (X25 sample), has a tensile strength of 23.0 MPa and a modulus of 1.48 MPa, the highest of any sample. This is stronger than the majority of previously reported values for TPS/CNF composites. Xanthan gum and CNF have a minor influence on the thermal stability of TPS, but nothing of note.

This work confirms that amura is a suitable source material for TPS. Xanthan gum is quantitatively proven to be an effective capping agent of CNF, increasing the ease of redispersion by limiting agglomeration. The synergistic effect between CNF and xanthan encourages further research on xanthan's use as a capping agent as well as reinforcement of other, maybe less CNF-compatible, biopolymers. The results of this work has applications in the production of redispersible dried CNFs and in improving the mechanical properties of biopolymers.

6 References

AAT Bioquest, Inc. (2023) *Quest Calculate™ Phosphate Buffer (pH 5.8 to 7.4) Preparation and Recipe* AAT BioQuest URL: https://www.aatbio.com/resources/buffer-preparations-and-recipes/phosphate-buffer-ph-5-8-to-7-4 (visited on 06/06/2023).

Abou-Zeid, R. E., Dacrory, S., Ali, K. A. and Kamel, S. (2018) "Novel method of preparation of tricarboxylic cellulose nanofiber for efficient removal of heavy metal ions from aqueous solution" *International Journal of Biological Macromolecules*, *119*, 207–214 ISSN: 0141-8130 DOI: 10.1016/J.IJBIOMAC.2018.07.127.

Abushammala, H. (2019) "A simple method for the quantification of free isocyanates on the surface of cellulose nanocrystals upon carbamation using toluene diisocyanate" *Surfaces*, *2*, 444–454 DOI: 10.3390/surfaces2020032.

Ahankari, S. S., Subhedar, A. R., Bhadauria, S. S. and Dufresne, A. (2021) "Nanocellulose in food packaging: A review" *Carbohydrate Polymers*, *255*, 117479 ISSN: 0144-8617 DOI: 10.1016/J.CARBPOL.2020.117479.

Ahlawat, V., Deopa, S. P. S. and Patil, S. (2022) "Quantitative elasticity of flexible polymer chains using interferometer-based AFM" *Nanomaterials*, *12*, (3) ISSN: 20794991 DOI: 10.3390/NANO12030526.

Almeida, T., Silvestre, A. J. D., Vilela, C., Freire, C. S. R. and Coburn, M. (2021) "Bacterial nanocellulose toward green cosmetics: Recent progresses and challenges" *International Journal of Molecular Sciences*, *22*, 2386 DOI: 10.3390/ijms22062836.

Altayan, M. M., Darouich, T. A. and Karabet, F. (2021) "Thermoplastic starch from corn and wheat: A comparative study based on amylose content" *Polymer Bulletin*, *78*, (6): 3131–3147 ISSN: 14362449 DOI: 10.1007/S00289-020-03262-9.

Ambouroue Avaro, M. R., Pan, Z., Yoshida, T. and Wada, Y. (2011) "Two alternative methods to predict amylose content of rice grain by using tristimulus CIE Lab values and developing a specific color board of starch-iodine complex solution" *Plant Production Science*, *14*, (2): 164–168 ISSN: 1349-1008 DOI: 10.1626/pps.14.164.

American Chemical Society (2023) *American Chemical Society national historic chemical landmarks. Bakelite: The world's first synthetic plastic* URL: https://www.acs.org/education/whatischemistry/landmarks/bakelite.html (visited on 06/06/2023).

Amin, A. M. M., Sauid, S. M., Musa, M. and Hamid, K. H. K. (2017) "The effect of glycerol content on mechanical properties, surface morphology and water absorption of thermoplastic films from *Tacca leontopetaloides* starch" *Jurnal Teknologi*, *79*, (5-3): 53–59 ISSN: 2180-3722 DOI: 10.11113/JT.V79.11327.

Araki, J. and Arita, T. (2017) "Production of ultrafine dry powders of surface-intact and unmodified cellulose nanowhiskers via homogenization in nonpolar organic solvents" *Chemistry Letters*, *46*, (9): 1438–1441 ISSN: 0366-7022 DOI: 10.1246/cl.170588.

Arvanitoyannis, I. and Biliaderis, C. G. (1999) "Physical properties of polyol-plasticized edible blends made of methyl cellulose and soluble starch" *Carbohydrate Polymers*, *38*, (1): 47–58 ISSN: 0144-8617 DOI: 10.1016/S0144-8617(98)00087-3.

Asquez-Cock, J. V., Ga, P., Omez, C. G., Posada, P., Castro, C., Dufresne, A. and Zuluaga, R. (2017) "Improved redispersibility of cellulose nanofibrils in water using maltodextrin as a green, easily removable and non-toxic additive" *Food Hydrocolloids*, *79*, 30–39 DOI: 10.1016/j.foodhyd.2017.12.024.

Babaee, M., Jonoobi, M., Hamzeh, Y. and Ashori, A. (2015) "Biodegradability and mechanical properties of reinforced starch nanocomposites using cellulose nanofibers" *Carbohydrate Polymers*, *132*, 1–8 ISSN: 0144-8617 DOI: 10.1016/j.carbpol.2015.06.043.

Baillie, C. (2004) *Green Composites : Polymer Composites and the Environment*, Boca Raton ISBN: 978-1-4557-2834-3.

Balea, A., Fuente, E., Blanco, A. and Negro, C. (2019) "Nanocelluloses: Natural-based materials for fiber-reinforced cement composites. A critical review" *Polymers*, *11*, 518 DOI: 10.3390/polym11030518.

Balla, B., Bartos, A., Kun, D., Csiszár, E., Móczó, J. and Fekete, E. (2021) "Improving mechanical and water sorption properties of thermoplastic starch by incorporating chitosan filler" *Polymer Testing*, *101*, 107278 ISSN: 0142-9418 DOI: 10.1016/J.POLYMERTESTING.2021.107278.

Baniasadi, H., Kimiaei, E., Polez, R. T., Ajdary, R., Rojas, O. J., Österberg, M. and Seppälä, J. (2022) "High-resolution 3D printing of xanthan gum/nanocellulose bio-inks" *International Journal of Biological Macromolecules*, *209*, 2020–2031 ISSN: 0141-8130 DOI: 10.1016/J.IJBIOMAC.2022.04.183.

Battegazzore, D., Bocchini, S., Nicola, G., Martini, E. and Frache, A. (2015) "Isosorbide, a green plasticizer for thermoplastic starch that does not retrogradate" *Carbohydrate Polymers*, *119*, 78–84 ISSN: 0144-8617 DOI: 10.1016/j.carbpol.2014.11.030.

Beaumont, M., König, J., Opietnik, M., Potthast, A. and Rosenau, T. (2017) "Drying of a cellulose II gel: Effect of physical modification and redispersibility in water" *Cellulose*, *24*, 1199–1209 DOI: 10.1007/s10570-016-1166-9.

Beaumont, M., Nypelö, T., König, J., Zirbs, R., Opietnik, M., Potthast, A. and Rosenau, T. (2016) "Synthesis of redispersible spherical cellulose II nanoparticles decorated with carboxylate groups" *Green Chemistry*, *18*, (6): 1465–1468 ISSN: 14639270 DOI: 10.1039/C5GC03031E.

Beck, S., Bouchard, J. and Berry, R. (2012) "Dispersibility in water of dried nanocrystalline cellulose" *Biomacromolecules*, *13*, (5): 1486–1494 ISSN: 15257797 DOI: 10.1021/BM300191K.

BeMiller, J. N. (2019) *Carbohydrate chemistry for food scientists*, English 3rd ed. WP, London ISBN: 978-0-12-812069-9.

BeMiller, J. N. and Whistler, R. L. (2009) *Starch: Chemistry and Technology*, 3rd ed. Academic Press, London ISBN: 9780127462752.

Ben Abdelouahab, N., Gossard, A., Ma, X., Dialla, H., Maillet, B., Rodts, S. and Coussot, P. (2021) "Understanding mechanisms of drying of a cellulose slurry by magnetic resonance imaging" *Cellulose*, *28*, (9): 5321–5334 ISSN: 1572882X DOI: 10.1007/S10570-021-03916-5.

Benítez, A. J. and Walther, A. (2017) "Counterion size and nature control structural and mechanical response in cellulose nanofibril nanopapers" *Biomacromolecules*, *18*, (5): 1642–1653 ISSN: 15264602 DOI: 10.1021/ACS.BIOMAC.7B00263.

Bertoft, E. (2013) "On the building block and backbone concepts of amylopectin structure" *Cereal Chemistry*, *90*, (4): 294–311 ISSN: 1943-3638 DOI: 10.1094/CCHEM-01-13-0004-FI.

Birdie, K. S. (2010) *Surface and Colloid Chemistry: Principles and Applications.* Taylor & Francis Group, Boca Rotan ISBN: 978-1-4200-9504-3.

Bisinella, V., Albizzati, P. F., Astrup, T. F. and Damgaard, A. (2018) *Life Cycle Assessment of grocery carrier bags* Environmental Project 1985 The Danish Environmental Protection Agency.

Brückner, S. (June 2000) "Estimation of the background in powder diffraction patterns through a robust smoothing procedure" *Journal of Applied Crystallography*, *33*, (3 II): 977–979 ISSN: 00218898 DOI: 10.1107/S0021889800003617.

Bui, D. N. and Son, Y. (2018) "Study on the rheological, thermal and mechanical properties of thermoplastic starch plasticized by glycerol" *Journal of the Korea Academia-Industrial cooperation Society*, *19*, (6): 21–26 ISSN: 1975-4701 DOI: 10.5762/KAIS.2018.19.6.21.

Butchosa, N. and Zhou, Q. (2014) "Water redispersible cellulose nanofibrils adsorbed with carboxymethyl cellulose" *Cellulose*, *21*, 4349–4358 ISSN: 1572882X DOI: 10.1007/s10570-014-0452-7.

Butler, M. (2016) *Xanthan Gum: Applications and Research Studies*, Nova Science Publishers, Inc, New York: p. 14 ISBN: 9781536100105.

Cael, J. J., Koenig, J. L. and Blackwell, J. (1975) "Infrared and Raman spectroscopy of carbohydrates. Part VI: Normal coordinate analysis of V-amylose" *Biopolymers*, *14*, 1885–1903 DOI: 10.1002/bip.1975.360140909.

Cai, J., Cai, C., Man, J., Zhou, W. and Wei, C. (2014) "Structural and functional properties of C-type starches" *Carbohydrate Polymers*, *101*, 289–300 ISSN: 0144-8617 DOI: 10.1016/j.carbpol.2013.09.058.

Carr, M. E. and Hermans, J. (1978) "Size and density of fibrin fibers from turbidity" *Macromolecules*, *11*, (1): 46–50 ISSN: 15205835 DOI: 10.1021/ma60061a009.

Carvalho, A. J. F., Curvelo, A. A. S. and Gandini, A. (2005) "Surface chemical modification of thermoplastic starch: Reactions with isocyanates, epoxy functions and stearoyl chloride" *Industrial Crops and Products*, *21*, (3): 331–336 ISSN: 0926-6690 DOI: 10.1016/J.INDCROP.2004.04.027.

Cazón, P., Morales-Sanchez, E., Velazquez, G. and Vázquez, M. (2022) "Measurement of the water vapor permeability of chitosan films: A laboratory experiment on food packaging materials" *Journal of Chemical Education*, *99*, (6): 2403–2408 ISSN: 19381328 DOI: 10.1021/ACS.JCHEMED.2C00449.

Chang, Y. P., Abd Karim, A. and Seow, C. C. (2006) "Interactive plasticizing-antiplasticizing effects of water and glycerol on the tensile properties of tapioca starch films" *Food Hydrocolloids*, *20*, (1): 1–8 ISSN: 0268-005X DOI: 10.1016/j.foodhyd.2005.02.004.

Cheetham, N. W. H. and Tao, L. (1998) "Variation in crystalline type with amylose content in maize starch granules: an X-ray powder diffraction study" *Carbohydrate Polymers*, *36*, (4): 277–284 ISSN: 0144-8617 DOI: 10.1016/S0144-8617(98)00007-1.

Cheng, D., Wen, Y., Wang, L., An, X., Zhu, X. and Ni, Y. (2015) "Adsorption of polyethylene glycol (PEG) onto cellulose nano-crystals to improve its dispersity" *Carbohydrate Polymers*, *123*, 157–163 ISSN: 0144-8617 DOI: 10.1016/j.carbpol.2015.01.035.

Chocyk, D., Gładyszewska, B., Ciupak, A., Oniszczuk, T., Mościcki, L. and Rejak, A. (2015) "Influence of water addition on mechanical properties of thermoplastic starch foils" *International Agrophysics*, *29*, 267–275 DOI: 10.1515/intag-2015-0031.

Chun, M.-S., Kim, C. and Lee, D. E. (2009) "Conformation and translational diffusion of a xanthan polyelectrolyte chain: Brownian dynamics simulation and single molecule tracking" *Physical Review E*, *79*, 051919 DOI: 10.1103/PhysRevE.79.051919.

Combariza, M. Y., Martínez-Ramírez, A. P. and Blanco-Tirado, C. (2021) "Perspectives in nanocellulose for crude oil recovery: A minireview" *Energy Fuels*, *35*, (19): 15381–15397 DOI: 10.1021/acs.energyfuels.1c02230.

Corradini, E., de Carvalho, A. J. F., da Silva Curvelo, A. A., Marcondes Agnelli, J. A. and Capparelli Mattoso, L. H. (2007) "Preparation and characterization of thermoplastic starch/zein blends" *Materials Research*, *10*, (3): 227–231 ISSN: 1516-1439 DOI: 10.1590/S1516-14392007000300002.

Csiszár, E., Kun, D. and Fekete, E. (2021) "The role of structure and interactions in thermoplastic starch–nanocellulose composites" *Polymers*, *13*, (18): 3186 ISSN: 2073-4360 DOI: 10.3390/POLYM13183186.

Da Matta Jr., M. D., Silveira Sarmento, S. B., De Oliveira, L. M. and Sandoval Zocchi, S. (2011) "Mechanical properties of pea starch films associated with xanthan gum and glycerol" *Starch - Stärke*, *63*, (5): 274–282 ISSN: 1521-379X DOI: 10.1002/STAR.201000088.

Da Róz, A. L., Carvalho, A. J. F., Gandini, A. and Curvelo, A. A. S. (2006) "The effect of plasticizers on thermoplastic starch compositions obtained by melt processing" *Carbohydrate Polymers*, *63*, (3): 417–424 ISSN: 0144-8617 DOI: 10.1016/j.carbpol.2005.09.017.

Daniels, P. H. (2009) "A brief overview of theories of PVC plasticization and methods used to evaluate PVC-plasticizer interaction" *Journal of Vinyl and Additive Technology*, *15*, (4): 219–223 ISSN: 1548-0585 DOI: 10.1002/VNL.20211.

Davison, A. and Hinkley, D. (1997) *Bootstrap Methods and Their Application*, Cambridge University Press, New York: pp. 28–29 ISBN: 978-0-521-57391-7.

de Graaf, R. A., Karman, A. P. and Janssen, L. P. B. M. (2003) "Material properties and glass transition temperatures of different thermoplastic starches after extrusion processing" *Starch - Stärke*, *55*, (2): 80–86 ISSN: 0038-9056 DOI: 10.1002/star.200390020.

Dias, O. A. T., Konar, S., Leão, A. L., Yang, W., Tjong, J. and Sain, M. (2020) "Current state of applications of nanocellulose in flexible energy and electronic devices" *Frontiers in Chemistry*, *8*, 420 DOI: 10.3389/fchem.2020.00420.

Diyana, Z. N., Jumaidin, R., Selamat, M. Z. and Suan, M. S. M. (2021) "Thermoplastic starch/beeswax blend: Characterization on thermal mechanical and moisture absorption properties" *International Journal of Biological Macromolecules*, *190*, 224–232 ISSN: 0141-8130 DOI: 10.1016/J.IJBIOMAC.2021.08.201.

Dogossy, G. and Czigany, T. (2011) "Thermoplastic starch composites reinforced by agricultural by-products: Properties, biodegradability, and application" *Journal of Reinforced Plastics and Composites*, *30*, (21): 1819–1825 ISSN: 15307964 DOI: 10.1177/0731684411429728.

Dome, K., Podgorbunskikh, E., Bychkov, A. and Lomovsky, O. (2020) "Changes in the crystallinity degree of starch having different types of crystal structure after mechanical pretreatment" *Polymers*, *12*, 641 ISSN: 20734360 DOI: 10.3390/POLYM12030641.

Dufresne, A. (2017) "Cellulose nanomaterial reinforced polymer nanocomposites" *Current Opinion in Colloid & Interface Science*, *29*, 1–8 DOI: 10.1016/j.cocis.2017.01.004.

Dufresne, A. (2018) "Cellulose nanomaterials as green nanoreinforcements for polymer nanocomposites" *Philosophical Transactions Royal Society A*, *376*, 1–23 DOI: 10.1098/rsta.2017.0040.

Ebnesajjad, S. (2013) *Handbook of Biopolymers and Biodegradable Plastics : Properties, Processing, and Applications*, Woodhead Publishing, Amsterdam ISBN: 978-1-85573-739-6.

Esmaeili, M., Pircheraghi, G. and Bagheri, R. (2017) "Optimizing the mechanical and physical properties of thermoplastic starch via tuning the molecular microstructure through co-plasticization by sorbitol and glycerol" *Polymer International*, *66*, (6): 809–819 ISSN: 0959-8103 DOI: 10.1002/pi.5319.

Espino-Pérez, E., Bras, J., Ducruet, V., Guinault, A., Dufresne, A. and Domenek, S. (2013) "Influence of chemical surface modification of cellulose nanowhiskers on thermal, mechanical, and barrier properties of poly(lactide) based bionanocomposites" *European Polymer Journal*, *49*, (10): 3144–3154 ISSN: 0014-3057 DOI: 10.1016/J.EURPOLYMJ.2013.07.017.

European Bioplastics (2022) *Bioplastics market data 2022* URL: https://www.european-bioplastics.org/market/ (visited on 07/15/2023).

Eyholzer, C., Bordeanu, N., Lopez-Suevos, F., Rentsch, D., Zimmermann, T. and Oksman, K. (2010) "Preparation and characterization of water-redispersible nanofibrillated cellulose in powder form" *Cellulose*, *17*, (1): 19–30 ISSN: 09690239 DOI: 10.1007/S10570-009-9372-3.

Fairman, E. (2014) “Avoiding aggregation during drying and rehydration of nanocellulose” *Honors College*, *172*, URL: https://digitalcommons.library.umaine.edu/honors/172.

Fall, A. B., Burman, A. and Wågberg, L. (2014) “Cellulosic nanofibrils from eucalyptus, acacia and pine fibers” *Nordic Pulp & Paper Research Journal*, *29*, (1): 176–184 ISSN: 2000-0669 DOI: 10.3183/NPPRJ-2014-29-01-P176-184.

Fall, A. B., Lindström, S. B., Sundman, O., Ödberg, L. and Wågberg, L. (2011) “Colloidal stability of aqueous nanofibrillated cellulose dispersions” *Langmuir*, *27*, 11332–11338 DOI: 10.1021/la201947x.

Felipe Bergel, B., Dias Osorio, S., Machado da Luz, L. and Campomanes Santana, R. M. (2018) “Effects of hydrophobized starches on thermoplastic starch foams made from potato starch” *Carbohydrate Polymers*, *200*, 106–114 ISSN: 0144-8617 DOI: 10.1016/J.CARBPOL.2018.07.047.

Felipe Bergel, B., Leite Araujo, L., dos Santos da Silva, A. L. and Campomanes Santana, R. M. (2020) “Effects of silylated starch structure on hydrophobization and mechanical properties of thermoplastic starch foams made from potato starch” *Carbohydrate Polymers*, *241*, 116274 ISSN: 0144-8617 DOI: 10.1016/j.carbpol.2020.116274.

Fernandes Diniz, J. M. B., Gil, M. H. and Castro, J. A. A. M. (2004) “Hornification—its origin and interpretation in wood pulps” *Wood Science and Technology*, *37*, 489–494 ISSN: 1432-5225 DOI: 10.1007/s00226-003-0216-2.

Foster, E. J., Moon, R. J., Agarwal, U. P., Bortner, M. J., Bras, J., Camarero-Espinosa, S., Chan, K. J., Clift, M. J. D., Cranston, E. D., Eichhorn, S. J., Fox, D. M., Hamad, W. Y., Heux, L., Jean, B., Korey, M., Nieh, W., Ong, K. J., Reid, M. S., Renneckar, S., Roberts, R., Shatkin, J. A., Simonsen, J., Stinson-Bagby, K., Wanasekara, N. and Youngblood, J. (2018) “Current characterization methods for cellulose nanomaterials” *Chemical Society Reviews*, *47*, 2609–2679 ISSN: 0306-0012 DOI: 10.1039/c6cs00895j.

Freundlich, H. (1909) *Kapillarchemie: eine Darstellung der Chemie der Kolloide und verwandter Gebiete*, Akademische Verlagsgesellschaf, Leipzig.

Fukuzumi, H., Tanaka, R., Saito, T. and Isogai, A. (2014) “Dispersion stability and aggregation behavior of TEMPO-oxidized cellulose nanofibrils in water as a function of salt addition” *Cellulose*, *21*, 1553–1559 DOI: 10.1007/s10570-014-0180-z.

Galat, A. (1980) "Study of the raman scattering and infrared absorption spectra of branched polysaccharides" *Acta biochimica Polonica*, *27*, (2): 135–142.

García-Ochoa, F., Santos, V. E., Casas, J. A. and Gómez, E. (2000) "Xanthan gum: production, recovery, and properties" *Biotechnology Advances*, *18*, (7): 549–579 ISSN: 0734-9750 DOI: 10.1016/S0734-9750(00)00050-1.

Gaudin, S., Lourdin, D., Botlan, D. L., Ilari, J. L. and Colonna, P. (1999) "Plasticisation and mobility in starch-sorbitol films" *Journal of Cereal Science*, *29*, (3): 273–284 ISSN: 0733-5210 DOI: 10.1006/JCRS.1999.0236.

Gaudin, S., Lourdin, D., Forssell, P. M. and Colonna, P. (2000) "Antiplasticisation and oxygen permeability of starch–sorbitol films" *Carbohydrate Polymers*, *43*, (1): 33–37 ISSN: 0144-8617 DOI: 10.1016/S0144-8617(99)00206-4.

Ghanbari, A., Tabarsa, T., Ashori, A., Shakeri, A. and Mashkour, M. (2018) "Preparation and characterization of thermoplastic starch and cellulose nanofibers as green nanocomposites: Extrusion processing" *International Journal of Biological Macromolecules*, *112*, ISSN: 18790003 DOI: 10.1016/j.ijbiomac.2018.02.007.

Ghasemlou, M., Daver, F., Ivanova, E. P., Habibi, Y. and Adhikari, B. (2021) "Surface modifications of nanocellulose: From synthesis to high-performance nanocomposites" *Progress in Polymer Science*, *119*, 101418 ISSN: 00796700 DOI: 10.1016/j.progpolymsci.2021.101418.

Goussé, C., Chanzy, H., Excoffier, G., Soubeyrand, L. and Fleury, E. (2002) "Stable suspensions of partially silylated cellulose whiskers dispersed in organic solvents" *Polymer*, *43*, (9): 2645–2651 ISSN: 0032-3861 DOI: 10.1016/S0032-3861(02)00051-4.

Greenspan, L. (1977) "Humidity fixed points of binary saturated aqueous solutions" *Journal of Research of the National Bureau of Standards-A. Physics and Chemistry*, *81*, (1): 89–96.

Guhados, G., Wan, W. and Hutter, J. L. (2005) "Measurement of the elastic modulus of single bacterial cellulose fibers using atomic force microscopy" *Langmuir*, *21*, 6642–6646 DOI: 10.1021/la0504311.

Guo, K., Zhang, L., Bian, X., Cao, Q. and Wei, C. (2020) "A-, B- and C-type starch granules coexist in root tuber of sweet potato" *Food Hydrocolloids*, *98*, 105279 ISSN: 0268-005X DOI: 10.1016/J.FOODHYD.2019.105279.

Hamid, S. B. A., Zain, S. K., Das, R. and Centi, G. (2016) "Synergic effect of tungstophosphoric acid and sonication for rapid synthesis of crystalline nanocellulose" *Carbohydrate Polymers*, *138*, 349–355 ISSN: 0144-8617 DOI: 10.1016/J.CARBPOL.2015.10.023.

Han, J., Zhou, C., Wu, Y., Liu, F. and Wu, Q. (2013) "Self-assembling behavior of cellulose nanoparticles during freeze-drying: Effect of suspension concentration, particle size, crystal structure, and surface charge" *Biomacromolecules*, *14*, (5): 1529–1540 ISSN: 15264602 DOI: 10.1021/BM4001734.

Hanif, Z., Jeon, H., Thang, Tran, H., Jegal, J., Park, S.-A., Kim, S.-M., Park, J., Hwang, S. Y. and Oh, D. X. (2018) "Butanol-mediated oven-drying of nanocellulose with enhanced dehydration rate and aqueous re-dispersion" *Journal of Polymer Research*, *25*, (191) DOI: 10.1007/s10965-017-1343-z.

Haque, M. M. U., Puglia, D., Fortunati, E. and Pracella, M. (2017) "Effect of reactive functionalization on properties and degradability of poly(lactic acid)/poly(vinyl acetate) nanocomposites with cellulose nanocrystals" *Reactive and Functional Polymers*, *110*, 1–9 ISSN: 1381-5148 DOI: 10.1016/J.REACTFUNCTPOLYM.2016.11.003.

Heggset, E. B., Aaen, R., Veslum, T., Henriksson, M., Simon, S. and Syverud, K. (2020) "Cellulose nanofibrils as rheology modifier in mayonnaise – A pilot scale demonstration" *Food Hydrocolloids*, *108*, 106084 ISSN: 0268-005X DOI: 10.1016/J.FOODHYD.2020.106084.

Hietala, M., Mathew, A. P. and Oksman, K. (2013) "Bionanocomposites of thermoplastic starch and cellulose nanofibers manufactured using twin-screw extrusion" *European Polymer Journal*, *49*, (4): 950–956 ISSN: 0014-3057 DOI: 10.1016/J.EURPOLYMJ.2012.10.016.

Hietala, M., Sain, S. and Oksman, K. (2017) "Highly redispersible sugar beet nanofibers as reinforcement in bionanocomposites" *Cellulose*, *24*, 2177–2189 DOI: 10.1007/s10570-017-1245-6.

Hizukuri, S., Kaneko, T. and Takeda, Y. (1983) "Measurement of the chain length of amylopectin and its relevance to the origin of crystalline polymorphism of starch granules" *Biochimica et Biophysica Acta (BBA) - General Subjects*, *760*, 188–191 ISSN: 0304-4165 DOI: 10.1016/0304-4165(83)90142-3.

Hoeng, F., Denneulin, A. and Bras, J. (2016) "Use of nanocellulose in printed electronics: A review" *Nanoscale*, *8*, 13131–13154 DOI: 10.1039/c6nr03054h.

Hoo, D. Y., Low, Z. L., Low, D. Y. S., Tang, S. Y., Manickam, S., Tan, K. W. and Ban, Z. H. (2022) "Ultrasonic cavitation: An effective cleaner and greener intensification technology in the extraction and surface modification of nanocellulose" *Ultrasonics Sonochemistry*, *90*, 106176 ISSN: 18732828 DOI: 10.1016/J.ULTSONCH.2022.106176.

Huang, J., Dufresne, A. and Lin, N. (2019) *Nanocellulose: From Fundamentals to Advanced Materials*, Wiley-VCH, Weinheim ISBN: 978-3-527-34269-3.

Huang, M., Yu, J. and Ma, X. (2005) "Ethanolamine as a novel plasticiser for thermoplastic starch" *Polymer Degradation and Stability*, *90*, (3): 501–507 ISSN: 0141-3910 DOI: 10.1016/j.polymdegradstab.2005.04.005.

Hubbe, M. A., Ferrer, A., Tyagi, P., Yin, Y., Salas, C., Pal, L. and Rojas, O. J. (2017) "Nanocellulose in thin films, coatings, and plies for packaging applications: A review" *BioResources*, *12*, (1): 2143–2233 ISSN: 19302126 DOI: 10.15376/biores.12.1.2143-2233.

Hui, Y. H. (2008) *Food Drying Science and Technology : Microbiology, Chemistry, Applications*, DEStech Publications, Lancaster ISBN: 978-1-932078-56-5.

Iwamoto, S., Kai, W., Isogai, A. and Iwata, T. (2009) "Elastic modulus of single cellulose microfibrils from tunicate measured by atomic force microscopy" *Biomacromolecules*, *10*, 2571–2576 DOI: 10.1021/bm900520n.

Iwamoto, S., Yamamoto, S., Lee, S. H. and Endo, T. (2014) "Mechanical properties of polypropylene composites reinforced by surface-coated microfibrillated cellulose" *Composites Part A: Applied Science and Manufacturing*, *59*, 26–29 ISSN: 1359-835X DOI: 10.1016/J.COMPOSITESA.2013.12.011.

James, G., Witten, D., Hastie, T. and Tibshirani, R. (2021) *An Introduction to Statistical Learning with Applications in R*, 2nd ed. Springer ISBN: 978-1-0716-1417-4.

Janick, J. and Freedman, B. (2022) *Tacca involucrata* URL: https://www.purdue.edu/hla/sites/famine-foods/famine_food/tacca-involucrata/ (visited on 04/14/2022).

Janssen, L. P. B. M. and Moscicki, L. (2010) *Thermoplastic Starch: A Green Material for Various Industries*, Wiley-VCH, Weinheim ISBN: 9783527325283 DOI: 10.1002/9783527628216.

Jiang, F. and Hsieh, Y.-L. (2014) "Assembling and redispersibility of rice straw nanocellulose: Effect of *tert*-butanol" *ACS Applied Materials and Interfaces*, *6*, (22): 20075–20084 ISSN: 19448252 DOI: 10.1021/AM505626A.

Jiugao, Y., Ning, W. and Xiaofei, M. (2005) "The effects of citric acid on the properties of thermoplastic starch plasticized by glycerol" *Starch - Stärke*, *57*, (10): 494–504 ISSN: 0038-9056 DOI: 10.1002/star.200500423.

Johnson, R. K., Zink-Sharp, A. and Glasser, W. G. (2011) "Preparation and characterization of hydrophobic derivatives of TEMPO-oxidized nanocelluloses" *Cellulose*, *18*, 1599–1609 DOI: 10.1007/s10570-011-9579-y.

Jonoobi, M., Mathew, A. P., Abdi, M. M., Makinejad, M. D. and Oksman, K. (2012) "A comparison of modified and unmodified cellulose nanofiber reinforced polylactic acid (PLA) prepared by twin screw extrusion" *Journal of Polymers and the Environment*, *20*, (4): 991–997 ISSN: 15662543 DOI: 10.1007/S10924-012-0503-9.

Kafy, A., Kim, H. C., Zhai, L., Kim, J. W., Hai, L. V., Kang, T. J. and Kim, J. (2017) "Cellulose long fibers fabricated from cellulose nanofibers and its strong and tough characteristics" *Scientific Reports*, *7*, (17683): 1–8 DOI: 10.1038/s41598-017-17713-3.

Kamboj, G., Gaff, M., Smardzewski, J., Haviarová, E., Hui, D., Rezaei, F. and Sethy, A. K. (2022) "Effect of cellulose nanofiber and cellulose nanocrystals reinforcement on the strength and stiffness of PVAc bonded joints" *Composite Structures*, *295*, 115821 ISSN: 0263-8223 DOI: 10.1016/J.COMPSTRUCT.2022.115821.

Kargarzadeh, H., Huang, J., Lin, N., Ahmad, I., Mariano, M., Dufresne, A., Thomas, S. and Gałęski, A. (2018) "Recent developments in nanocellulose-based biodegradable polymers, thermoplastic polymers, and porous nanocomposites." *Progress in Polymer Science*, *87*, 197–227 DOI: 10.1016/j.progpolymsci.2018.07.008.

Karimi, S., Dufresne, A., Tahir, P. M., Karimi, A. and Abdulkhani, A. (2014) "Biodegradable starch-based composites: Effect of micro and nanoreinforcements on composite properties" *Journal of Material Science*, *49*, 4513–4521 ISSN: 15734803 DOI: 10.1007/s10853-014-8151-1.

Kaushik, A., Singh, M. and Verma, G. (2010) "Green nanocomposites based on thermoplastic starch and steam exploded cellulose nanofibrils from wheat straw" *Carbohydrate Polymers*, *82*, 337–345 ISSN: 0144-8617 DOI: 10.1016/j.carbpol.2010.04.063.

Ketola, A. E., Leppänen, M., Turpeinen, T., Papponen, P., Strand, A., Sundberg, A., Arstila, K. and Retulainen, E. (2019) "Cellulose nanofibrils prepared by gentle drying methods reveal the limits of helium ion microscopy imaging" *RSC Advances*, *9*, 15668–15677 ISSN: 20462069 DOI: 10.1039/C9RA01447K.

Khalil, H. P. S. A., Davoudpour, Y., Islam, M. N., Mustapha, A., Sudesh, K., Dungani, R. and Jawaid, M. (2014) "Production and modification of nanofibrillated cellulose using various mechanical processes: A review" *Carbohydrate Polymers*, *99*, 649–665 DOI: 10.1016/j.carbpol.2013.08.069.

Khan, B., Niazi, M. B. K., Jahan, Z., Farooq, W., Naqvi, S. R., Ali, M., Ahmed, I. and Hussain, A. (2019) "Effect of ultra-violet cross-linking on the properties of boric acid and glycerol co-plasticized thermoplastic starch films" *Food Packaging and Shelf Life*, *19*, 184–192 ISSN: 2214-2894 DOI: 10.1016/j.fpsl.2018.05.006.

Khoshkava, V. and Kamal, M. R. (2014) "Effect of drying conditions on cellulose nanocrystal (CNC) agglomerate porosity and dispersibility in polymer nanocomposites" *Powder Technology*, *261*, 288–298 ISSN: 0032-5910 DOI: 10.1016/J.POWTEC.2014.04.016.

Kim, D.-Y., Nishiyama, Y. and Kuga, S. (2002) "Surface acetylation of bacterial cellulose" *Cellulose*, *9*, (3-4): 361–367 DOI: 10.1023/A:1021140726936.

Kim, J., Bang, J., Kim, Y., Kim, J.-C., Hwang, S.-W., Yeo, H., Choi, I.-G. and Kwak, H. W. (2022) "Eco-friendly alkaline lignin/cellulose nanofiber drying system for efficient redispersion behavior" *Carbohydrate Polymers*, *282*, 119122 ISSN: 0144-8617 DOI: 10.1016/J.CARBPOL.2022.119122.

Kiziltas, A., Nazari, B., Kiziltas, E. E., Gardner, D. J. S., Han, Y. and Rushing, T. S. (2016) "Cellulose nanofibre-polyethylene nanocomposites modified by polyvinyl alcohol" *Journal of Applied Polymer Science*, *133*, (6): 42933 ISSN: 1097-4628 DOI: 10.1002/APP.42933.

Kokol, V., Božič, M., Vogrinčič, R. and Mathew, A. P. (2015) "Characterisation and properties of homo- and heterogenously phosphorylated nanocellulose" *Carbohydrate Polymers*, *125*, 301–313 ISSN: 0144-8617 DOI: 10.1016/J.CARBPOL.2015.02.056.

Kwak, H. W., You, J., Lee, M. E. and Jin, H.-J. (2019) "Prevention of cellulose nanofibril agglomeration during dehydration and enhancement of redispersibility by hydrophilic gelatin" *Cellulose*, *26*, (7): 4357–4369 ISSN: 1572882X DOI: 10.1007/S10570-019-02387-Z.

Lamy, B. and Baley, C. (2000) "Stiffness prediction of flax fibers-epoxy composite materials" *Journal of Materials Science Letter*, *19*, 979–980 DOI: 10.1023/A:1006776423764.

Langari, M. M., Nikzad, M., Ghoreyshi, A. A. and Mohammadi, M. (2019) "Isolation of nanocellulose from broomcorn stalks and its application for nanocellulose/xanthan film preparation" *ChemistrySelect*, *4*, 11987–11994 DOI: 10.1002/slct.201902533.

Langmuir, I. (1918) "The adsorption of gases on plane surfaces of glass, mica and platinum" *Journal of the American Chemical Society*, *40*, (9): 1361–1403 ISSN: 15205126 DOI: 10.1021/ja02242a004.

Laohakunjit, N. and Noomhorm, A. (2004) "Effect of plasticizers on mechanical and barrier properties of rice starch film" *Starch - Stärke*, *56*, (8): 348–356 ISSN: 0038-9056 DOI: 10.1002/star.200300249.

Leloup, V. M., Colonna, P. and Buleon, A. (1991) "Influence of amylose-amylopectin ratio on gel properties" *Journal of Cereal Science*, *13*, (1): 1–13 ISSN: 0733-5210 DOI: 10.1016/S0733-5210(09)80023-4.

Leroy, L., Stoclet, G., Lefebvre, J.-M. and Gaucher, V. (2022) "Mechanical behavior of thermoplastic starch: Rationale for the temperature-relative humidity equivalence" *Polymers*, *14*, (13): 2531 ISSN: 2073-4360 DOI: 10.3390/POLYM14132531.

Li, A., Xu, D., Luo, L., Zhou, Y., Yan, W., Leng, X., Dai, D., Zhou, Y., Ahmad, H., Rao, J. and Fan, M. (2021) "Overview of nanocellulose as additives in paper processing and paper products" *Nanotechnology Reviews*, *10*, (1): 264–281 ISSN: 21919097 DOI: 10.1515/NTREV-2021-0023.

Li, J., Song, Z., Li, D., Shang, S. and Guo, Y. (2014) "Cotton cellulose nanofiber-reinforced high density polyethylene composites prepared with two different pretreatment methods" *Industrial Crops and Products*, *59*, 318–328 ISSN: 0926-6690 DOI: 10.1016/J.INDCROP.2014.05.033.

Li, Q., McGinnis, S., Sydnor, C., Wong, A. and Renneckar, S. (2013) "Nanocellulose life cycle assessment" *ACS Sustainable Chemistry and Engineering*, *1*, (8): 919–928 ISSN: 21680485 DOI: 10.1021/sc4000225.

Li, W., Leong, T. S. H., Ashokkumar, M. and Martin, G. J. O. (2017) "A study of the effectiveness and energy efficiency of ultrasonic emulsification" *Physical Chemistry Chemical Physics*, *20*, 86–96 ISSN: 14639076 DOI: 10.1039/C7CP07133G.

Lian, X., Cheng, K., Wang, D., Zhu, W. and Wang, X. (2018) "Analysis of crystals of retrograded starch with sharp X-ray diffraction peaks made by recrystallization of amylose and amylopectin" *International Journal of Food Properties*, *20*, (3): S3224–S3236 ISSN: 15322386 DOI: 10.1080/10942912.2017.1362433.

Lin, N. and Dufresne, A. (2013) "Physical and/or chemical compatibilization of extruded cellulose nanocrystal reinforced polystyrene nanocomposites" *Macromolecules*, *46*, (14): 5570–5583 ISSN: 00249297 DOI: 10.1021/MA4010154.

Liu, Y. (2018) "Strong and flexible nanocomposites of carboxylated cellulose nanofibril dispersed by industrial lignin" *ACS Sustainable Chemistry and Engineering*, *6*, (4): 5524–5532 ISSN: 21680485 DOI: 10.1021/ACSSUSCHEMENG.8B00402.

Lizundia, E., Fortunati, E., Dominici, F., Vilas, J. L., León, L. M., Armentano, I., Torre, L. and Kenny, J. M. (2016) "PLLA-grafted cellulose nanocrystals: Role of the CNC content and grafting on the PLA bionanocomposite film properties" *Carbohydrate Polymers*, *142*, 105–113 ISSN: 0144-8617 DOI: 10.1016/J.CARBPOL.2016.01.041.

Lowys, M.-P., Desbrières, J. and Rinaudo, M. (2001) "Rheological characterization of cellulosic microfibril suspensions. Role of polymeric additives" *Food Hydrocolloids*, *15*, (1): 25–32 ISSN: 0268-005X DOI: 10.1016/S0268-005X(00)00046-1.

Lutfi, Z., Nawab, A., Alam, F., Hasnain, A. and Haider, S. Z. (2017) "Influence of xanthan, guar, CMC and gum acacia on functional properties of water chestnut (*Trapa bispinosa*) starch" *International Journal of Biological Macromolecules*, *103*, 220–225 ISSN: 0141-8130 DOI: 10.1016/j.ijbiomac.2017.05.046.

Ma, X., Chang, P. R., Yang, J. and Yu, J. (2009) "Preparation and properties of glycerol plasticized-pea starch/zinc oxide-starch bionanocomposites" *Carbohydrate Polymers*, *75*, (3): 472–478 ISSN: 0144-8617 DOI: 10.1016/J.CARBPOL.2008.08.007.

Ma, X. and Yu, J. (2004) "The effects of plasticizers containing amide groups on the properties of thermoplastic starch" *Starch - Stärke*, *56*, (11): 545–551 ISSN: 0038-9056 DOI: 10.1002/star.200300256.

Mackenzie, W. (2022) *Cost competitiveness of PET, aluminium and glass beverage containers* tech. rep. International Aluminium URL: https://international-aluminium.org/wp-content/uploads/2022/09/Cost-competitiveness-of-PET-aluminium-and-glass-beverage-containers-1.pdf.

Mahardika, M., Abral, H., Kasim, A., Arief, S. and Asrofi, M. (2018) "Production of nanocellulose from pineapple leaf fibers via high-shear homogenization and ultrasonication" *Fibers*, *6*, (2) DOI: 10.3390/fib6020028.

Mahfoudhi, N. and Boufi, S. (2017) "Nanocellulose as a novel nanostructured adsorbent for environmental remediation: A review" *Cellulose*, *24*, (3): 1171–1197 ISSN: 1572-882X DOI: 10.1007/S10570-017-1194-0.

Makhtar, N. S. M., Hamdan, N., Rodhi, M. N. M., Musa, M. and Ku Hamid, K. H. (2014) "The potential use of *Tacca leontopetaloides* as green material in manufacturing automotive part" *Applied Mechanics and Materials*, *575*, 65–72 ISSN: 1662-7482 DOI: 10.4028/www.scientific.net/AMM.575.65.

Makhtar, N. S. M., Rodhi, M. N. M., Musa, M. and Hamid, K. H. K. (2013) "Thermal behavior of *Tacca leontopetaloides* starch-based biopolymer" *International Journal of Polymer Science*, *2013*, DOI: 10.1155/2013/373854.

Mali, S., Grossmann, M. V. E., García, M. A., Martino, M. N. and Zaritzky, N. E. (2006) "Effects of controlled storage on thermal, mechanical and barrier properties of plasticized films from different starch sources" *Journal of Food Engineering*, *75*, (4): 453–460 ISSN: 0260-8774 DOI: 10.1016/j.jfoodeng.2005.04.031.

Malucelli, L. C., Matos, M., Jordão, C., Lomonaco, D., Lacerda, L. G., Carvalho Filho, M. A. and Magalhães, W. L. (2019) "Influence of cellulose chemical pretreatment on energy consumption and viscosity of produced cellulose nanofibers (CNF) and mechanical properties of nanopaper" *Cellulose*, *26*, (3): 1667–1681 ISSN: 1572882X DOI: 10.1007/S10570-018-2161-0.

Mandala, I. G., Palogou, E. D. and Kostaropoulos, A. E. (2002) "Influence of preparation and storage conditions on texture of xanthan–starch mixtures" *Journal of Food Engineering*, *53*, (1): 27–38 ISSN: 0260-8774 DOI: 10.1016/S0260-8774(01)00136-4.

Mark, R. E. (1967) *Cell Wall Mechanics of Tracheids.* Yale University Press, New Haven.

Mattox, D. M. (2010) *Handbook of Physical Vapor Deposition (PVD) Processing*, 2nd ed. Elsevier Science & Technology Books, Norwich ISBN: 978-0-8155-2037-5.

Mautner, A. (2020) "Nanocellulose water treatment membranes and filters: A review" *Polymer International*, *69*, (9): 741–751 ISSN: 1097-0126 DOI: 10.1002/PI.5993.

Mazeau, K. and Wyszomirski, M. (2012) "Modelling of Congo red adsorption on the hydrophobic surface of cellulose using molecular dynamics" *Cellulose*, *19*, (5): 1495–1506 ISSN: 09690239 DOI: 10.1007/S10570-012-9757-6.

Melo, C. P. B., Grossman, M. V. E., Yamashita, F., Youssef, E. Y., Dall'Antônia, L. H. and Mali, S. (2011) "Effect of manufacturing process and xanthan gum addition on the properties of cassava starch films" *Journal of Polymer and the Environment*, *19*, 739–749 DOI: 10.1007/s10924-011-0325-1.

Meneguin, A. B., da Silva Barud, H., Sábio, R. M., de Sousa, P. Z., Manieri, K. F., de Freitas, L. A. P., Pacheco, G., Alonso, J. D. and Chorilli, M. (2020) "Spray-dried bacterial cellulose nanofibers: A new generation of pharmaceutical excipient intended for intestinal drug delivery" *Carbohydrate Polymers*, *249*, 116838 ISSN: 0144-8617 DOI: 10.1016/j.carbpol.2020.116838.

Meng, L., Liu, H., Yu, L., Duan, Q., Chen, L., Liu, F., Shao, Z., Shi, K. and Lin, X. (2019) "How water acting as both blowing agent and plasticizer affect on starch-based foam" *Industrial Crops and Products*, *134*, 43–49 ISSN: 0926-6690 DOI: 10.1016/J.INDCROP.2019.03.056.

Michelin, M., Gomes, D. G., Romaní, A., T.M. Polizeli, M. and Teixeira, J. A. (2020) "Nanocellulose production: Exploring the enzymatic route and residues of pulp and paper industry" *Molecules*, *25*, (15): 3411 ISSN: 1420-3049 DOI: 10.3390/MOLECULES25153411.

Mikus, P.-Y., Alix, S., Soulestin, J., Lacrampe, M. F., Krawczak, P., Coqueret, X. and Dole, P. (2014) "Deformation mechanisms of plasticized starch materials" *Carbohydrate Polymers*, *114*, 450–457 ISSN: 0144-8617 DOI: 10.1016/J.CARBPOL.2014.06.087.

Missoum, K., Bras, J. and Belgacem, M. N. (2012) "Water redispersible dried nanofibrillated cellulose by adding sodium chloride" *Biomacromolecules*, *13*, (12): 4118–4125 ISSN: 15257797 DOI: 10.1021/BM301378N.

Morán, J. I., Alvarez, V. A., Cyras, V. P. and Vázquez, A. (2008) "Extraction of cellulose and preparation of nanocellulose from sisal fibers" *Cellulose*, *15*, (1): 149–159 ISSN: 09690239 DOI: 10.1007/S10570-007-9145-9.

Mordor Intelligence (2023) *Thermoplastic starch (TPS) market - growth, trends, COVID-19 impact, and forecasts (2022 - 2028)* URL: https://www.mordorintelligence.com/industry-reports/thermoplastic-starch-market (visited on 07/15/2023).

Moser, C., Henriksson, G. and Lindström, M. (2018) "Improved dispersibility of once-dried cellulose nanofibers in the presence of glycerol" *Nordic Pulp and Paper Research Journal*, *33*, (4): 647–650 ISSN: 20000669 DOI: 10.1515/NPPRJ-2018-0054.

Moser, C., Henriksson, G. and Lindström, M. E. (2016) "Specific surface area increase during cellulose nanofiber manufacturing related to energy input" *BioResources*, *11*, (3): 7124–7132 ISSN: 19302126 DOI: 10.15376/BIORES.11.3.7124-7132.

Müller, C. M., Laurindo, J. B. and Yamashita, F. (2012) "Composites of thermoplastic starch and nanoclays produced by extrusion and thermopressing" *Carbohydrate Polymers*, *89*, (2): 504–510 ISSN: 0144-8617 DOI: 10.1016/J.CARBPOL.2012.03.035.

Myllärinen, P., Partanen, R., Seppälä, J. and Forssell, P. (2002) "Effect of glycerol on behaviour of amylose and amylopectin films" *Carbohydrate Polymers*, *50*, 355–361 ISSN: 1868-7075 DOI: 10.1016/S0144-8617(02)00042-5.

Nardi, R., Silveira, M. H. L. and Siqueira, G. (2020) "Understanding important aspects of spray drying microfibrillated cellulose through statistical analysis" *Cellulose*, *27*, 10707–10717 DOI: 10.1007/s10570-020-03392-3.

Nashed, G., Rutgers, R. P. G. and Sopade, P. A. (2003) "The plasticisation effect of glycerol and water on the gelatinisation of wheat starch" *Starch - Stärke*, *55*, 131–137 ISSN: 1521-379X DOI: 10.1002/STAR.200390027.

Nawab, A., Alam, F., Haq, M. A. and Hasnain, A. (2016) "Effect of guar and xanthan gums on functional properties of mango (*Mangifera indica*) kernel starch" *International Journal of Biological Macromolecules*, *93*, 630–635 ISSN: 0141-8130 DOI: 10.1016/j.ijbiomac.2016.09.011.

Nechyporchuk, O., Belgacem, M. N. and Bras, J. (2016) "Production of cellulose nanofibrils: A review of recent advances" *Industrial Crops and Products*, *93*, 2–25 DOI: 10.1016/j.indcrop.2016.02.016.

Nelson, M. L. and O'Connor, R. T. (May 1964) "Relation of certain infrared bands to cellulose crystallinity and crystal latticed type. Part I. Spectra of lattice types I, II, III and of amorphous cellulose" *Journal of Applied Polymer Science*, *8*, (3): 1311–1324 ISSN: 1097-4628 DOI: 10.1002/APP.1964.070080322.

Nevoralová, M., Koutný, M., Ujčić, A., Horák, P., Kredatusová, J., Šerá, J., Růžek, L., Růžková, M., Krejčíková, S., Šlouf, M. and Kruliš, Z. (2019) "Controlled biodegradability of functionalized thermoplastic starch based materials" *Polymer Degradation and Stability*, *170*, 108995 ISSN: 0141-3910 DOI: 10.1016/J.POLYMDEGRADSTAB.2019.108995.

Niazi, M. B. K., Zijlstra, M. and Broekhuis, A. A. (2015) "Influence of plasticizer with different functional groups on thermoplastic starch" *Journal of Applied Polymer Science*, *132*, (22): 42012 ISSN: 1097-4628 DOI: 10.1002/APP.42012.

Nicu, R., Ciolacu, F. and Ciolacu, D. E. (2021) "Advanced functional materials based on nanocellulose for pharmaceutical/medical applications" *Pharmaceutics*, *13*, 1125 DOI: 10.3390/pharmaceutics13081125.

Niemand, D. (2023) *Xanthan gum as an additive in oven-dried nanocellulose to prevent agglomeration* Department of Chemical Engineering, University of Pretoria.

Niu, F., Li, M., Huang, Q., Zhang, X., Pan, W., Yang, J. and Li, J. (2017) "The characteristic and dispersion stability of nanocellulose produced by mixed acid hydrolysis and ultrasonic assistance" *Carbohydrate Polymers*, *165*, 197–204 ISSN: 0144-8617 DOI: 10.1016/J.CARBPOL.2017.02.048.

Nordenström, M., Kaldéus, T., Erlandsson, J., Pettersson, T., Malmström, E. and Wågberg, L. (2021) "Redispersion strategies for dried cellulose nanofibrils" *ACS Sustainable Chemistry and Engineering*, *9*, (33): 11003–11010 ISSN: 21680485 DOI: 10.1021/ACSSUSCHEMENG.1C02122.

Nowak, F. M. (2010) *Sonochemistry: Theory, Reactions, Syntheses, and Applications.* Nova Science Publishers, New York ISBN: 9781617286520.

Nwokocha, L., Senan, C. and Williams, P. A. (2011) "Structural, physicochemical and rheological characterization of *Tacca involucrata* starch" *Carbohydrate Polymers*, *86*, 789–796 DOI: 10.1016/j.carbpol.2011.05.024.

OECD (2022) *Global Plastics Outlook: Economic Drivers, Environmental Impacts and Policy Options*, OECD Publishing, Paris DOI: 10.1787/de747aef-en.

Omojola, M. O. (2013) "Tacca starch: A review of its production, physicochemical properties, modification and industrial uses" *Nigerian Food Journal*, *31*, (2): 8–21 ISSN: 1684 5374 URL: http://www.bioline.org.br/pdf?nd13061.

Osswald, T. A. (2017) *Understanding Polymer Processing: Processes and Governing Equations*, 2nd ed. Hanser Publications, Munich ISBN: 978-1-56990-647-7.

Othman, S. H., Wane, B. M., Nordin, N., Noor Hasnan, N. Z., Talib, R. A. and Karyadi, J. N. W. (2021) "Physical, mechanical, and water vapor barrier properties of starch/cellulose nanofiber/thymol bionanocomposite films" *Polymers*, *13*, (23): 4060 DOI: 10.3390/polym13234060.

Ougiya, H., Hioki, N., Watanabe, K., Morinaga, Y., Yoshinaga, F. and Samejima, M. (1998) "Relationship between the physical properties and surface area of cellulose derived from adsorbates of various molecular sizes" *Bioscience, Biotechnology and Biochemistry*, *62*, (10): 1880–1884 ISSN: 13476947 DOI: 10.1271/BBB.62.1880.

Özeren, H. D., Guivier, M., Olsson, R. T., Nilsson, F. and Hedenqvist, M. S. (2020) "Ranking plasticizers for polymers with atomistic simulations: PVT, mechanical properties, and the role of hydrogen bonding in thermoplastic starch" *ACS Applied Polymer Materials*, *2*, (5): 2016–2026 ISSN: 26376105 DOI: 10.1021/acsapm.0c00191.

Pääkkö, M., Ankerfors, M., Kosonen, H., Nykänen, A., Ahola, S., Österberg, M., Ruokolainen, J., Laine, J., Larsson, P. T., Ikkala, O. and Lindström, T. (2007) "Enzymatic hydrolysis combined with mechanical shearing and high-pressure homogenization for nanoscale cellulose fibrils and strong gels" *Biomacromolecules*, *8*, (6): 1934–1941 ISSN: 1525-7797 DOI: 10.1021/bm061215p.

Paluch, M., Ostrowska, J., Tyński, P., Sadurski, W. and Konkol, M. (2022) "Structural and thermal properties of starch plasticized with glycerol/urea mixture" *Journal of Polymers and the Environment*, *30*, (2): 728–740 ISSN: 15728919 DOI: 10.1007/S10924-021-02235-X.

Pawlicka, A., Tavares, F. C., Dörr, D. S., Cholant, C. M., Ely, F., Santos, M. J. L. and Avellaneda, C. O. (2019) "Dielectric behavior and FTIR studies of xanthan gum-based solid polymer electrolytes" *Electrochimica Acta*, *305*, 232–239 ISSN: 0013-4686 DOI: 10.1016/J.ELECTACTA.2019.03.055.

Pedregosa, F., Varoquaux, G., Gramfort, A., Michel, V., Thirion, B., Grisel, O., Blondel, M., Prettenhofer, P., Weiss, R., Dubourg, V., Vanderplas, J., Passos, A., Cournapeau, D., Brucher, M., Perrot, M. and Duchesnay, E. (2011) "Scikit-learn: Machine learning in Python" *Journal of Machine Learning Research*, *12*, 2825–2830.

Peng, Y., Duan, C., Elias, R., Lucia, L. A. and Fu, S. (2019) "A new protocol for efficient and high yield preparation of cellulose nanofibrils" *Cellulose*, *26*, 877–887 DOI: 10.1007/s10570-018-2112-9.

Peng, Y., Nair, S. S., Chen, H., Yan, N. and Cao, J. (2018) "Effects of lignin content on mechanical and thermal properties of polypropylene composites reinforced with micro particles of spray dried cellulose nanofibrils" *ACS Sustainable Chemistry & Engineering*, *6*, 11078–11086 DOI: 10.1021/acssuschemeng.8b02544.

Peng, Y., Gardner, D. J. and Han, Y. (2012a) "Drying cellulose nanofibrils: In search of a suitable method" *Cellulose*, *19*, (1): 91–102 ISSN: 09690239 DOI: 10.1007/S10570-011-9630-Z.

Peng, Y., Gardner, D. J., Han, Y., Kiziltas, A., Cai, Z. and Tshabalala, M. A. (2013) "Influence of drying method on the material properties of nanocellulose I: Thermostability and crystallinity" *Cellulose*, *20*, 2379–2392 DOI: 10.1007/s10570-013-0019-z.

Peng, Y., Han, Y. and Gardner, D. J. (2012b) "Spray-drying cellulose nanofibrils: Effect of drying process parameters on particle morphology and size distribution" *Wood and Fibre Science*, *44*, (4): 448–461.

Pereda, M., Kissi, N. E. and Dufresne, A. (2014) "Extrusion of polysaccharide nanocrystal reinforced polymer nanocomposites through compatibilization with poly(ethylene oxide)" *ACS Applied Materials and Interfaces*, *6*, (12): 9365–9375 ISSN: 19448252 DOI: 10.1021/AM501755P.

Perumal, A. B., Nambiar, R. B., Moses, J. A. and Anandharamakrishnan, C. (2022) "Nanocellulose: Recent trends and applications in the food industry" *Food Hydrocolloids*, *127*, 107484 ISSN: 0268-005X DOI: 10.1016/J.FOODHYD.2022.107484.

Pozo, C., Rodríguez-Llamazares, S., Bouza, R., Barral, L., Castaño, J., Müller, N. and Restrepo, I. (2018) "Study of the structural order of native starch granules using combined FTIR and XRD analysis" *Journal of Polymer Research*, *25*, (12): 1–8 ISSN: 15728935 DOI: 10.1007/S10965-018-1651-Y.

Pushpadass, H. A., Kumar, A., Jackson, D. S., Wehling, R. L., Dumais, J. J. and Hanna, M. A. (2009) "Macromolecular changes in extruded starch-films plasticized with glycerol, water and stearic acid" *Starch - Stärke*, *61*, (5): 256–266 ISSN: 1521-379X DOI: 10.1002/STAR.200800046.

Qian, S., Sheng, K., Yu, K., Xu, L. and Fontanillo Lopez, C. A. (2018) "Improved properties of PLA biocomposites toughened with bamboo cellulose nanowhiskers through silane modification" *Journal of Materials Science*, *53*, (15): 10920–10932 ISSN: 15734803 DOI: 10.1007/S10853-018-2377-2.

Rindlav-Westling, Å., Stading, M. and Gatenholm, P. (2002) "Crystallinity and morphology in films of starch, amylose and amylopectin blends" *Biomacromolecules*, *3*, (1): 84–91 ISSN: 15257797 DOI: 10.1021/BM010114I.

Rol, F., Belgacem, M. N., Gandini, A. and Bras, J. (2019) "Recent advances in surface-modified cellulose nanofibrils" *Progress in Polymer Science*, *88*, 241–264 ISSN: 00796700 DOI: 10.1016/j.progpolymsci.2018.09.002.

Saito, T., Kuramae, R., Wohlert, J., Berglund, L. A. and Isogai, A. (2012) "An ultrastrong nanofibrillar biomaterial: the strength of single cellulose nanofibrils revealed via sonication-induced fragmentation" *Biomacromolecules*, *14*, 248–253 DOI: 10.1021/bm301674e.

Santmarti, A., Tammelin, T. and Lee, K.-Y. (2020) "Prevention of interfibril hornification by replacing water in nanocellulose gel with low molecular weight liquid poly(ethylene glycol)" *Carbohydrate Polymers*, *250*, 116870 ISSN: 0144-8617 DOI: 10.1016/J.CARBPOL.2020.116870.

Sasaki, T., Yasui, T. and Matsuki, J. (2000) "Effect of amylose content on gelatinization, retrogradation, and pasting properties of starches from waxy and nonwaxy wheat and their F1 seeds" *Cereal Chemistry*, *77*, (1): 58–63 ISSN: 1943-3638 DOI: 10.1094/CCHEM.2000.77.1.58.

Sato, T., Norisuye, T. and Fujita, H. (1984) "Double-stranded helix of xanthan: Dimensional and hydrodynamic properties in 0.1 M aqueous sodium chloride" *Macromolecules*, *17*, (12): 2696–2700 ISSN: 15205835 DOI: 10.1021/ma00142a043.

Savadekar, N. R. and Mhaske, S. T. (2012) "Synthesis of nano cellulose fibers and effect on thermoplastics starch based films" *Carbohydrate Polymers*, *89*, 146–151 ISSN: 0144-8617 DOI: 10.1016/j.carbpol.2012.02.063.

Saxena, A., Elder, T. J., Kenvin, J. and Ragauskas, A. J. (2010) "High oxygen nanocomposite barrier films based on xylan and nanocrystalline cellulose" *Nano-Micro Letters*, *2*, (4): 235–241 DOI: 10.5101/NML.V2I4.P235-241.

Schmitt, H., Guidez, A., Prashantha, K., Soulestin, J., Lacrampe, M. F. and Krawczak, P. (2015) "Studies on the effect of storage time and plasticizers on the structural variations in thermoplastic starch" *Carbohydrate Polymers*, *115*, 364–372 ISSN: 0144-8617 DOI: 10.1016/j.carbpol.2014.09.004.

Seabold, S. and Perktold, J. (2010) "Statsmodels: Econometric and statistical modeling with python" in: *9th Python in Science Conference*.

Seddiqi, H., Oliaei, E., Honarkar, H., Jin, J., Geonzon, L. C., Bacabac, R. G. and Klein-Nulend, J. (2021) "Cellulose and its derivatives: towards biomedical applications" *Cellulose*, *28*, 1893–1931 DOI: 10.1007/s10570-020-03674-w.

Shang, Z., An, X., Seta, F. T., Ma, M., Shen, M., Dai, L., Liu, H. and Ni, Y. (2019) "Improving dispersion stability of hydrochloric acid hydrolyzed cellulose nano-crystals" *Carbohydrate Polymers*, *222*, 115037 ISSN: 0144-8617 DOI: 10.1016/J.CARBPOL.2019.115037.

Shimizu, M., Saito, T., Nishiyama, Y., Iwamoto, S., Yano, H., Isogai, A. and Endo, T. (2016) "Fast and robust nanocellulose width estimation using turbidimetry" *Macromolecular Rapid Communications*, *37*, (19): 1581–1586 ISSN: 1521-3927 DOI: 10.1002/MARC.201600357.

Singh, V., Ali, S. Z., Somashekar, R. and Mukherjee, P. S. (2007) "Nature of crystallinity in native and acid modified starches" *International Journal of Food Properties*, *9*, (4): 845–854 ISSN: 10942912 DOI: 10.1080/10942910600698922.

Sjöö, M. and Nilsson, L. (2018) *Starch in Food: Structure, Function and Applications*, 2nd ed. Woodhead Publishing, Duxford ISBN: 9780081008683.

Soares Faria, L. U., Soares Pacheco, B. J., Couto Oliveira, G. and Lacerda Silva, J. (2020) "Production of cellulose nanocrystals from pineapple crown fibers through alkaline pretreatment and acid hydrolysis under different conditions" *Journal of Materials Research and Technology*, *9*, (6): 12346–12353 ISSN: 2238-7854 DOI: 10.1016/J.JMRT.2020.08.093.

Suzuki, K., Sato, A., Okumura, H., Hashimoto, T., Nakagaito, A. N. and Yano, H. (2014) "Novel high-strength, micro fibrillated cellulose-reinforced polypropylene composites using a cationic polymer as compatibilizer" *Cellulose*, *21*, (1): 507–518 ISSN: 09690239 DOI: 10.1007/S10570-013-0143-9.

Swan, S. H. and Colino, S. (2021) *Count Down: How Our Modern World Is Threatening Sperm Counts, Altering Male and Female Reproductive Development, and Imperiling the Future of the Human Race*, Scribner, New York ISBN: 9781982113667.

Tadmor, Z. (1976) "Forces in dispersive mixing" *Industrial and Engineering Chemistry Fundamentals*, *15*, (4): 346–348 ISSN: 01964313 DOI: 10.1021/I160060A022.

Talja, R. A., Helén, H., Roos, Y. H. and Jouppila, K. (2007) "Effect of various polyols and polyol contents on physical and mechanical properties of potato starch-based films" *Carbohydrate Polymers*, *67*, (3): 288–295 ISSN: 0144-8617 DOI: 10.1016/j.carbpol.2006.05.019.

Tan, I., Wee, C. C., Sopade, P. A. and Halley, P. J. (2004) "Investigation of the starch gelatinisation phenomena in water-glycerol systems: application of modulated temperature differential scanning calorimetry" *Carbohydrate Polymers*, *58*, (2): 191–204 ISSN: 0144-8617 DOI: 10.1016/j.carbpol.2004.06.038.

Tanpichai, S., Quero, F., Nogi, M., Yano, H., Young, R. J., Lindströ, T., Sampson, W. W. and Eichhorn, S. J. (2012) "Effective young's modulus of bacterial and microfibrillated cellulose fibrils in fibrous networks" *Biomacromolecules*, *13*, 1340–1349 DOI: 10.1021/bm300042t.

Tardos, T. F. (2015) *Interfacial Phenomena and Colloid Stability: Basic Principles*, vol. 1 De Gruyter, Berlin ISBN: 978-3-11-028340-2.

Teixeira, E. M., Pasquini, D., Curvelo, A. A. S., Corradini, E., Belgacem, M. N. and Dufresne, A. (2009) "Cassava bagasse cellulose nanofibrils reinforced thermoplastic cassava starch" *Carbohydrate Polymers*, *78*, (3): 422–431 ISSN: 01448617 DOI: 10.1016/J.CARBPOL.2009.04.034.

The Editors of Encyclopaedia (2008) *Dioscoreaceae* URL: https://www.britannica.com/plant/Dioscoreaceae (visited on 04/14/2022).

Thunwall, M., Kuthanová, V., Boldizar, A. and Rigdahl, M. (2008) "Film blowing of thermoplastic starch." *Carbohydrate Polymers*, *71*, (4): 583–590 ISSN: 0144-8617 DOI: 10.1016/J.CARBPOL.2007.07.001.

Trache, D., Hussin, M. H., Haafizc, M. K. M. and Thakur, V. K. (2017) "Recent progress in cellulose nanocrystals: Sources and production" *Nanoscale*, *9*, 1763–1786 DOI: 10.1039/c6nr09494e.

Ubwa, S., Abah, J., Asemave, K. and Shambe, T. (Oct. 2012) "Studies on the gelatinization temperature of some cereal starches" *International Journal of Chemistry*, *4*, 22–28 DOI: 10.5539/ijc.v4n6p22.

Uetani, K. and Yano, H. (2011) "Nanofibrillation of wood pulp using a high-speed blender" *Biomacromolecules*, *12*, (2): 348–353 ISSN: 1525-7797 DOI: 10.1021/bm101103p.

United Nations (2015) *Transforming our world: The 2030 agenda for sustainable development* URL: https://wedocs.unep.org/20.500.11822/9814 (visited on 06/06/2023).

Valenzuela, C. P. and Rodriguez-Llamazares, S. (2016) *Calculate the relative crystallinity of starch by XRD and FTIR* R package version >= 3.0 URL: https://CRAN.R-project.org/package=cryst.

Van Der Burgt, M. C., Van Der Woude, M. E. and Janssen, L. P. B. M. (1996) "The influence of plasticizer on extruded thermoplastic starch" *Journal of Vinyl and Additive Technology*, *2*, (2): 170–174 ISSN: 1083-5601 DOI: 10.1002/vnl.10116.

Van Soest, J. J. G. and Knooren, N. (1997) "Influence of glycerol and water content on the structure and properties of extruded starch plastic sheets during aging" *Journal of Applied Polymer Science*, *64*, 1411–1422 DOI: 10.1002/(SICI)1097-4628(19970516)64:7<1411::AID-APP21>3.0.CO;2-Y.

Van Soest, J. J. G., Bezemer, R. C., de Wit, D. and Vliegenthart, J. F. G. (Mar. 1996a) "Influence of glycerol on the melting of potato starch" *Industrial Crops and Products*, *5*, (1): 1–9 ISSN: 0926-6690 DOI: 10.1016/0926-6690(95)00047-X.

Van Soest, J. J. G., de Wit, D. and Vliegenthart, J. F. G. (1996b) "Mechanical properties of thermoplastic waxy maize starch" *Journal of Applied Polymer Science*, *61*, (11): 1927–1937 DOI: 10.1002/(SICI)1097-4628(19960912)61:11<1927::AID-APP7>3.0.CO;2-L.

Van Soest, J. J. G. and Essers, P. (1997) "Influence of amylose-amylopectin ratio on properties of extruded starch plastic sheets" *Journal of Macromolecular Science*, *34*, (9): 1665–1689 ISSN: 10601325 DOI: 10.1080/10601329708010034.

Van Soest, J. J. G., Hulleman, S. H. D., de Wit, D. and Vliegenthart, J. F. G. (1996c) "Changes in the mechanical properties of thermoplastic potato starch in relation with changes in B-type crystallinity" *Carbohydrate Polymers*, *29*, (3): 225–232 ISSN: 01448617 DOI: 10.1016/0144-8617(96)00011-2.

Van Soest, J. J. G., Hulleman, S. H. D., de Wit, D. and Vliegenthart, J. F. G. (1996d) "Crystallinity in starch bioplastics." *Industrial Crops and Products*, *5*, 1–22 ISSN: 0926-6690.

Van Soest, J. J. G. and Vliegenthart, J. F. G. (1997) "Crystallinity in starch plastics: Consequences for material properties" *Trends in Biotechnology*, *15*, (6): 208–213 ISSN: 0167-7799 DOI: 10.1016/S0167-7799(97)01021-4.

Van't Land, C. M. (2011) *Drying in the Process Industry*, John Wiley & Sons Inc., Hoboken ISBN: 9780470131176.

VanDer Kamp, K. A., Qiang, D., Aburub, A. and Wurster, D. E. (2005) "Modified langmuir-like model for modeling the adsorption from aqueous solutions by activated carbons" *Langmuir*, *21*, (1): 217–224 ISSN: 07437463 DOI: 10.1021/LA0400930.

Varavinit, S., Shobsngob, S., Varanyanond, W., Chinachoti, P. and Naivikul, O. (2003) "Effect of amylose content on gelatinization, retrogradation and pasting properties of flours from different cultivars of thai rice" *Starch - Stärke*, *55*, (9): 410–415 ISSN: 1521-379X DOI: 10.1002/STAR.200300185.

Velásquez-Cock, J., Gómez H., B. E., Posada, P., G, A. S., Gómez H., C., Castro, C., Gañán, P. and Zuluaga, R. (2018) "Poly (vinyl alcohol) as a capping agent in oven dried cellulose nanofibrils" *Carbohydrate Polymers*, *179*, 118–125 ISSN: 0144-8617 DOI: 10.1016/J.CARBPOL.2017.09.089.

Verseput, R. (2000) "Digging into DOE: Selecting the right central composite design for response surface methodology applications" *Quality Digest*, URL: https://www.qualitydigest.com/june01/html/doe.html.

Vineeth, S. K., Gadhave, R. V. and Gadekar, P. T. (2019) "Nanocellulose applications in wood adhesives — Review" *Open Journal of Polymer Chemistry*, *9*, (4): 63–75 ISSN: 2165-6681 DOI: 10.4236/OJPCHEM.2019.94006.

Virtanen, P., Gommers, R., Oliphant, T. E., Haberland, M., Reddy, T., Cournapeau, D., Burovski, E., Peterson, P., Weckesser, W., Bright, J., van der Walt, S. J., Brett, M., Wilson, J., Millman, K. J., Mayorov, N., Nelson, A. R. J., Jones, E., Kern, R., Larson, E., Carey, C. J., Polat, İ., Feng, Y., Moore, E. W., VanderPlas, J., Laxalde, D., Perktold, J., Cimrman, R., Henriksen, I., Quintero, E. A., Harris, C. R., Archibald, A. M., Ribeiro, A. H., Pedregosa, F., van Mulbregt, P. and SciPy 1.0 Contributors (2020) "SciPy 1.0: Fundamental algorithms for scientific computing in python" *Nature Methods*, *17*, 261–272 DOI: 10.1038/s41592-019-0686-2.

Wang, P., Chen, F., Zhang, H., Meng, W., Sun, Y. and Liu, C. (2017) "Large-scale preparation of jute-fiber-reinforced starch-based composites with high mechanical strength and optimized biodegradability" *Starch - Stärke*, *69*, (11-12): 1700052 ISSN: 1521-379X DOI: 10.1002/STAR.201700052.

Wiedmann, W. and Strobel, E. (1991) "Compounding of thermoplastic starch with twin-screw extruders" *Starch - Stärke*, *43*, (4): 138–145 ISSN: 1521-379X DOI: 10.1002/STAR.19910430404.

Wiercigroch, E., Szafraniec, E., Czamara, K., Pacia, M. Z., Majzner, K., Kochan, K., Kaczor, A., Baranska, M. and Malek, K. (2017) "Raman and infrared spectroscopy of carbohydrates: A review" *Spectrochimica Acta Part A: Molecular and Biomolecular Spectroscopy*, *185*, 317–335 ISSN: 1386-1425 DOI: 10.1016/J.SAA.2017.05.045.

Wu, B.-c. and McClements, D. J. (2015) "Design of reduced-fat food emulsions: Manipulating microstructure and rheology through controlled aggregation of colloidal particles and biopolymers" *Food Research International*, *76*, 777–786 ISSN: 0963-9969 DOI: 10.1016/J.FOODRES.2015.06.034.

Wyatt, N. B. and Liberatore, M. W. (2009) "Rheology and viscosity scaling of the polyelectrolyte xanthan gum" *Journal of Applied Polymer Science*, *114*, (6): 4076–4084 ISSN: 1097-4628 DOI: 10.1002/APP.31093.

Wypych, G. (2016) *Handbook of Polymers*, 2nd ed. ChemTec Publishing, Toronto ISBN: 9781927885116 URL: http://app.knovel.com/web/toc.v/cid:kpHPE00012/viewerType:toc/root_slug:handbook-polymers-2nd.

Wypych, G. (2021) *Handbook of Fillers*, 5th ed. ChemTec Publishing, Toronto ISBN: 978-1-927885-79-6.

Xu, X., Liu, F., Jiang, L., Zhu, J. Y., Haagenson, D. and Wiesenborn, D. P. (2013) "Cellulose nanocrystals vs. cellulose nanofibrils: A comparative study on their microstructures and effects as polymer reinforcing agents" *ACS Applied Materials & Interfaces*, *5*, 2999–3009 DOI: 10.1021/am302624t.

Xu, Y., Xu, Y., Chen, H., Gao, M., Yue, X. and Ni, Y. (2022) "Redispersion of dried plant nanocellulose: A review" *Carbohydrate Polymers*, *294*, 119830 ISSN: 0144-8617 DOI: 10.1016/J.CARBPOL.2022.119830.

Yang, G., Ma, G., He, M., Ji, X., Li, W., Youn, H. J., Lee, H. L. and Chen, J. (2021) "Comparison of effects of sodium chloride and potassium chloride on spray drying and redispersion of cellulose nanofibrils suspension" *Nanomaterials*, *11*, (2): 439 ISSN: 2079-4991 DOI: 10.3390/NANO11020439.

Yang, J.-h., Yu, J.-g. and Ma, X.-f. (2006) "Study on the properties of ethylenebisformamide and sorbitol plasticized corn starch (ESPTPS)" *Carbohydrate Polymers*, *66*, (1): 110–116 ISSN: 0144-8617 DOI: 10.1016/j.carbpol.2006.02.029.

Yeromonahos, C., Polack, B. and Caton, F. (2010) "Nanostructure of the fibrin clot" *Biophysical Journal*, *99*, (7): 2018–2027 ISSN: 0006-3495 DOI: 10.1016/J.BPJ.2010.04.059.

Young, R. J. and Lovell, P. A. (2011) *Introduction to Polymers.* 3rd ed. CRC Press, Boca Raton ISBN: 978-1-4398-9415-6.

Yu, L. and Christie, G. (2005) "Microstructure and mechanical properties of orientated thermoplastic starches" *Journal of Materials Science*, *40*, (1): 111–116 ISSN: 1573-4803 DOI: 10.1007/S10853-005-5694-1.

Zaku, S., Aguzue, O., Thomas, S. and Barminas, J. (2009) "Studies on the functional properties and the nutritive values of amura plant starch (*Tacca involucrata*) a wild tropical plant" *African Journal of Food Science*, *3*, (10): 320–322.

Zaman, M., Xiao, H., Chibante, F. and Ni, Y. (2012) "Synthesis and characterization of cationically modified nanocrystalline cellulose" *Carbohydrate Polymers*, *89*, (1): 163–170 ISSN: 0144-8617 DOI: 10.1016/J.CARBPOL.2012.02.066.

Zdanowicz, M. and Spychaj, T. (2011) "Ionic liquids as starch plasticizers or solvents" *Polimery*, *56*, (11-12): 861–864 URL: http://ichp.vot.pl/index.php/p/article/view/978.

Zdanowicz, M., Jędrzejewski, R. and Pilawka, R. (2019) "Deep eutectic solvents as simultaneous plasticizing and crosslinking agents for starch" *International Journal of Biological Macromolecules*, *129*, 1040–1046 ISSN: 0141-8130 DOI: 10.1016/J.IJBIOMAC.2019.02.103.

Žepič, V., Fabjan, E. Š., Kasunič, M., Korošec, R. C., Hančič, A., Oven, P., Perše, L. S. and Poljanšek, I. (2014) "Morphological, thermal, and structural aspects of dried and redispersed nanofibrillated cellulose (NFC)" *Holzforschung*, *68*, (6): 657–667 ISSN: 1437434X DOI: 10.1515/hf-2013-0132.

Zha, L., Wang, S., Berglund, L. A. and Zhou, Q. (2023) "Mixed-linkage (1,3;1,4)-β-d-glucans as rehydration media for improved redispersion of dried cellulose nanofibrils" *Carbohydrate Polymers*, *300*, 120276 ISSN: 0144-8617 DOI: 10.1016/J.CARBPOL.2022.120276.

Zhang, J. Z., Peng, X. Y., Liu, S., Jiang, B. P., Ji, S. C. and Shen, X. C. (2019) "The persistence length of semiflexible polymers in lattice Monte Carlo simulations" *Polymers*, *11*, (2): 295 ISSN: 20734360 DOI: 10.3390/POLYM11020295.

Zhang, P., Gao, D., Zou, P. and Wang, B. (2017) "Preparation and thermomechanical properties of nanocrystalline cellulose reinforced poly(lactic acid) nanocomposites" *Journal of Applied Polymer Science*, *134*, (14): 44683 ISSN: 1097-4628 DOI: 10.1002/APP.44683.

Zhang, Y. and Han, J. H. (2006) "Mechanical and thermal characteristics of pea starch films plasticized with monosaccharides and polyols" *Journal of Food Science*, *71*, (2): 109–118 ISSN: 0022-1147 DOI: 10.1111/j.1365-2621.2006.tb08891.x.

Zhang, Y. and Han, J. H. (2010) "Crystallization of high-amylose starch by the addition of plasticizers at low and intermediate concentrations" *Journal of Food Science*, *75*, N8–N16 ISSN: 1750-3841 DOI: 10.1111/J.1750-3841.2009.01404.X.

Zhang, Y., Liu, Q., Hrymak, A. and Han, J. H. (2013) "Characterization of extruded thermoplastic starch reinforced by montmorillonite nanoclay" *Journal of Polymers and the Environment*, *21*, (1): 122–131 ISSN: 15662543 DOI: 10.1007/S10924-012-0528-0.

Zhang, Y., Xu, Y., Gao, M., Xiong, J. and Dai, L. (2021) "Water-redispersible cellulose nanocrystals adsorption of glucose via alcohol precipitation" *Journal of Wood Chemistry and Technology*, *41*, (4): 169–176 ISSN: 15322319 DOI: 10.1080/02773813.2021.1954032.

Zhou, Y., Wei, J., Lv, Y., Bian, H., Wang, W., Wang, F., Wang, J., Sun, J., Cui, M. and Shao, Z. (2019) "Methodology of redispersible dry cellulose nanofibrils powder synthesis under waterless condition" *ACS Sustainable Chemistry and Engineering*, *7*, (12): 10690–10698 ISSN: 21680485 DOI: 10.1021/acssuschemeng.9b01340.

Zhu, Z., Wang, W., Wang, X., Zhao, X., Xia, N., Kong, F. and Wang, S. (2021) "Easy way to prepare dispersible CNC dry powder by precipitation and conventional evaporation" *Cellulose*, *28*, (15): 9661–9676 ISSN: 1572882X DOI: 10.1007/S10570-021-04123-Y.

Zuo, Y., Gu, J., Tan, H. and Zhang, Y. (2015) "Thermoplastic starch prepared with different plasticizers: Relation between degree of plasticization and properties" *Journal of Wuhan University of Technology-Mater. Sci. Ed. 30*, (2): 423–428 ISSN: 1993-0437 DOI: 10.1007/s11595-015-1164-z.